Biological and synthetic membranes: What can be learned from a coarse-grained description?

Marcus Müller [a] * Kirill Katsov [b] † and Michael Schick [c] ‡

[a]Institut für Theoretische Physik, Georg-August Universität, Friedrich Hund Platz 1, D37077 Göttingen, Germany

[b]Materials Research Laboratory, University of California, Santa Barbara, CA 93106, USA

[c]Department of Physics, University of Washington, Box 351560, Seattle, WA 98195-1560, USA

We discuss the role coarse-grained models play in the investigation of the structure and thermodynamics of bilayer membranes, and we place them in the context of alternative approaches. Because they reduce the degrees of freedom and employ simple and soft effective potentials, coarse-grained models can provide rather direct insight into collective phenomena in membranes on large time and length scales. We present a summary of recent progress in this rapidly evolving field, and pay special attention to model development and computational techniques. Applications of coarse-grained models to changes of the membrane topology are illustrated with studies of membrane fusion utilizing simulations and self-consistent field theory.

Contents

*mmueller@theorie.physik.uni-goettingen.de
†katsov@mrl.ucsb.edu
‡schick@phys.washington.edu

1. Introduction

The incredible complexity of biological systems combined with their immediate importance makes them the most recent subject for the application of the coarse-grained models of soft condensed matter physics [1, 2, 3]. While developed earlier for the elucidation of the statics and dynamics of melts and solutions of very long and uniform polymers [4, 5, 6, 7, 8, 9, 10, 11], coarse-grained models seem particularly well suited to the study of biological constituents [12, 13, 14, 15, 16, 17], such as the heteropolymers DNA and RNA, as well as relatively short-chain lipids which comprise all biological membranes.

Systems of polymers and of lipids share many common features, and exhibit universal collective phenomena, those which involve many molecules [13]. Examples of such phenomena include thermodynamic phase transitions, e.g., the main chain transition in lipid bilayers from a fluid, liquid crystalline to a gel phase [18, 19], and the lateral phase separation which appears to be implicated in "raft" formation in the plasma membrane [20, 21, 22, 23], as well as thermally activated processes such as vesicle fusion and fission [24, 25, 26, 27, 28, 29, 30], important in endocytosis and exocytosis, and electroporation [31, 32, 33, 34, 35] used in the micro-encapsulation of drugs and drug-delivery systems[36, 37].

Since collective phenomena involve many molecules and entail large length and time scales – 10-1000 nm and μs-ms, respectively – details of the structure and dynamics on short, atomistic length scales are often irrelevant, and the behavior is dictated by only a small number of key properties, e.g., the amphiphilic nature of the molecule. This imparts a large degree of universality to the collective phenomena. These terms are borrowed from the theory of critical phenomena [38]. However the clear separation in length, time and energy scales assumed by this approach, is often missing in membrane systems. Thus the universality of collective phenomena, or the ability of coarse-grained models to describe collective phenomena, cannot be taken for granted. It is important, therefore, to compare the behavior of different experimental realizations among each other and with the results of coarse-grained models.

In the following we shall highlight some recent developments in this active research area in which many new models and computational techniques are being developed. We do not attempt to provide a comprehensive overview of this rapidly evolving field, but rather try to give an introduction both to the basic concepts involved in creating a coarse-grained model, and to the simulation techniques specific to membranes and interfaces. We shall emphasize the connection to polymer science whenever appropriate. In particular, we will also discuss application of field-theoretic techniques to calculate membrane properties. These techniques employ very similar coarse-grained models as do the particle-based simulation schemes, and they permit the calculation of free energies, and free energy barriers, which are often difficult to obtain in computer simulations. An application of coarse-grained models in the context of computer simulations and field-theoretic techniques is illustrated by the study of membrane fusion, a choice biased by our own research focus on this area.

Many important applications are not covered by this manuscript. Most notably we do not discuss important progress in the study of collective phenomena exhibited by single molecules, as in the folding of a protein [39, 40, 41] or the processes that ensue when a protein is inserted into a membrane [42, 43, 44, 45, 46], or those exhibited by assemblies of a small number of molecules, as in the formation and subsequent function of a channel [47, 48, 49]. In our view, details of the specific molecular architecture are very important for these processes, and they lack the type of universality which undergirds the application of coarse-grained models.

In the next section we place coarse-grained models in the context of atomistic ones that deal with molecular details, and of phenomenological Hamiltonians that do not retain the notion of

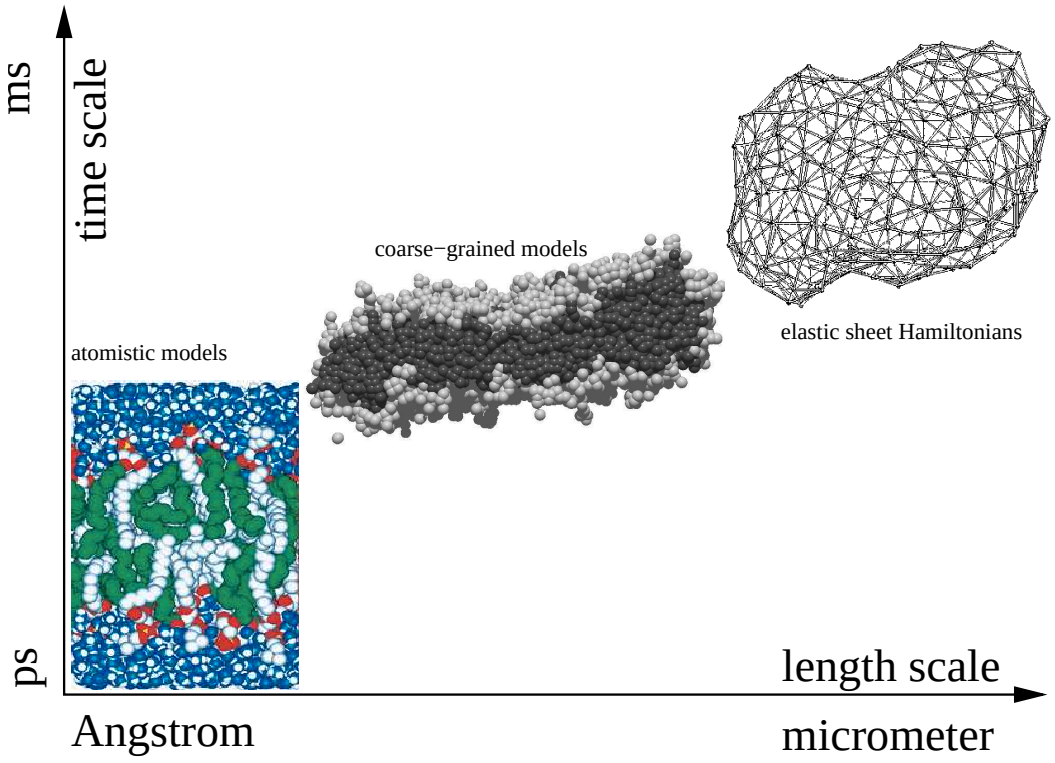

Figure 1. Illustration of different models used to tackle problems in membrane physics. (left) snapshot of an atomistic simulation of a 1-stearoyl- 2-docosahexaenoyl-sn-glycero-3-phosphocholine (SDPC, 18:0/22:6 PC) lipid bilayer from Ref. [50]. (middle) tensionless bilayer of a coarse-grained model from Ref. [51] (right) snapshot of a randomly triangulated surface from Ref. [52].

individual molecules. We then discuss briefly a selection of simulation and self-consistent field techniques utilized for coarse-grained models of membranes. We illustrate the combination of computer simulation and field-theoretic approach with the example of membrane fusion. The paper closes with an outlook on further exciting, and open, questions in this area.

2. Atomistic modeling, coarse-grained models and phenomenological Hamiltonians

Processes in membranes evolve on vastly different scales of time, length and energy. Consequently a variety of membrane models and computational techniques have been devised to investigate specific questions at these different scales. We divide them roughly into atomistic, coarse-grained, and phenomenological models as illustrated in Fig. 1.

2.1. Atomistic molecular dynamics simulations

Atomistic models, which describe bilayer membrane properties with chemical accuracy, have been successfully utilized to investigate the detailed properties of particular membrane systems and lipid-protein complexes. Such models have a longstanding tradition. The first Molecular Dynamics simulation of lipid bilayers, carried out in the early 1990's [53, 54], were able to sim-

ulate only a small patch of a bilayer, one nanometer in extent, over a very short time interval, typically 0.1ns. Since then, much effort has been directed to the improvement of simulation algorithms, (e.g., multiple time step algorithms [55]), and to the implementation of the simulation code on parallel computers. Consequently atomistic simulations have advanced significantly. Today, there are many complete simulation packages that comprise standard routines for Molecular Dynamics simulations. Among them are NAMD Molecular Dynamics Software (NAMD) [56], the Groningen Machine for Chemical Simulation (GROMACS) [57, 58], Groningen Molecular Simulation (GROMOS) [59, 60], MDynaMix [61], Assisted Model Building with Energy Refinement (AMBER) [62], NWChem [63, 64], Integrated Model Program, Applied Chemical Theory (IMPACT) [65], Biochemical and Organic Simulation System (BOSS)/ Monte Carlo for Proteins (MCPRO) [66], DL_POLY [67, 68], Large-scale Atomic/Molecular Massively Parallel Simulator (LAMMPS) [69], and Extensible Simulation Package for Research on Soft Matter Systems (ESPResSo) [70]. The first four packages in this list are tailored to simulate lipid bilayers and proteins in atomistic details, while the latter codes stem from polymer simulations and have also been applied to coarse-grained simulations of soft matter. Most of the program packages (NAMD, GROMACS, DL_POLY, LAMMPS and ESPResSo) are freely available. A nominal fee is charged for the use of GROMOS, while other packages, (e.g., IMPACT), are commercial products. Most of the programs run on parallel computing platforms using the Message Passing Interface (MPI). Differences exist in the way the information is distributed among the processors (e.g., spatial domain decomposition vs. particle decomposition), the force fields that are implemented, and their ease of use and the availability of tutorials. In addition to ensuring that the code is error-free and computational efficient, the developers make efforts to keep it transparent and extendable. Often the data formats allow exchange of information with other software packages, such as high level quantum chemistry packages (QM/MM methods), or visualization software (e.g., Visual Molecular Dynamics (VMD) [71] or PyMol [72]).

In atomistic models the attempt is made to describe faithfully the molecular architecture and the interactions between components. The interactions include those specifically describing a chemical bond (two particle, bond angle potentials and dihedral, torsional, potentials), as well as those between atoms not bonded to one another, such as electrostatic and van der Waals interactions. The quality of the interaction potentials is crucial for a successful description. In lieu of a first-principles calculation, one would like the interactions to fit the results of quantum chemical calculations of small fragments of the molecules. Often parameters are additionally fitted to experimental observations of various quantities. Many sets of potentials have been devised for lipids in an aqueous environment, but there is still a need to refine the interactions and devise more accurate models. The parameters of the interactions can be adjusted to standard force fields, e.g., CHARMM [73], GROMOS96 [74], OPLS-AA [75, 76], or Encad [77]. Often there exists the possibility of including customized, tabulated, potentials.

Atomistic force fields typically include Coulomb interactions. They arise from ionic groups or "partial charges" that account for the ability of atomic species to share charges on a common bond. For very small systems, the long-ranged Coulomb interactions are handled by Ewald summation. Most modern applications, however, employ Particle-Mesh-Ewald techniques [78, 79, 80] which yield a scaling of the order $\mathcal{O}(N \ln N)$, with the number of charges, N, or fast multipole expansions (e.g., IMPACT [65]) which scale linearly with N. ESPResSo [70], however, can additionally deal with Coulomb interactions via a strictly local, field-theoretic, algorithm [81, 82, 83], and provides routines for simulating systems that are periodic in one or two directions.

Typically, atomistic models are studied by Molecular Dynamics simulations [84]. The advantage of this simulation scheme consists in its rather realistic description of the microscopic

dynamics of the constituents. It thereby permits the investigation of kinetic processes, e.g., the transport of small molecules across the bilayer, the lateral self-diffusion of lipid molecules in the bilayer, the tumbling motion of the lipid tails, or the dynamics of the hydrogen-bond network of water at the hydrophilic/hydrophobic interface. The simulation packages often use the time-reversible, symplectic Velocity Verlet or Leapfrog algorithms [85, 86] and allow for multiple time step integration [55].

Most of the atomistic simulation packages also include a limited selection of methods to calculate free energies. The most popular techniques comprise thermodynamic integration and umbrella-sampling methods [87]. Sometimes replica-exchange Monte Carlo, or parallel tempering methods, are employed [88, 89, 90, 91].

In the simplest case, the simulation follows the trajectory of the particles by integrating Newton's equations of motion in time. The time step is set by the shortest period in the system, e.g., that of the stretching mode of a covalent bond. Since the time scale for these bond vibrations is orders of magnitude smaller than the time scale of interest, the bond lengths are often constrained, thus eliminating the smallest periods and allowing for a larger time step of the integrator. Common algorithms that incorporate these constraints into the Molecular Dynamics scheme are SHAKE [92], RATTLE [93], and LINCS [94]. Moreover the simulation packages also allow the possibility of constraining the position of atoms, or distances between constituents, a constraint often applied during the relaxation period.

Newton's equations of motion lead to a microcanonical trajectory. Unfortunately, most numerical integrations do not conserve the energy on long time scales. Therefore one often couples the system to a thermostat, and uses the temperature, T, as a control variable. Analogously, it is often desirable to simulate the system at constant pressure, or more usually, surface tension, using the Berendsen thermostat [95] or the Anderson-Nosé-Hoover algorithm [96, 97, 98, 99]. This allows the volume, or area, to fluctuate. Some programs also permit the geometry of the simulation box to change in order to equilibrate stresses in crystalline phases via the Parrinello-Rahman technique [100]. These simulation methodologies are very similar to what is utilized in coarse-grained simulations.

In addition to interactions between atoms, external forces have also been included in recent simulation schemes. In these "steered Molecular Dynamics simulations" one can mimic, for example, the action of an AFM cantilever on a biopolymer. This allows one to "push" the system over a free energy barrier. If this is repeated often enough, Jarzynski's equation [101, 102, 103, 104, 105] can be used to calculate free energies by integrating the corresponding Boltzmann factor.

While atomistic simulations in the early 1990s could simulate only an extremely small patch of a pure lipid bilayer membrane on the order of a nanometer, [53, 54], current Molecular Dynamics simulations study membrane patches of a few tens of nanometers over time scales of a few tens of nanoseconds. The time scale of observation has increased by two orders of magnitude over the earliest attempts. These simulations provide valuable information about the molecular organization and dynamics of the lipids and of the water, both in the bilayer and at the hydrophobic/hydrophilic interface [106, 107, 108, 109]. For example, recent atomistic simulations revealed the molecular structure of the ripple phase in phosphatidylcholine bilayers [110]. However, calculation of these basic properties (e.g., free energy differences between different morphologies) still pose challenges to computer simulations because of the large time scales which are introduced by the interactions between head groups due to charge pairing or water bridging.

Another important aspect of atomistic simulations is that they are able to correlate the detailed lipid architecture (e.g., particular head group structure, length, and degree of saturation

of the tails) with the physical properties of the bilayer (thickness, orientation of segments, liquid-crystalline ordering, and elastic moduli). Such physical properties can be obtained, for example, by increasing sufficiently the length and time scale of the simulation, so that one can observe the fluctuations of the bilayer membrane. From an analysis of the undulations and peristaltic fluctuations of the local thickness, one obtains the bending rigidity and area compressibility of the membrane, as well as the pertinent relaxation times [111, 112]. For instance, atomistic simulations of monoolein, which is an extremely simple lipid with only one mono-unsaturated tail of eighteen carbon atoms and a very small headgroup consisting solely of two hydroxyls, reveal that fluctuations on the length scale of 20 nm have relaxation times of more than 5 ns. This time scale is expected to be longer in the usual double-tailed phospholipids [112].

The combination of sophisticated simulation codes and powerful parallel computers has permitted atomistic simulations to investigate some collective phenomena in bilayer membranes. The transformation from an inverted cubic phase to an inverted hexagonal phase in the monoolein system has been studied [113]. The transition, as a function of areal density, between liquid-condensed and liquid-expanded phases of a monolayer of DPPC at an air-water interface has been studied, as well as the monolayer's eventual rupture [114]. Recent applications can even cope with the protracted time scales associated with the spontaneous self-assembly of lipids into a bilayer [115], or the formation of small vesicles [116].

Another thrust of applications is the study of membranes that consist of lipid mixtures, or membranes that have molecules adsorbed onto them. The atomistic description provides a detailed view of the role that small inclusions, like cholesterol, or adsorbents, like sugars or polymers, play in modifying the structure of the bilayer. In the following, we give several examples.

The addition of a surfactant [117] or cholesterol [118, 119, 120] to a lipid bilayer tends to increase the ordering of the lipid tails, which causes them to lengthen. Because the liquid-like interior of the bilayer is highly incompressible, this results in a decrease of the area per head group. In the case of high concentrations of cholesterol [119], the decrease of the area per head group is accompanied by an increase of the bending modulus and a decrease in the lateral self-diffusion coefficient of the lipids. The change of the lipid packing also affects the distribution of voids. They become rarer, and those that remain elongate along the bilayer normal as the concentration of cholesterol increases [120]. Addition of salicylate to a lipid bilayer also decreases the area per head group. However in this case, the mechanical properties of the bilayer are hardly affected [121]. The effect of halothane, an anesthetic, is quite different. This small molecule preferentially segregates to the upper part of the lipid acyl chains, increases the area per head group, and decreases the lipid chain order [122].

Large sugar molecules do not penetrate into the hydrophobic interior of the bilayer, but do impact the hydrogen bonding at the interface between the head groups and the water. An interesting example is provided by trehalose, a disaccharide, which is found in animals capable of enduring cold temperatures or dry environments. Experiments indicate that it prevents leakage and fusion during drying and freeze-drying, a property which has been exploited for practical applications [123, 124]. Atomistic simulations [125, 126, 127, 128, 129, 130] show that the area per head group remains unaffected. In addition, the total number of hydrogen bonds of the lipid heads is conserved. However, hydrogen bonds with trehalose now replace some of the bonds which had been made with water. A single trehalose molecule can interact with multiple lipids simultaneously. This result suggests that, at sufficiently high concentrations, disaccharides might serve as an effective replacement for water.

The largest-scale simulations carried out on the atomistic level are able to study lipid-protein, or lipid-DNA, interactions [131], and to investigate channels [47, 132] through a bilayer lipid

membrane. The added complexity brought about by incorporating proteins into the membrane poses huge challenges to both the simulation techniques and computational requirements due to the large number of additional interactions which have to be accurately described. Some examples of the systems studied are as follows.

A protein's conformations when it is inserted into the membrane, and the distortion of the lipid bilayer in its vicinity, can be studied by atomistic simulation. The protein's interactions with the lipids are both strong, compared to the thermal energy scale, k_BT, and specific. They are difficult to simplify, with the result that the details of the complex architecture on the molecular level have to be considered for a quantitative description. Proteins can create interactions within the bilayer due to the strain field generated by a mismatch of its hydrophobic region with that of the bilayer in which it is embedded. Large molecules like DNA [131] and proteins [47, 132, 133] also give rise to significant interactions outside of the bilayer.

Often proteins are not isolated in the lipid membrane, but aggregate to structures such as pores, or ion channels [46, 47, 48]. The detailed structure of these channels has attracted great interest in understanding how they function to let some ions pass while stopping others. It has been possible to study the permeation of water through an acquaporin pore [47, 132]. These simulations reveal the motion of a single water molecule as it passes through the channel. The trajectories provide insights into the specificity mechanism by which the channel allows water, but not ions, to pass. Recently, the permeability for water and ions of the α-hemolysin/lipid bilayer complex has been studied by large-scale computer simulations involving 300 000 atoms [133]. The application of external electrical fields permitted the ion permeability to be obtained as a function of bias voltage, and the selectivity of α-hemolysin to chlorine ions to be elucidated.

The bilayer structure in almost all of these atomistic simulations has to be pre-assembled because the time scale of self-assembly from a homogeneous mixture of lipids and water typically far exceeds the simulation time scale. (For an exception, see Ref. [115].) This leaves unanswered the question of the thermodynamic stability of the pre-assembled membrane. Even though the atomistic potentials are parameterized from the interaction of atoms, the manner in which these potentials determine the global stability of the different lipid morphologies is subtle, and unknown. Furthermore, the transitions between these lipid morphologies, and the formation of out-of-plane structures as occurs in budding, are beyond the scope of atomistic modeling.

2.2. Coarse-grained models

2.2.1. Why are coarse-grained models useful?

While atomistic simulations provide valuable, detailed, information about the local structural properties of lipid membranes, they cannot access the time and length scales involved in collective membrane phenomena, which are milliseconds and micrometers respectively. One strategy to overcome this difficulty is to eliminate some of the detail by coarse-graining the description. Coarse-grained models do not attempt to describe the large scale phenomena by starting from the smallest atomic length scale, but rather by lumping a small number of atoms into an effective particle [12, 14, 15, 134, 135, 136, 137, 138, 139, 140, 141, 142, 143, 144]. These particles then interact via coarse-grained, simplified, interactions, ones which typically do not include electrostatic and torsional potentials, for example. The reduced number of degrees of freedom, and the softer interactions on the coarsened scale lead to a significant computational speed-up with the consequence that larger systems and longer time scales are accessible. This makes possible the study of collective phenomena in membranes, a study not possible via ab-initio methods now, or in the foreseeable future. However the loss of chemical detail limits some of the predictive power of coarse-grained models.

The objectives of mesoscopic modeling are twofold: on the one hand, to help to identify those

interactions which are necessary to bring about collective phenomena on a mesoscopic scale, such as self-assembly, and on the other to elucidate the universal behavior on the mesoscopic scale itself. These include the role of thermal fluctuations, or the existence of phase transitions between self-assembled morphologies. Mesoscopic models are also an ideal testing ground for phenomenological concepts.

The obvious question which presents itself is how the coarse-graining is to be achieved. What are the relevant degrees of freedom and interactions to be retained at the coarse-grained scale in order to incorporate the essential physics of the system? This is a fundamental question of *any* model-building procedure which must be addressed when one abandons ab-initio calculations.

One can respond that, due to the experimentally observed universality of self-assembled structures, any coarse-grained model that includes the relevant interactions will capture the qualitative features. Consequently one should use the simplest possible model in order to take maximum advantage of the computational benefits of coarse-graining. This is the strategy of minimal models which were the first to study self-assembly. They are still very popular. The question that remains is just what are the "relevant" interactions necessary to bring about the collective phenomena observed in experimental systems. Within the framework of minimal models, one can start with a simple model and successively augment it with additional interactions until the phenomenon of interest is captured. While this method appears to be rather crude, it does provide insight into which interactions, on the length scales of a few atomic units, are necessary to bring about collective behavior in membranes. It also contributes to identifying those mechanisms that underly the phenomena and the degree of universality. Alternatively one can try to "derive" coarse-grained models from a specific atomistic system, a procedure which is termed "systematic coarse-graining". We shall discuss both techniques in turn.

2.2.2. Minimal models

The idea of successively eliminating degrees of freedom from a specific mixture of lipid and water to "derive" a coarse-grained model is a beautiful and potentially powerful concept. This concept of coarse-grained models has a long-standing tradition in polymer physics [4], and during the last three years much progress has been made in the area of biological and synthetic membranes. Unfortunately, the coarse-graining procedure is often impractical to implement explicitly. Notable exceptions are dilute and semi-dilute polymer solutions for which the concept of coarse-graining can be formulated in terms of a consistent theory, one which has been extensively exploited [5, 6, 7].

The configurations of long, flexible, linear polymers in dilute or semi-dilute solutions are characterized by a self-similar, fractal structure. This self-similarity extends from the structure of a few monomeric repeat units to the size of the entire molecule, which is comprised of hundreds or thousands of monomers. For long chain molecules, there is a clear separation between the structure on the length scale of a monomeric unit, which strongly depends on the chemical structure and details of the interactions on the atomic scale, and the mesoscopic structure of the entire molecule. Clearly the chain dimensions depend on the chemical identity of the monomeric units in a very subtle manner, but for the description of the large scale properties a single, coarse-grained, parameter, the end-to-end distance, suffices. The background of this statement is the observation of de Gennes, in 1972, that the behavior of a long, self-avoiding, walk is intimately related to the properties of a critical point in a n-component field theory in the limit $n \to 0$ [145]. This opened the way for the use of the machinery of the Renormalization Group for the description of polymer solutions, and placed the heuristic observation of the universality of the behavior of long chain molecules within a rigorous theoretical framework. The inverse chain length plays the role of the distance to the critical point. The behavior at the critical

point is universal, i.e., it does not depend on the microscopic interactions but only on a few, relevant, features that characterize a universality class. For polymer solutions the relevant properties are the connectivity of the monomeric units along the backbone and the excluded volume interaction between monomeric units. By virtue of universality, any model characterized by these two properties will capture the behavior of polymer solutions in the limit of long chain lengths. The theory has provided detailed insights into the large scale chain conformations in dilute and semi-dilute solutions, and has been utilized to describe quantitatively the screening of the excluded volume interactions, and the cross-over from dilute to semi-dilute solutions [5, 6, 7].

Biological systems do not exhibit the sort of scale invariance that lies at the heart of the Renormalization Group approach to polymer systems. In particular, there is no parameter, like the chain length, that tunes the separation between the microscopic scale of the atomic interactions and the mesoscopic structure. Another practical complication is that, in contrast to polymer systems in which one considers systems of very few components and with simple interactions between them, biological systems are composed of many different, complex, structural units which are connected by means of several different interactions. As a consequence, the development of coarse-grained models for membranes is more an art than a science. It is often guided by physical intuition, computational constraints, and a large degree of trial-and-error. The underlying assumption is that, just as in polymer solutions, the qualitative behavior of the membrane depends only on a few coarse-grained parameters that characterize the relevant interactions of the mesoscopic model. This assumption is not justified by a rigorous formal theory. Consequently it is *a priori* unknown what the relevant interactions are that have to be incorporated in order for a coarse-grained model to faithfully capture the behavior on mesoscopic length scales. The answer to this crucial question depends on the specific system, and on the properties in which one is interested. For example, the experimental fact that systems which differ chemically a great deal, such as biologically relevant lipids in aqueous solution and amphiphilic water-soluble polymers, do exhibit a great number of common morphologies implies that the existence of these morphologies can be traced back to a small number of simple interactions.

A key ingredient is the connectivity of two strongly repelling entities within a single molecule. Since these two parts are joined together they cannot separate and form macroscopic domains, but organize instead into supermolecular structures so as to minimize the unfavorable contacts between their parts. The particular physical mechanisms that cause the repulsion between the two entities appear to be less important.

Another significant experimental observation is the correlation that exists between the gross amphiphilic architecture of the components of the system and the system's phase behavior. Not only does the size of the molecule set the scale of the self-assembled structures, such as the bilayer thickness, but also its "architecture", the relative volumes of the two antagonistic molecular parts, can be directly correlated with the various morphologies. This correlation has been stressed by Israelachvili [146, 147]. Lipids in which the head and tail groups are of similar volumes tend to form bilayers. If the lipid tails volume is enlarged or the headgroup reduced (e.g. by replacing a phosphatidylcholine with a phosphatidylethanolamine) then the lipids are said to be "cone-shaped" and they tend to form inverted hexagonal phases. In this phase, the lipids assemble into tubes with the heads directed inward and the tails outward, and the tubes form a periodic hexagonal lattice. This concept also carries over to AB diblock copolymers which consist of two blocks composed of N_A and N_B, monomeric units. In this case, the fraction, $f \equiv N_A/(N_A + N_B)$, of one block is employed to parameterize the molecular architecture, and it also correlates with the observed phase behavior. From these observations, one can conclude that it is crucial to conserve the basic geometry of the molecules during the mapping onto a

coarse-grained model.

Notwithstanding these important universal aspects, the details of the molecular architecture, interactions and the mechanisms of self-assembly, do vary from system to system. In block copolymers, for example, the geometrical conformations of polymers strongly fluctuate and, therefore, the average geometrical shape of a diblock copolymer is strongly affected by its environment. The balance between the repulsive interaction energy of the two components and the conformational entropy that describes the change of available molecular conformations dictates the self-assembled morphology. In lipid systems, however, the molecules are short and rigid. The reduced number of molecular conformations severely limits their ability to alter their average geometric shape to adapt to the environment. Thus, the concept of packing rigid, wedge-shaped, objects is useful, i.e. the "shape" of the molecules does not depend significantly on the environment. A mismatch between the molecular geometry and packing constraints cannot be completely accommodated by changes of molecular orientation, so that this mismatch also alters the local fluid-like packing. It is this interplay between universal and specific aspects that make the development of coarse-grained models in biological systems a challenging one.

The amphiphilic nature of the molecules and the important molecular geometry are characteristic of self-assembling systems. These two relevant properties must be captured by a coarse-grained model. They differ in detail as to how these properties are incorporated, and they have been augmented by additional interactions to provide a more detailed description of specific systems.

One of the simplest self-assembling system is that of oil and water and amphiphile, and many simple lattice models were introduced to study it [134, 148, 149]. Larson was one of the first to ask how some of the simplest specific features of the amphiphile, such as the presence of a multi-atom hydrophobic tail and the relative volume of head and tail units, would affect the phase structure. While water and oil were represented by a single site on a lattice, amphiphiles were modeled as a linear string of nearest or next-nearest sites. Interactions between hydrophilic units, water or lipid heads, and hydrophobic units, oil or lipid tails, were described by square-well potentials that extended over the nearest and next-nearest neighbors. Like units attracted each other while unlike units repelled each other. Monte Carlo simulations of this model yielded information about possible phase diagrams of ternary water, oil, and amphiphile solutions [134, 150, 151]. This simple lattice model was even able to reproduce the complex gyroid morphology that has been observed both in amphiphile solutions and block copolymers. Not surprisingly the Larson model shares many features with simple lattice models that have been utilized to study the universal characteristics of polymer solutions and melts. In the latter context, simple lattice models have been employed to problems ranging from the scaling properties of isolated chains in good solvent [152], the equation of state of solutions and mixtures [153, 154], to the ordering of diblock copolymers [155, 156].

To study further how microscopic details affect macroscopic behavior, one must flesh out these schematic models by various structural details. Unfortunately, it is difficult to capture details of the geometric shape of the amphiphiles in simple lattice models. The restricted number of angles between bonds that connect neighboring amphiphilic units makes very difficult a realistic description of the rather stiff tails. Further, in lattice models, the head and tail segments invariably occupy identical volumes. Some of these difficulties can be overcome by complex lattice models, such as in the bond fluctuation model of Carmesin and Kremer [138, 157, 158]. In this model, each segment occupies the eight corners of a unit cell of a simple cubic lattice. Monomers along the amphiphile are connected by one of 108 bond vectors that are allowed to take lengths, $2, \sqrt{5}, \sqrt{6}, 3$ or $\sqrt{10}$ in units of the lattice spacing. This set of bond vectors is chosen such that the excluded volume constraint guarantees that bonds do not cross in the course of

local random monomer displacements by one unit in one of the lattice axis. Thus, effects due to entanglements are captured. The large number of bond vectors and the extended shape of the monomers yields a rather good description of continuum space. For instance, the eighty-seven different bond angles permit a rather realistic description of stiffness. Artifacts due to lattice discretization are strongly reduced, yet the computational advantages of a lattice model (e.g., early rejection of trial moves) are retained [155, 156]. Moreover, sophisticated Monte Carlo simulation techniques have been implemented for lattice models that allow for a very efficient relaxation of the molecular conformations and the calculation of free energies. The model can be quantitatively mapped onto the standard Gaussian chain model that is used in self-consistent field (SCF) calculations (cf. Sec. 2.3). This allows for a computationally efficient way to explore a wide parameter range as well as to calculate corresponding free energies. Amphiphiles have been modeled as flexible chains consisting of a hydrophilic and a hydrophobic block. The solvent can be described by a homopolymer chain that consists of hydrophilic segments. Like segments attract each other via a square well potential that extends over the nearest fifty-four lattice sites, while hydrophilic and hydrophobic segments within this range of interaction repel each other. The strength of the interaction between the segments controls the free energy of the hydrophilic/hydrophobic interface, where as the relative length of the hydrophilic block, f, tunes the spontaneous curvature of a monolayer. The model has been successfully employed to study self-assembly in diblock copolymers and their mixtures with homopolymers [159], and pore formation of bilayers under tension [160]. The bending rigidity of a monolayer and tension of a bilayer have been measured via the spectrum of interface fluctuations and bilayer undulations [159, 160], and the fusion of membranes has also been studied [161, 51] within this framework.

Although this lattice model includes only the bare essentials necessary to bring about self-assembly, it is sufficient to describe its universal properties. A mapping of length scale between lattice model and experimental realizations can be established by comparing an experimental bilayer thickness in nanometers with the bilayer thickness of the model expressed in lattice constants. Similarly the model's energy scale can be deduced by comparing the experimental and calculated free energy of the hydrophilic/hydrophobic interface. Additional characteristics, such as the bending rigidity, or the area compressibility modulus, then can be combined in dimensionless ratios. A comparison of such dimensionless ratios between liposomes, polymersomes, and the bond fluctuation model is presented in Table 1. One observes that these mesoscopic characteristics do not strongly differ between membranes formed by long amphiphilic diblock copolymers and biological lipids in aqueous solution and that the lattice model is able to reproduce the order of magnitude estimate of these properties. Therefore, this table quantifies the universality of amphiphilic systems and justifies the use of highly simplified models [13].

An alternative procedure to include molecular detail is to use off-lattice models. Clearly these models allow for much flexibility in describing the molecular geometry and they can be studied by Molecular Dynamics. A generic off-lattice model has been utilized by Smit and co-workers [168] to elucidate micelle formation. Water and oil molecules are modeled by Lennard-Jones particles while the amphiphile is represented by a collection of particles bonded together via harmonic springs. The hydrophobic beads form a linear chain tail, while the hydrophilic head beads are all bonded to a single, central bead which, in turn, is attached to the tail. This mimics the bulkiness of the lipid head.

Goetz and Lipowsky [136] employed a model in which the amphiphiles are comprised of a single head bead and four tail segments. Water is modeled by a single bead. The interactions between the like beads (head-head, water-water, head-water and tail-tail) are of Lennard-Jones type with a cut-off at $r_c = 2.5\sigma$. The energy, ϵ, and range, σ, of the Lennard-Jones potential set the scales. The hydrophobic interaction between water and tail or head and tail is a purely

	polymersomes	liposomes	bond fluctuation model
d_c	80Å	30Å(DOPE$^{(a)}$), 25Å(DOPC$^{(b)}$)	21u
f	0.39	0.35 ± 0.10	0.34375
$C_0 d_c$	no data	-1.1 (DOPE$^{(d)}$), -0.29 (DOPC$^{(c)}$)	-0.68
$\Delta A/A_0$	0.19	0.05	0.19
$\kappa_a/\gamma_{\rm int}$	2.4	4.4 (DOPE$^{(b)}$), 2.9 (DOPC$^{(b)}$)	4.1
$\kappa_b/\gamma_{\rm int} d_c^2$	0.044	0.10 (DOPE$^{(c)}$), 0.12 (DOPC$^{(d)}$)	0.048

Table 1
Structural and elastic properties of bilayer membranes formed by amphiphilic diblock copolymers, biological lipids and a coarse-grained lattice model. d_c - thickness of membrane hydrophobic core in the tensionless state, f - hydrophilic fraction, C_0 - monolayer spontaneous curvature, $\Delta A/A_0$ - bilayer area expansion (critical value for the experimental systems, and the actual strain used in simulations), κ_a - bilayer area compressibility modulus, κ_b - monolayer bending modulus, $\gamma_{\rm int}$ - hydrophilic/hydrophobic interface tension (oil/water tension of 50pN/nm for the experimental systems, and A/B homopolymer tension for the simulations). Data on EO7 polymersomes is taken from [162]; and on lipids from (a): [163], (b): [164], (c): [165], and (d): [166] (see also http://aqueous.labs.brocku.ca/lipid/). Values of d_c, C_0 and κ_a for DOPE were obtained by linear extrapolation from the results on DOPE/DOPC(3:1) mixture. Values of κ_b, $\gamma_{\rm int}$, and C_0 for the simulated model were calculated by us using the method of [167]. From Ref. [13].

repulsive soft potential,

$$V_{\rm sc}(r) = 4\epsilon(\sigma_{\rm sc}/r)^9, \tag{1}$$

with $\sigma_{\rm rep} = 1.05\sigma$, that is cut-off at $r_c = 2.5\sigma$. The potentials are truncated and shifted so that both the potential and the force are continuous at the cut-off:

$$V_{\rm trunc}(r) = \begin{cases} V(r) - V(r_c) - \left.\frac{dV}{dr}\right|_{r_c}(r - r_c) & \text{for } r \le r_c \\ 0 & \text{for } r > r_c. \end{cases} \tag{2}$$

Beads along the amphiphile are bonded together via harmonic springs

$$V_{\rm bond}(r) = k_{\rm bond}(|\mathbf{r}| - \sigma)^2. \tag{3}$$

The rather large value $k_{\rm bond}\sigma^2/\epsilon = 5000$ is chosen to constrain the average bond length to a value very close to σ. Additionally a bending potential of the form

$$V_{\rm bend} = k_{\rm bend}(1 - \cos(\theta)), \tag{4}$$

where θ denotes the bond angle, is included. By increasing the bending stiffness $k_{\rm bend} \le 5\epsilon$, one can change the conformations from those typical of a very flexible molecule to those characteristic of a rigid one.

A further step in the coarse-graining procedure is to eliminate the solvent particles while preserving their effects implicitly. Since the two-dimensional membrane is embedded in a three-dimensional volume filled with solvent, the number of solvent particles increases much faster than the number of amphiphiles as one studies ever larger systems sizes. Yet the role of the solvent often is only to stabilize the bilayer membrane whose properties are the focus of attention.

Therefore, if the solvent could be eliminated, it would result in a huge computational speed-up. Typically, one can assume that the amphiphile-solvent mixture is incompressible on a coarse scale. Then the system configuration is completely described by the configuration of the amphiphiles, and the interaction between solvent and amphiphiles can be integrated out giving rise to an effective interaction between the amphiphilic units.

The resultant *implicit* solvent models have enjoyed long-standing popularity in polymer physics where the behavior of polymers in solvents of different qualities often is described by polymers in vacuum with effective interactions between the monomeric units. Attractive interactions correspond to a bad solvent and result in a collapse of the polymer, while repulsive interactions correspond to a good solvent because the isolated polymer adopts a swollen, self-avoiding-walk like shape [6, 169]. While there exists a formal one-to-one correspondence between the thermodynamic properties of an incompressible polymer-solvent mixture and the corresponding compressible polymer model with effective interactions, these effective interactions might not be well represented by *density-independent pair potentials*. For instance, by replacing the repulsion between solvent and polymer by an effective attraction between the polymer segments, one might observe a much higher local polymer density than in the original incompressible mixture where the maximal value of the local polymer density is limited by the incompressibility constraint. The differences between incompressible mixtures and effective compressible systems comprised of only amphiphiles are even more pronounced when one regards dynamical properties because (i) the density variations in the implicit solvent model results in variations in the local mobility of the amphiphilic units that are absent in the original incompressible system and (ii) the solvent carries momentum, and the concomitant hydrodynamic flow might promote cooperative re-arrangements. These considerations illustrate that integrating out the solvent degrees of freedom, though conceptually straightforward, does involve some practical subtleties.

Initial attempts to construct solvent-free membrane models using simple pairwise interactions were rather unsuccessful. The model of Drouffe et al. [170] represented amphiphiles by single beads interacting via a spherical hard-core repulsion and an orientation-dependent short-ranged attraction. They found that increasing the attraction between the lipid tails resulted in the formation of membranes. These membranes consisted of a *single* layer of particles and the membranes were crystalline (gel), i.e. the lipids laterally condensed onto a triangular lattice. This solid phase was characterized by the pronounced reduction of lateral lipid diffusion. When the temperature was raised the membrane did not form a fluid membrane, but simply disassembled. To overcome this difficulty, a many-body interaction was introduced to mimic the hydrophobic effect and to stabilize a fluid membrane. Additionally these interactions limited the number of neighbors and thereby suppressed three-dimensional aggregation in favor of sheet-like structures. These multi-body, or density-dependent, interactions made the calculation of thermodynamic quantities rather subtle (see below).

Noguchi and Takasu [171] modeled the amphiphiles by rigid rods comprised of three interaction centers, a head and two tail beads. These beads interact via a rotationally symmetric potential but the multi-body character of the attraction of the hydrophobic tail beads is used to stabilize the membrane. Particles repel each other via a soft core potential which defines the energy scale, ϵ, and the monomeric length scale, σ. The potential is of the form

$$V_{\rm rep}(r) = \epsilon e^{-20(r/\sigma-1)}, \tag{5}$$

and it is truncated and shifted at a cut-off 1.3σ. The multi-body potential takes the form

$$V_{\rm multi}[\bar{\rho}] = \begin{cases} -0.5\bar{\rho} & \text{for } \bar{\rho} < \rho^* - 1 \\ 0.25(\bar{\rho} - \rho^*)^2 - c & \text{for } \rho^* - 1 \le \bar{\rho} < \rho^* \\ -c & \text{for } \bar{\rho}^* \le \rho \end{cases} \tag{6}$$

with parameters $\rho^* = 10$ and $c = 4.75$ for the tail bead nearest to the head and $\rho^* = 14$ and $c = 6.75$ for the tail bead at the end. The smoothed density, $\bar{\rho}$, quantifies the local number of hydrophobic particles in a small sphere around the reference particle at position, $\mathbf{r}$, according to

$$\bar{\rho} = \sum_{\mathbf{r}'} h(|\mathbf{r} - \mathbf{r}'|) \qquad \text{with} \qquad h(r) = \begin{cases} 1 & \text{for } r < 1.6\sigma, \\ \frac{1}{\exp[20(r/\sigma - 1.9)]+1} & \text{for } 1.6\sigma \le r < 2.2\sigma, \\ 0 & \text{for } 2.2\sigma \le r. \end{cases} \tag{7}$$

where the sum over $\mathbf{r}'$ includes all hydrophobic segments on other amphiphiles. At small smoothed densities, $\bar{\rho} < \rho^* - 1$, the multi-body potential is linear in the density and, thus, represents a pairwise attraction between neighboring hydrophobic beads on different molecules. At higher densities, the attractive strength levels off and adopts a constant value independent of the local density. This feature avoids the collapse of the hydrophobic tails into extremely dense structures and thus prevents crystallization. In contrast to the previous model of Drouffe and co-workers [170] the membranes in Noguchi's model are bilayer, i.e., they are comprised to two layers of amphiphilic molecules.

Wang and Frenkel [172] described another variant of solvent-free models with multi-body interactions, where amphiphiles were modeled as flexible chains consisting of three coarse-grained beads. A bending potential along the backbone was utilized to tune the molecular flexibility. They employed a qualitatively similar density dependence of the multi-body term, but used an anisotropic weighting function to construct the smoothed density, $\bar{\rho}$.

The first solvent-free model that resulted in the formation of a fluid bilayer from particles that interact via simple pairwise isotropic interactions was devised by Farago [173]. In this model, amphiphiles consist of rigid, linear trimers comprising one head-bead and two tail-beads. The interactions were tuned by a rather lengthy "trial and error" process to make the attraction between molecules sufficiently strong to support the stability of the membrane, but still weak enough so that the membrane would not crystallize. They are as follows. Let (1) denote the hydrophilic head bead and (2) and (3) the hydrophobic beads along the rigid amphiphile that are spaced at a distance, σ. Beads of the same type interact via a Lennard-Jones potential

$$V_{ii}(r) = 4\epsilon_{ii}\left[\left(\frac{\sigma_{ii}}{r}\right)^{12} - \left(\frac{\sigma_{ii}}{r}\right)^{6}\right]. \tag{8}$$

Interactions between the head and the first hydrophobic bead are repulsive

$$V_{12}(r) = 4\epsilon_{12}\left(\frac{\sigma_{12}}{r}\right)^{12}, \tag{9}$$

and the repulsion between the head and the end tail bead is even harsher

$$V_{13}(r) = 4\epsilon_{13}\left(\frac{\sigma_{13}}{r}\right)^{18}. \tag{10}$$

The attraction between different hydrophobic beads, however, has a broad attractive minimum

$$V_{23}(r) = 4\epsilon_{23}\left[\left(\frac{\sigma_{23}}{r}\right)^{2} - \frac{\sigma_{23}}{r}\right]. \tag{11}$$

All potentials are truncated and shifted at a cut-off distance $2.5\sigma_{33}$. The potential parameters are detailed in Table 2.

Deserno and co-workers [174, 175] argued that an increase of the range of the interaction is crucial for stabilizing fluid bilayers. They represented amphiphiles as flexible trimers. All

σ_{ij}/σ_{33}	head (1)	tail (2)	tail (3)	ϵ_{ij}/k_BT	1	2	3
1	1.1	1.15	1.4		0.1875	1.1375	200
2		1.05	0.525			1.75	375
3			1				1.875

Table 2
Parameters of the interaction potentials in Equations (8)-(11) of Farago's solvent-free model. From Ref. [173].

beads repel each other via a Lennard-Jones potential of the type of Eq. (8) which is truncated and shifted at the minimum, $r_{\min} = \sqrt[6]{2}\sigma_{ii}$, resulting in a purely repulsive potential. The size of the tails defines the length scale, $\sigma_{33} = \sigma_{22}$ while the heads are smaller, $\sigma_{11} = 0.95\sigma_{33}$ and the repulsive interactions between head and tails are non-additive, $\sigma_{12} = \sigma_{13} = 0.95\sigma_{33}$. In addition to this purely repulsive interaction, hydrophobic tail beads interact with each other via an attraction with tunable range, w_c (see inset of Fig. 2):

$$V_{\rm att}(r) = \begin{cases} -\epsilon & \text{for } r < r_{\min}, \\ -\epsilon \cos^2\left(\frac{\pi(r-r_{\min})}{2w_c}\right) & \text{for } r_{\min} \le r < r_{\min} + w_c, \\ 0 & \text{for } r_{\min} + w_c < r. \end{cases} \tag{12}$$

The beads are linked together via a FENE potential

$$V_{\rm bond} = -\frac{1}{2} k_{\rm bond} r_0^2 \ln\left[1 - \left(\frac{r}{r_0}\right)^2\right], \tag{13}$$

with $k_{\rm bond} = 30\epsilon/\sigma_{33}^2$ and maximal bond length, $r_0 = 1.5\sigma_{33}$. There is no bond angle potential, but the flexibility is tuned by applying a harmonic spring between the head and the last tail bead

$$V_{\rm bend}(r_{13}) = \frac{1}{2} k_{\rm bend} \left(r_{13} - 4\sigma_{33}\right)^2. \tag{14}$$

with $k_{\rm bend} = 10\epsilon/\sigma_{33}^2$.

Figure 2 presents the phase diagram at zero lateral tension as a function of rescaled temperature and the range of the attractive interaction, w_c. If the range of the attraction, w_c, is small compared to the effective hard core diameter, σ_{33}, the membrane assembles into a solid sheet upon cooling. Only if the range of the attraction is sufficiently large does one encounter two transitions upon cooling. As the system is cooled, the amphiphiles first assemble into a fluid membrane. Upon further cooling, the membrane crystallizes. In this solid phase the lateral mobility of the amphiphiles is strongly reduced. The temperature interval in which the fluid membrane is stable increases with the range of the attraction and extends to higher temperatures.

The role of the range of the attractive interactions in stabilizing fluid, self-assembled membranes qualitatively resembles the role it plays in stabilizing a fluid phase of simple molecules. If such molecules interact via a hard-core repulsion and a weak, but longer-ranged, attraction a fluid phase exists only if the range of the attraction is sufficiently large, roughly greater than 20% of the hard core diameter. Otherwise the fluid directly condenses into a solid [176, 177, 178].

Another solvent-free model has been devised by Brannigan and co-workers [179, 180, 181, 182, 183]. The amphiphiles consist of five beads. The first bead (h) corresponds to the hydrophilic head, the second bead (i) is associated with the interface between hydrophilic and hydrophobic

entities, and the other three beads constitute the hydrophobic tail (t). The distance between neighboring beads along the amphiphile are constrained to a distance σ, which defines the length scale. A bending potential of the form $V_{\rm bend}(\theta) = k_{\rm bend}\cos\theta$, with $5\epsilon \le k_{\rm bend} \le 10\epsilon$, tunes the geometrical shape of the molecules. A repulsive interaction

$$V_{\rm rep}(r) = c_{\rm rep}\left(\frac{\sigma}{r}\right)^{12} \qquad \text{with} \qquad c_{\rm rep} = 0.4\epsilon, \tag{15}$$

is applied between all beads except intramolecular pairs separated by less than three bonds. Tail beads, and a tail and an interface bead, attract each other via a standard van-der-Waals attraction:

$$V_{\rm att}(r) = -\epsilon\left(\frac{\sigma}{r}\right)^{6}. \tag{16}$$

Both, repulsion and attraction, are truncated at a distance, 2σ. The interface beads, however, interact among each other via a longer-ranged potential

$$V_{\rm int}(r) = -c_{\rm int}\left(\frac{\sigma}{r}\right)^{2} \qquad \text{with} \qquad c_{\rm int} = 3\epsilon, \tag{17}$$

which is cut off at 3σ. This longer-ranged attraction, which acts only between the interface beads, is sufficient to stabilize fluid bilayer membranes at reduced temperature, $k_BT/\epsilon = 0.9$.

A different path to the development of generic coarse-grained models has been pursued by Groot [184, 185], Smit [186, 187, 188, 189, 190, 191], Shillcock [142, 192, 193, 194] and Mouritsen [195, 196] with their co-workers. These coarse-grained models utilize ultra-soft interactions in conjunction with a dissipative particle dynamics (DPD) thermostat [197, 198, 199, 200, 201]. Unlike the Langevin thermostat that adds random noise and friction to each particle, the DPD thermostat adds random noise and friction to each neighboring pair of particles. Thus, momentum is locally conserved and hydrodynamic flow can be described. The use of ultra-soft potentials allows for rather large time steps for integrating the equation of motions (see Refs. [202, 203, 196, 204] for a detailed discussion). Their use can be justified by recognizing that the center of mass positions of the group of atoms that constitute a coarse-grained segment can overlap and their interaction is much softer than the harsh repulsions on the atomistic scale (cf. Sec. 2.2.3). This is a generic feature of coarse-grained models: the larger the length scale the weaker the interactions. By the same token, the density of the soft beads exceeds unity when measured in units of the particles' interaction radius.

In DPD simulations, particles of type i and j (denoting water (w), head (h), glycerol-linking (e) and tail (t)) interact via a very simplistic soft force of the form:

$$\mathbf{F}_{ij}(\mathbf{r}) = \begin{cases} -a_{ij}\left(1-\frac{|\mathbf{r}|}{r_c}\right)\frac{\mathbf{r}}{|\mathbf{r}|} & \text{for } r \le r_c \\ 0 & \text{for } r > r_c \end{cases} \tag{18}$$

where $\mathbf{r}$ is the distance vector between the particles' positions. The range of the interactions, r_c, between these soft beads sets the length scale.

Originally, the DPD simulation scheme had been devised to simulate fluid flow, and a soft bead was thought of as a fluid volume comprising many molecules but still being macroscopically small. In the context of membrane simulations, a soft bead represents a rather small fluid volume that consists only of several molecular groups comprising the amphiphile. Often one identifies the range of interaction, r_c, with 1 nm, i.e., one tail bead corresponds to three or four methyl units.

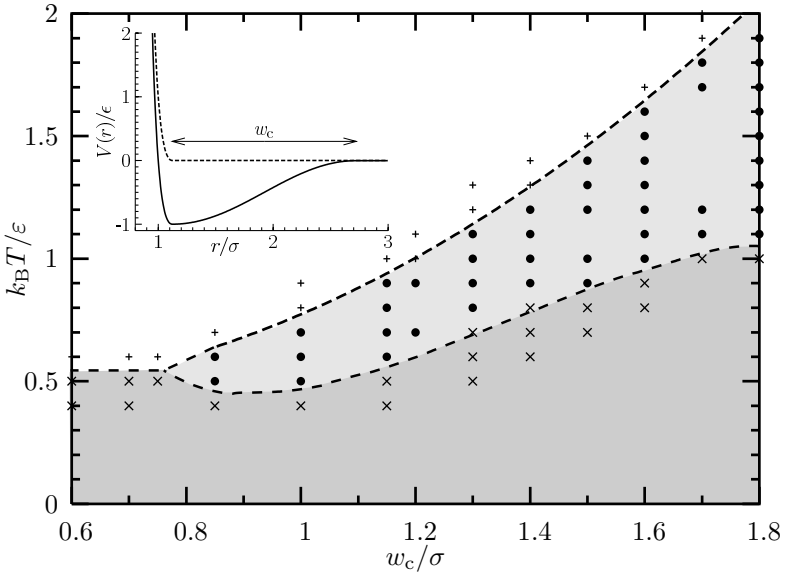

Figure 2. Phase diagram resulting from Deserno's model as a function of rescaled temperature, k_BT/ϵ and range, w_c/σ_{33} of the attraction between tail beads according to Eq. (12). The areal density corresponds to zero tension. Each symbol corresponds to one simulation and identifies different bilayer phases: × – gel/crystalline, • – fluid, + – unstable. Lines are merely guides to the eye. The inset shows the pair-potential between tail lipids (solid line) and the purely repulsive head-head and head-tail interaction (dashed line). From Ref. [174].

By the same token, a solvent bead corresponds to a small number of water molecules. (Attempts to map a single methyl unit onto a soft bead were rather unsuccessful [188] in reproducing the internal bilayer structure and resulted in a significant interdigitation of the apposed monolayers.) Typically the amphiphilic molecules consist of only a very small number of beads – one to three hydrophilic head beads and four to ten hydrophobic tail beads. The longer the amphiphiles the more stable and rigid the bilayer is.

The strength of the interaction simultaneously describes the repulsion between unlike species, and the excluded volume of the coarse-grained beads which imparts a small compressibility to the liquid. The parameters of the model are tailored to reproduce key characteristics of the amphiphiles in solution (e.g., the compressibility of the solvent and the bilayer compressibility).

A typical set of interaction strength is:

a_{ij}/k_BT	w	t	h
w	15(25)	80	15
t	80	25	80
h	15	80	35

(19)

These values were originally proposed by Groot to parameterize the interactions of ionic surfactants [185]. Smit and co-workers [188] increased a_{ww} from 15 to 25 to avoid very high densities in the bilayer's hydrophobic core. Different sets of parameters have been devised for double-tail lipids. Shillcock and Lipowsky [142] used the set

a_{ij}/k_BT	w	t	h
w	25	75	35
t	75	25	50
h	35	50	25

(20)

Interactions along the amphiphile determine the molecular shape of the amphiphile. They include a harmonic bonding potential of the form [185]

$$V_{\rm bond}(r) = k_{\rm bond}\mathbf{r}^2, \tag{21}$$

or [186]

$$V_{\rm bond}(r) = k_{\rm bond}(|\mathbf{r}| - r_0)^2. \tag{22}$$

Additionally, bending potentials of the form [186]

$$V_{\rm bend} = \frac{1}{2}k_{\rm bend}(\theta - \theta_0)^2, \tag{23}$$

or [142]

$$V_{\rm bend} = k_{\rm bend}(1 - \cos(\theta - \theta_0)), \tag{24}$$

have been applied. Shillcock and Lipowsky [142] highlight the role of the bending potential on the internal structure of the bilayer membrane. The earlier DPD model by Groot [185], and also self-consistent field models [205], describe the lipid tails as completely flexible which leads to a broad distribution of the tail ends throughout the bilayer. This interdigitation of the two apposing monolayers that form the membrane typically is not observed in biological membranes. A very large incompatibility between hydrophobic and hydrophilic entities would be required to stretch the monolayers sufficiently to reproduce the structure of a biological membrane.

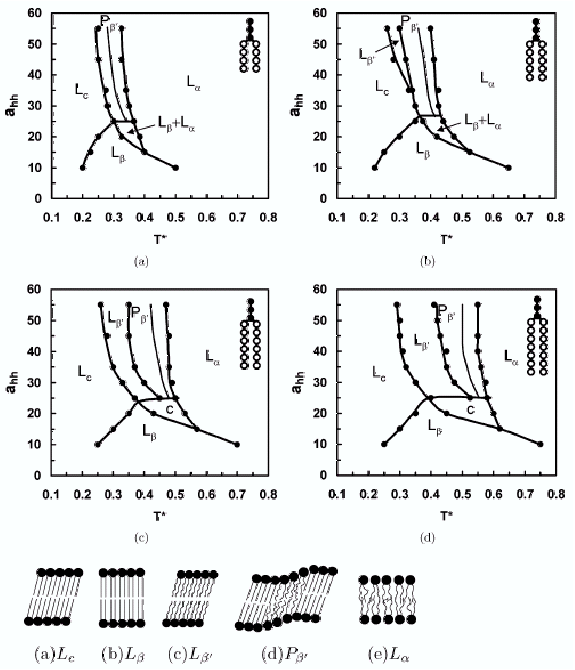

Figure 3. Phase diagrams of model lipids as a function of head-head repulsion, a_{hh}, and temperature, T^* for various lipid architectures as indicated in the key. The different bilayer phases are sketch in the bottom row: L_c – tilted subgel phase, L_β – gel phase, L'_β – tilted gel phase, P'_β – ripple phase, L_α – fluid phase. In the two lower phase diagrams "c" denotes a coexistence region, of which the exact structure was difficult to determine. From Ref. [191].

This example illustrates that bilayer structure and properties do sensitively depend on the model parameters of the minimal coarse-grained models. Since the potentials of these models are not directly related to molecular interactions, the parameters have to be adjusted so as to reproduce macroscopic observables. Although the minimal coarse-grained models are quite simple, they have been shown to form several of the known bilayer phases: fluid, gel and crystalline [187, 180, 206, 207, 208, 191, 175], as well as more exotic ones, like the ripple phase [187, 191]. The different phases that can be obtained by the DPD model of Smit and co-workers are illustrated in Fig. 3. The phase diagram as well as the area compressibility modulus, bending stiffness and spontaneous curvature [193, 183, 209] have been explored as a function of model parameters. This ensures that one can choose parameters that make the coarse-grained model mimic, qualitatively, the behavior of an experimental system.

2.2.3. Systematic coarse-graining: potential and limitations

While the above minimal coarse-grained models are able to explore the generic features of the behavior of amphiphiles in solution, much recent interest has focused on "deriving" coarse-grained models for a specific chemical substance [12, 210, 14, 15, 16, 17]. The general feature of these systematic coarse-graining schemes is the attempt to utilize information about the microscopic structure, obtained by atomistic simulations, for instance, in order to parameterize the interactions between the coarse-grained entities.

These techniques have originally been developed for polymer systems, and they have been extensively employed to describe quantitatively the structure and dynamics of polymer melts and solutions [8, 10, 11, 211, 212, 213, 214, 215]. While the universal properties of amphiphilic systems only require a coarse-grained model to capture a few relevant interactions, the systematic construction of such a model that quantitatively reproduces the behavior of the underlying microscopic system is a very ambitious task. From the onset, it is obvious that decimating the degrees of freedom will result in a loss of information, and will generate very complicated multi-body interactions [216]. The latter imparts additional complications on extracting ther-

modynamic information from coarse-grained models. Commonly the multi-body interactions are, in turn, approximated by pairwise interactions in order to retain the computational efficiency of the coarse-grained representation, and these effective pairwise interactions depend on the thermodynamic state of the system (i.e., they depend on density or temperature, and they are different in different thermodynamic phases).

The general principles of systematic coarse-graining consist in (i) choosing a set of key characteristics that the coarse-grained model shall reproduce, and (ii) determining the interactions between the coarse-grained degrees of freedom so as to reproduce these characteristics. The first step is the most crucial, and is guided by insight into the physics of the phenomena that one wants to investigate. Three qualitatively different properties can be distinguished – structural quantities, thermodynamic properties, and dynamic characteristics.

Structural quantities are related to the geometry of the molecules on different length scales. In order to capture the specific details of the molecular architecture, a coarse-grained model should not only reproduce the overall size of the molecule (e.g., the end-to-end distance), but it should also include finer details of the molecular architecture (e.g., the stiffness along the molecular backbone, the bulkiness of the lipid's head, the location of double bonds in the hydrocarbon tails). It is essential to capture the rough features of the molecular geometry and its fluctuations, or ability to deform in response to its environment.

In the ideal case the parameterization of a coarse-grained model is based on the detailed atomistic information about the molecular conformations under the same thermodynamic conditions, i.e., the same temperature and density. Then, one explicitly defines a mapping from a configuration of the atomistic model, $\{\mathbf{r}\}$, onto a configuration of the coarse-grained model, $\{\mathbf{R}\}$. Utilizing a large equilibrated sample of atomistic configurations, one can obtain the probability distribution of distances between coarse-grained entities.

This procedure is illustrated in Fig. 4 for the case of a polybutadiene melt at 240 K and atmospheric pressure. The rich structure of local correlations is specific to the chosen system, but the qualitative features discussed in the following are born out by a wide class of systems and have been observed in a large variety of studies [10, 213, 218, 219, 220, 221, 222, 223, 224, 14, 225, 15, 226, 17, 227, 228, 229, 230, 231, 232, 233, 234, 235]. The two panels of the figure present the intramolecular and intermolecular pair correlation function as obtained from a simulation within a united atom model [236, 237, 238, 239]. The *intramolecular* correlations exhibit a rich structure on short length scales that mirrors both the correlations due to bond length and torsional interactions, as well as the delicate packing of the dense polymeric fluid. At large distances, those correlations have died away, and the intramolecular pair correlation function smoothly decays like $g_{\rm intra}(r) \sim 1/r$ as expected for a Gaussian polymer in a melt [4]. The *intermolecular* pair correlation function describes the probability of finding two coarse-grained segments on different molecules at a distance, r. It exhibits qualitatively a form that one also expects for a simple liquid. At small distances the correlation function vanishes – this distance characterizes the "thickness" of the polymer. There is a broad nearest-neighbor peak around 5 A, and there are a few further oscillations at larger distances. The long-range approach of the intermolecular correlation function to unity is dictated by the polymeric correlation hole effect and it is identical to the decay of the intramolecular correlations because the two cancel one another at length scales larger than the correlation length of density fluctuations due to the near incompressibility of the dense liquid [4].

One can use the explicit configurations of an atomistic simulation, and lump n successive carbon atoms along the backbone of the polymer into an effective coarse-grained segment. In this specific example, the location of the coarse-grained bead is taken to be the center of mass of its constituents, without accounting for the differences in molecular mass of CH and CH_2 units.

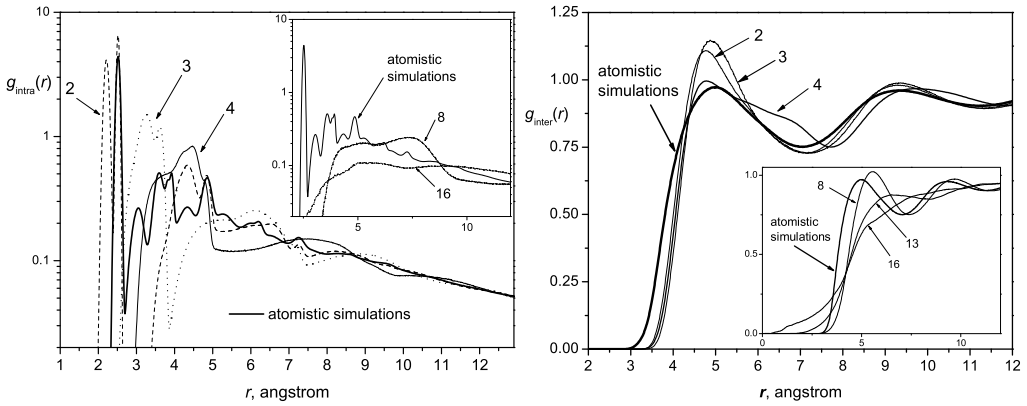

Figure 4. (a) Coarse-graining of the intramolecular segment-segment correlation function of polybutadiene (240 K). The numbers mark data with different degrees of the coarse-graining. For example, the coarse-graining degree $n = 4$ yields a chain molecule for which four united atoms are approximated by one effective segment. The bold curve is the correlation function calculated using the united-atom model (δ-type peaks at $r = 1.34$ Å, 1.5 Å, 1.53 Å arising from the CH=CH, CH_2-CH and CH_2-CH_2 bonding distances are omitted). (b) Coarse-graining of the intermolecular segment-segment correlation function of polybutadiene at 240 K. For $n \leq 8$, the correlation function changes quantitatively. For large degree of the coarse-graining (e.g., $n > 13$), the correlation peaks and minima disappear and the correlation hole at $r < 3$A shrinks. The bold curve is the correlation function calculated using the united-atom model. From Ref. [217].

The correlations between the coarse-grained beads constructed in this manner for different levels, n, of coarse-graining are also depicted in Fig. 4. Two general characteristics can be observed: First, the larger the degree of coarse-graining, the smoother are the intra- and intermolecular pair correlation functions. This behavior stems from the fact that the coarse-grained beads can partially overlap. This softening increases with the degree of coarse-graining, n. Second, the local structure is very sensitive to n, while the large distance behavior is not. In the specific example, constructing a coarse-grained bead from $n = 3$ segments yields a rather poor representation of the intramolecular and intermolecular correlations: The first peak of g_{intra} coincides with the minimum of the data for the united atom model and the first peak of g_{inter} is too high. The value $n = 4$ yields a better description. Increasing the value of n even further, one finds that the local structure gradually fades away and the beads become so soft that there is a significant probability that the coarse-grained beads overlap (c.f., inset of Fig. 4 b). Thus there is an optimal degree of coarse-graining. Values of n which are too small lead to comparably harsh coarse-grained potentials which, in turn, give rise to packing effects that are not related to the structure of the underlying atomistic systems. Large values of n result in a loss of local structure and thereby of chemical specificity.

The thermodynamic equilibrium properties of a coarse-grained model can be constructed formally via a partial trace, i.e., a summation over all microscopic configurations compatible with a fixed set of coarse-grained degrees of freedom. This procedure is in complete analogy with Renormalization Group calculations which have successfully been employed in polymer physics and critical phenomena [5, 6, 7]. Let $\{\mathbf{r}\}$ denote the coordinates of the detailed microscopic model (e.g., the atom positions in a chemically realistic model) and let $\{\mathbf{R}\}$ denote the coarse-grained degrees of freedom. There is a mapping from the detailed degrees of freedom, $\{\mathbf{r}\}$, onto the coarse-grained ones, $\mathbf{R}[\{\mathbf{r}\}]$. For instance, $\{\mathbf{R}\}$, might be the center of mass of a small group of atoms or the location of a particular group of a lipid molecule. Let $E[\{\mathbf{r}\}]$ denote the pairwise interactions of the microscopic system, so one can calculate an effective interaction, $U[\{\mathbf{R}\}]$ between the coarse-grained degrees of freedom via [216]

$$\exp\left(-\frac{U[\{\mathbf{R}\}]}{k_BT}\right) = \int \mathcal{D}[\{\mathbf{r}\}] \exp\left(-\frac{E[\{\mathbf{r}\}]}{k_BT}\right) \delta\left(\mathbf{R} - \mathbf{R}[\{\mathbf{r}\}]\right) \tag{25}$$

With this definition of the effective interaction, U, the partition function of the microscopic system $\mathcal{Z}$ can be obtained according to

$$\mathcal{Z} = \int \mathcal{D}[\{\mathbf{R}\}] \exp\left(-\frac{U[\{\mathbf{R}\}]}{k_BT}\right) \tag{26}$$

and the probability of the coarse-grained degrees of freedom is identical to that generated by equilibrium configurations of the microscopic model. There are, however, two caveats:

(i) U does not possess the typical characteristics of an interaction but rather those of a free energy. In particular, U depends on the thermodynamic state characterized by temperature, pressure, etc. Due account of this state dependence has to be taken if thermodynamic quantities are extracted. For example, the internal energy is calculated according to [240]:

$$\langle E \rangle \equiv \frac{\int \mathcal{D}[\{\mathbf{r}\}] E[\{\mathbf{r}\}] \exp\left(-\frac{E[\{\mathbf{r}\}]}{k_BT}\right)}{\int \mathcal{D}[\{\mathbf{r}\}] \exp\left(-\frac{E[\{\mathbf{r}\}]}{k_BT}\right)} \tag{27}$$

$$= k_BT^2 \frac{\partial \ln \mathcal{Z}}{\partial T} \tag{28}$$

$$= \frac{\int \mathcal{D}[\{\mathbf{R}\}] \left(U[\{\mathbf{R}\}] - T\frac{\partial}{\partial T}U[\{\mathbf{R}\}]\right) \exp\left(-\frac{U[\{\mathbf{r}\}]}{k_B T}\right)}{\int \mathcal{D}[\{\mathbf{R}\}] \exp\left(-\frac{U[\{\mathbf{r}\}]}{k_B T}\right)} \tag{29}$$

$$= \left\langle U[\{\mathbf{R}\}] - T\frac{\partial}{\partial T}U[\{\mathbf{R}\}] \right\rangle_{|\{\mathbf{R}\}} \tag{30}$$

By the same token, the effective potential depends on density, ρ, and care has to be taken when calculating derivatives of thermodynamic quantities with respect to the number of particles or volume. For density-dependent central pair potentials, $U(R, \rho, T, \cdots)$ the pressure is given by [241]

$$p \equiv -\frac{\partial F}{\partial V} \tag{31}$$

$$= p_{\text{ideal}} + p_{\text{virial}} + \frac{\rho^3}{2}\int \mathrm{d}^3 R\, \frac{\partial U(R,\rho,T,\cdots)}{\partial \rho} g(R,\rho,T,\cdots) \tag{32}$$

$$\text{with} \qquad p_{\text{ideal}} = k_B T \rho \qquad \text{and} \qquad p_{\text{virial}} = -\frac{\rho^2}{6}\int \mathrm{d}^3 R\, R \frac{\partial U(R)}{\partial R} g(R) \tag{33}$$

where the first terms are the familiar ideal gas term and the viral expression for the pressure which ignore the density dependence of the effective potential. The additional second term arises due to the dependence of the effective interaction, U, on the thermodynamic conditions under which it has been obtained [241, 240]. $g(R)$ is the pair correlation function of the coarse-grained fluid (cf. Eq. (36)).

(ii) Generally, $U[\{\mathbf{R}\}]$ cannot be decomposed into pairwise interactions but it consists of complicated many-body interactions. It is neither feasible to construct these many-body interactions numerically through the formal coarse-graining procedure outlined by Eq. (25) (see Refs [242, 243, 244, 245] for explicit schemes for simple lattice models), nor can they be utilized in an efficient computational model.

In order to obtain a computationally tractable model, one has to approximate the effective, many-body interaction by pairwise potentials, and one often ignores the state dependence of the effective interaction. To this end, one seeks an approximation of the form

$$U[\{\mathbf{R}\}, \rho, T, \cdots] \approx \sum_i \sum_{j<i} V(\mathbf{R}_i - \mathbf{R}_j) \tag{34}$$

The detailed form of V is unknown. Often one utilizes a generic form that contains several free parameters. These parameters are adjusted to the specific system (see below). Moreover, one requires that even after ignoring the state dependence of the interactions, the model still reproduces thermodynamic properties such as the equation of state, the interfacial tension, etc. It is this uncontrolled approximation in the construction of coarse-grained models that requires physical insight.

Once the general type of the interactions to be included and the key characteristics the coarse-grained model should reproduce have been chosen, the second step of constructing the detailed form of the coarse-grained interactions, V, is conceptually straightforward but tedious. As a first approximation one utilizes the *potential of mean force*, V_{mf} obtained via the pair correlation function of coarse-grained degrees of freedom:

$$g(\mathbf{R}_{ij}) \equiv \exp\left(-\frac{V_{\text{mf}}(\mathbf{R}_{ij})}{k_B T}\right) \tag{35}$$

with $\mathbf{R}_{ij} = \mathbf{R}_i - \mathbf{R}_j$, and where the pair correlation function is given by

$$g(\mathbf{R}) = V \left\langle \delta\left(\mathbf{R} - (R_i[\{\mathbf{r}\}] - R_j[\{\mathbf{r}\}])\right)\right\rangle \tag{36}$$

through the microscopic configurations.

By definition this construction procedure works well if the coarse-grained degrees of freedom are dilute, but fails if higher order correlations become important (condensed phase effect). Nevertheless this potential of mean force serves as an initial guess for more sophisticated procedures. One strategy consists in using the Ornstein-Zernike equation

$$h(\mathbf{R}_{12}) = c(\mathbf{R}_{12}) + \rho \int \mathrm{d}\mathbf{R}_3 \; h(\mathbf{R}_{23}) c(\mathbf{R}_{13}) \tag{37}$$

to obtain the direct correlation function, $c(\mathbf{R})$ from the total correlation function, $h(\mathbf{R}) = g(\mathbf{R}) - 1$. Then, one can use an approximate closure relation to express the direct correlation function in terms of the interparticle potential. Liquid state theory provides guidance in choosing accurate closures. An example is the hypernetted chain closure (HNC) [232]

$$\frac{V(\mathbf{R})}{k_B T} = -\ln g(\mathbf{R}) + h(\mathbf{R}) - c(\mathbf{R}) \tag{38}$$

which differs from the potential of mean force in Eq. (35) by the last two terms.

This scheme provides a systematic, yet approximate, approach for constructing the effective pair interactions. In polymer physics, one often employs a numerical method – iterative Boltzmann inversion [246, 247, 231, 230, 232]. One starts with an initial guess for the pair interactions, V_0. This pair interaction is used in a computer simulation of the coarse-grained system, and the correlation function, g_0, is monitored. In the next step of the iteration, $i = 1$, the potential is improved according to

$$V_i(\mathbf{R}) = V_{i-1}(\mathbf{R}) + k_B T \ln \frac{g_{i-1}(\mathbf{R})}{g(\mathbf{R})} \tag{39}$$

where $g(\mathbf{R})$ is the reference pair correlation function obtained from the microscopic system. The procedure is continued until the coarse-grained simulations with the potential V_i reproduce the reference pair correlation function with sufficient accuracy. Other iterative scheme, e.g., self-adjusting Wang-Landau-type methods [248], can be envisioned as well.

In addition to these structural quantities the potential parameters of the coarse-grained representation are tailored to reproduce thermodynamic properties such as pressure, interface tension or elastic moduli. Some quantities (like pressure or membrane tension) can be included in the iterative Boltzmann inversion scheme utilizing constant pressure or tension simulations [230]. Alternatively, non-bonded interactions that do not strongly impact the molecular structure are adjusted to reproduce the desired thermodynamic properties.

While the mapping of equilibrium properties between atomistic and coarse-grained models is conceptually well understood, the mapping of dynamical properties might prove an even bigger challenge. The softer interactions in coarse-grained models typically speed up the dynamics on large length scales. This is a major computational benefit of coarse-graining. However the speed up is not uniform, but rather depends upon the specific dynamic property. For instance, the ratio of time constants between lateral diffusion of the lipids' center of mass, the structural relaxation of the lipid conformations and the rotational diffusion around the bilayer's normal differ between the coarse-grained model and atomistic simulations [15]. Several factors contribute to the non-uniform speed-up:

The mobility of lipid head groups is coupled to the structural rearrangement of water in their vicinity, but the local structure (e.g., hydrogen bonding) is not faithfully reproduced by coarse-grained models. Likewise, the elimination of degrees of freedom of the hydrophobic

tails (C–C bond stretching, bond angle and torsional potentials) in the course of the coarse-graining procedure speeds up the structural relaxation of the lipid tails. Moreover, the neglect of topological constraints in the molecules' dynamics (non-crossability) by very soft potentials (e.g., DPD models) will selectively speed up the dynamics of extended molecules compared to e.g., small solvent molecules. These effects have quite different origins and, in general, will result in different speed-up factors. Moreover, electrostatic interactions omitted in coarse-grained models might be not essential for structural properties, but still may significantly alter the dynamics [249]. Likewise, integrating out the solvent molecules results in strong attractions between like units of the amphiphilic molecules. This might dramatically influence the dynamics (see e.g., Ref. [250] for a careful discussion of the role of explicit solvent on the dynamics of the collapse of a polymer chain in a bad solvent). Therefore, one cannot expect that a *single* scale factor relates the characteristic times of different motions and dynamic processes between atomistic and coarse-grained models [13, 15, 251]. Thus particular care has to be exerted when non-equilibrium process are to be described by coarse-grained models. Nevertheless, a natural and common identification of the time scale in coarse-grained models consists in matching the characteristic time of the slowest process of relevance, e.g., the lateral diffusion of a amphiphilic molecule in the bilayer.

2.3. Coarse-grained field-theoretic models and molecular field theories

An alternative approach to a particle-based description has its roots in statistical field theory [252, 253]. In this framework one operates with collective variables, such as density and interaction fields instead of the coordinates of the individual molecules. The formal advantage of this approach is that it allows one to decouple many-body (particle-particle) interactions and to replace them with one-body (particle-field) interactions. This "simplification" comes at a price – to calculate the partition function one has to perform thermodynamic averages over the field variables. Nevertheless, under suitable conditions, one can introduce controlled approximations that make the field-based approaches tractable.

Formally, the particle-based canonical partition function of a system of n particles, occupying volume V and interacting through a (multi-body) potential $U(\{\mathbf{r}\})$

$$\mathcal{Z} \propto \prod_{j=1}^{n} \int_V \mathrm{d}^3\mathbf{r}_j \; e^{-U(\{\mathbf{r}\})/k_BT}, \tag{40}$$

can be transformed into the following field-theoretic partition function:

$$\mathcal{Z} \propto \int \mathcal{D}w_\alpha \int \mathcal{D}\phi_\beta \; e^{-\mathcal{H}[w_\alpha,\phi_\beta]/k_BT}, \tag{41}$$

where $\mathcal{H}[w_\alpha, \phi_\beta]$ is usually called an effective action or Hamiltonian of the system, and it depends on density and interaction field variables, $\phi_\beta(\mathbf{r})$ and $w_\alpha(\mathbf{r})$. Here, the indices α and β run over different *types* of microscopic units (monomers, segments), and the functional integration $\int \mathcal{D}f$ is performed over all spatial realizations of the field variables.

Despite the fact that the field-theoretic transformation replaces one very hard problem, Eq. (40), with another, Eq. (41), in this representation it is simple to implement the *mean-field* approximation which, in polymer systems, is quite accurate [254, 255]. Physically, the mean-field approximation amounts to the assumption that the statistics of a system is dominated by a particular field configuration, so that the partition function is also dominated by a single term and takes the simple, approximate form

$$\mathcal{Z} \propto e^{-\mathcal{H}[w^*_\alpha,\phi^*_\beta]/k_BT}, \tag{42}$$

where the dominant field configurations, w^*_α and ϕ^*_β, are the stationary (and, actually, saddle point) configurations of the effective Hamiltonian:

$$\left.\frac{\delta\mathcal{H}}{\delta w_\alpha(\mathbf{r})}\right|_{w^*,\phi^*} = \left.\frac{\delta\mathcal{H}}{\delta \phi_\beta(\mathbf{r})}\right|_{w^*,\phi^*} = 0 \tag{43}$$

This approximation is usually not very accurate for systems composed of low-molecular weight species with short-ranged interactions, but it becomes more so for particles with long-ranged interactions and for high-molecular weight polymers at high concentrations. Depending on the system of interest, one can frequently quantify deviations away from the mean-field solution caused by long-wavelength fluctuations, and define the corresponding Ginzburg parameter [254, 255]. In polymer systems with short-ranged segment interactions, it is usually the dimensionless overlap parameter, or invariant degree of polymerization, $\bar{\mathcal{N}} \equiv (\rho R_e^3/N)^2$, which characterizes the number of polymer chains interacting directly with a given chain. Here R_e is the molecules' end-to-end distance, N denotes the number of monomeric units (segments) per molecule and, ρ is the segment number density. This parameter can be compared to that in the case of simple lattice models. In the latter systems, the mean-field approximation usually becomes accurate at large enough site coordination number, commonly achieved either at high spatial dimensionality or for long-ranged interaction potential. In polymer systems, however, high effective coordination numbers can be achieved by increasing the polymerization index at a constant segment density.

There are two basic issues that have to be addressed within any mean-field approach: (i) calculation of the average molecular-field acting on a given molecule due to a density distribution of all other molecules present in the system, (ii) evaluation of a single-molecule partition function in the presence of this field, which can be formally written as:

$$Z_1[w] = \sum_{\{s\}} g_s e^{-w(s)/k_B T}. \tag{44}$$

Here $w(s)$ is the mean-molecular field felt by the chain in microscopic state s. These states have *a priori* statistical weights g_s, that are solely determined by intra-chain degrees of freedom and characterize the molecular architecture in a spatially homogeneous system. Ultimately, the two ingredients of a mean-field approach have to be solved self-consistently for all the species, therefore the name *self-consistent field (SCF) theory*. The variety of the SCF approaches in the literature can be classified by the types of approximations used for solving the two problems above. Below, we describe a number of such approaches as applied to modeling of bilayer membranes.

2.3.1. Anchored chain models

One of the first molecular-field theories of a lipid bilayer was proposed by Marcelja [256, 257]. In this model, lipid head groups and solvent molecules are modeled by a simple boundary to which lipid tails are anchored at a given areal density. Intra-chain degrees of freedom are sampled using Flory's Rotational Isomeric State (RIS) model [258, 259] and the segments interact through an anisotropic aligning potential of Maier-Saupe kind:

$$w(\Theta_{12}) = V_0 \left[\frac{3}{2}\cos^2(\Theta_{12}) - \frac{1}{2}\right], \tag{45}$$

where Θ_{12} is the angle between segment axes. This potential is borrowed from the theory of nematic liquid crystals, and in the context of lipid packing the aligning tendency between segments stems from the fact that all-*trans* chains pack at a higher density and, hence, experience stronger dispersive van der Waals attractions. Further, being better aligned, they are subject to

fewer hard core repulsions. In the mean-molecular field approximation the two-body interactions in Eq. (45) are replaced by a one-body interaction with the scalar order parameter field:

$$\eta = \left\langle \frac{3}{2}\cos^2(\Theta) - \frac{1}{2} \right\rangle, \tag{46}$$

where Θ denotes now the angle between the segment and the average axis of orientation. This relatively simple theory is capable of a quantitative (albeit phenomenological) description of experimental data on the liquid-gel ordering transition thermodynamics.

Gruen [260, 261, 262, 263] extended Marcelja's model by replacing the phenomenological Maier-Saupe ordering interaction with a local incompressibility condition in the lipid tail region imposed through an inhomogeneous Lagrange multiplier field, $\pi(z)$, coupled to the local microscopic segmental density $\hat{\phi}(z) = \sum_{i=1}^{N} \delta(z - z_i)$, where z is the coordinate across the laterally homogeneous bilayer and the sum runs over all the positions z_i of the N units per molecule. Results derived with this model show semi-quantitative agreement with results of molecular simulations both for thermodynamics as well as for the structural properties of bilayers. Minor modifications of this approach allow the study of properties of cylindrical and spherical micelles [264, 265, 266].

Similar ideas of imposing packing constraints on anchored chain systems have been explored by a number of researchers. Differences between these methods are mostly technical. Dill et al. [267, 268] and Scheutjens and co-workers [269] use a lattice to describe both chain conformations as well as molecular field configurations, which can be treated with efficient transfer matrix methods originally proposed by Kramers and Wannier for solving the Ising model. Ben-Shaul et al. [270, 271, 272, 273] enumerate a very large set of the most probable chain configurations off-lattice and use iterative techniques to reach self-consistency. For a more detailed exposition of these ideas we refer the reader to excellent reviews of these works [268, 270].

Recently Elliott et al. [274, 275] has extended the mean-field approach to study mixtures of saturated and unsaturated lipids and cholesterol. It has been shown that the incompressibility (or packing) constraint is not sufficient to provide a quantitative description of both liquid and gel lipid membranes and the corresponding main-chain transition. This deficiency can be eliminated by including additional explicit orientational interaction, similar in spirit to the original ideas of Marcelja and Gruen. The following form of pairwise interaction potential has been proposed:

$$V(\mathbf{u}, \mathbf{u}') \to V(\mathbf{u}\cdot\mathbf{c}, \mathbf{u}'\cdot\mathbf{c}) \approx -Jf(\mathbf{u}\cdot\mathbf{c})f(\mathbf{u}'\cdot\mathbf{c}), \tag{47}$$

where $\mathbf{u}$ and $\mathbf{u}'$ are the local orientations of CH_2 groups, $\mathbf{c}$ is the bilayer normal, and J characterizes the coupling strength. In the absence of head group orientational interactions, the chain tails on average will align parallel to the bilayer normal, which implies that $f(x)$ should be a monotonically decreasing function of its argument. Elliott et al. [274] utilize the generic form

$$f(\cos\Theta) = \frac{2m+1}{2}(\cos^2\Theta)^m \approx m\exp(-m\Theta^2), \tag{48}$$

where Θ is the angle between the local chain orientation $\mathbf{u}$ and the bilayer normal $\mathbf{c}$. The parameter m controls the width of the orientational interaction and the case $m = 1$ is comparable to the original Maier-Saupe interaction function used by Marcelja [276]. Elliot et al. [274] take $m = 18$. The higher power dependence was first proposed by Gruen [262, 263].

The experimental value of the main-chain transition temperature of a single component DPPC system is used to fit the strength, J, of the orientational interaction whereas the power, m, is estimated from the average alignment of an acyl tail in the bilayer. The same set of parameters can be used to describe membranes containing unsaturated dioleoylphosphatidylcholine

(DOPC) lipids. This theory successfully predicts the absence of the liquid-gel transition in DOPC membranes due to disordering effect of the unsaturated double bond. Binary dipalmitoyl phosphatidylcholine (DPPC)/DOPC model bilayers exhibit phase coexistence between a saturated-lipid-rich gel phase and an unsaturated-lipid-rich liquid crystalline phase with the transition temperature below that of the pure saturated-lipid system. An extended model of a ternary system containing saturated and unsaturated lipids and cholesterol has been used to provide strong evidence for the existence of a liquid-ordered to liquid-disordered phase transition [275].

Despite the fact that the anchored chain models provide a detailed description of chain-packing in both gel and liquid lipid bilayers, their description of the interfacial polar-head region is very rudimentary. It is either completely ignored in favor of fixing the lipid areal density or treated essentially phenomenologically. The inequivalence of tail, head and solvent segments effectively makes the bilayers *pre-assembled* structures, as opposed to *self-assembled* ones. Since this limitation does not come from the mean-field approximation, it can be completely eliminated within a more general self-consistent field-theoretic framework.

2.3.2. Self-assembled membrane models

The self-consistent theory of polymer systems, both for solutions and melts of long-chain molecules, was formulated by Edwards [277]. Helfand and Tagami [278, 279, 280] pioneered the use of this approach for the study of multicomponent polymer systems with diffuse interfaces. Since then the self-consistent field theory has been utilized for a wide range of polymeric systems [269, 281, 282, 283, 284, 253, 255, 285], notably it has been highly successful in studying self-assembly of block copolymers [286, 287, 288] and copolymer-homopolymer mixtures [289, 290, 291, 292, 293].

Leermakers et al. used similar ideas to study self-assembled bilayers composed of polymer chains with random-walk and RIS (Rotational Isomeric State) statistics [205]. For the sake of computational convenience, chain configurations are restricted to a tetragonal lattice aligned with the bilayer interface. The segment-segment dispersive interactions are modeled by a set of Flory-Huggins parameters: χ_{AW} for tail segment/water, χ_{BW} for head group/water and $\chi_{AB}(\approx \chi_{AW})$ tail segment/head group interactions. The harshly repulsive interactions at short distances are taken into account by imposing the common incompressibility condition $\phi_A(z) + \phi_B(z) + \phi_W(z) = 1$, where $\phi_{A,B,W}(z)$ are local volume fractions of the tail, head, and water segments, respectively. The authors use two types of chain statistics to describe the intramolecular conformations. The first one is a random walk on the tetragonal lattice, which allows neighboring bonds to overlap and does not distinguish between the *trans* and *gauche* conformations. The second more elaborate model, based on the RIS scheme, takes into account the small energy difference between the local bond configurations and also forbids direct backfolding of the chain onto itself. In both approaches the chain partition function and density distributions can be evaluated using straightforward matrix algebra. Nevertheless, for computational tractability only laterally homogeneous structures are considered.

This fully self-consistent framework is capable of describing stable, tensionless, self-assembled bilayers, provided the interaction parameters are within certain limits. The random-chain and the RIS-chain models both result in membranes with qualitatively similar segment distributions and thermodynamic properties. Quantitatively, however, this approach underestimates the experimentally measured membrane thickness by about 50%, suffers from an excessive chain-disorder and fails to predict the gel-liquid main-chain transition. Despite these deficiencies, this simple framework is very flexible and efficient and it has been extended to studies of bilayer vesicles, membrane elasticity, bilayer-bilayer interactions and effects of surfactants on bilayer

structure and stability [294].

The absence of the main-chain transition in this model has been traced to the inability of the simple incompressibility constraint to properly describe *anisotropic* packing of the chains. To cure this problem, Leermakers et al. formulated an anisotropic SCF theory [295]. The idea is based on a generalization of Flory's and Di Marzio's treatment of rigid rod statistics in anisotropic states and results in an effective entropic aligning interaction between chains (cf. Elliott et al. [274]). The modified theory predicts a first order main-chain transition and the existence of two gel phases: one with intercalated monolayers in the dilute regime, and the other with almost non-overlapping monolayers in the concentrated regime.

With straightforward modifications, this theory was used to investigate mechanical properties of the lecithin bilayer membranes. To calculate the bending moduli of the lecithin vesicles, Leermakers et al. [294] proposed to use spherically curved lattices that can accommodate either lattice random-walks or RIS chains. The fact that the underlying lattice is "commensurate" with the segment structure of the chains, leads to strong lattice artifacts. These numerical artifacts give rise to strong variations of both structural and thermodynamic properties as a function of vesicle radius. To resolve this problem, the authors propose to consider only vesicles with radii that are commensurate with the underlying lattice. Despite the fact that the model then provides a reasonable account of the stability and structure of the curved, pure lecithin bilayers, this approach has been criticized in a later work (see below). Bending moduli of multicomponent vesicles are predicted to be smaller than those of pure vesicles composed of either of the components. This prediction is in agreement with the earlier studies on anchored chains grafted to curved interfaces [296].

Oversteegen et al. [297] studied in detail the dependence of elastic constants on microscopic interaction parameters. In particular, they found that the bending modulus, κ_b, strongly depends on the strength of interactions between the head groups and the solvent. As the strength of head group hydration decreases, so does the bending modulus, apparently vanishing for sufficiently weak head group/solvent interaction parameters. Interestingly, under the same conditions the saddle splay modulus, $\bar{\kappa}$, progressively becomes less negative and eventually adopts positive values. This favors formation of saddle-like structures and should lead to the instability of a flat bilayer. The authors also carefully investigate the spherical lattice artifacts mentioned above and conclude that there is actually no completely consistent way to eliminate them, despite earlier claims to the contrary. Nevertheless, the authors argue that the lattice model may still prove to be a valuable tool to to make qualitative predictions. The same approach was used [298] to study elastic properties of surfactant monolayers. It was found that the monolayer spontaneous curvature does not vanish, as in the case of the bilayers, and strongly depends on molecular architecture. The monolayer bending modulus was found to be essentially half of that of the corresponding bilayer, in agreement with previous studies which used an anchored chain model [299].

Meijer et al. [300] used extensions of the lattice mean-field model to study inclusions of foreign molecules in bilayer membranes utilizing a detailed description of both rigid and flexible molecules with, and without, electrostatic interactions. To handle the rigid inclusions whose segment structure is not necessarily commensurate with the underlying tetragonal lattice (used to generate RIS hydrocarbon chain configurations), the authors must make several approximations to preserve efficiency of the propagator scheme. This approach is implemented in a computer program called GOLIATH. Partitioning coefficients for a wide range of molecules into bilayer membranes were predicted in reasonable agreement with experimental data. Detailed theoretical information on the density and orientational distributions of these inclusions allowed the authors to conclude that it is possible to design isomeric molecules that can have roughly the same

partitioning coefficient, but would differ greatly with respect to the position and orientation of the inclusion in the membrane. This could be potentially of use in designing membrane-incorporated drug systems.

In a more recent work, Leermakers et al. refined their SCF approach by including several new features [301]. First, the introduction of different segment volumes for CH_2 and CH_3 groups counteracted the interdigitation of hydrocarbon chains from apposing monolayers. Second, by allowing the formation of clusters of water molecules [302], they were able to prevent excessive penetration of the water molecules into the membrane's hydrophobic region. Third, polarizability of chain segments was included for thermodynamic consistency. The predictions of this detailed approach compare favorably with all-atom MD simulations by the same authors [303] of SOPC and SDPC bilayers. This validates the SCF parameter set, which can then be used to investigate other membrane properties.

Whitmore et al. extended the lattice, self-consistent, anisotropic field theory to compressible, fully hydrated, phospholipid membranes [304]. The authors assumed that the lipid headgroups are strongly confined both positionally and orientationally throughout the temperature range of interest. This approximation considerably simplifies the numerical solution of the set of self-consistent equations, and emphasizes the bond density and orientation in the hydrocarbon region of the bilayer. The assumption, however, is in disagreement with the the rather wide interfaces observed by Leermakers et al. in a similar model bilayer system [301]. Similarly, the solvent molecules (water) were excluded from the hydrocarbon layer. To determine the microscopic interaction parameters the authors used the main-chain transition temperature for DPPE, its dependence on the chain length, and the change in thickness of the hydrocarbon layer at the transition. The so-parameterized model exhibits a first order phase transition between the highly ordered gel phase, L_β, to the partially disordered liquid crystalline phase, L_α. It also provides a reasonable account of equilibrium changes in the bilayer thickness and hydrocarbon density across the main chain transition. The predicted increase of the transition temperature with the hydrocarbon chain length is in qualitative agreement with experimental observation, but is still weaker by a factor of 3. The authors attribute this inaccuracy to the neglect of orientational effects of water on the gel-to-liquid transition.

In an alternative approach, Müller and Schick [305] used an off-lattice representation of the field theory, and obtained the single-chain partition function via a partial enumeration [306] over a large set of molecular conformations of a lipid chain with the RIS statistics. The model takes into account an explicit solvent, which permits the study of thermotropic, as well as lyotropic, phase transitions between lamellar, L_α, and inverted hexagonal, $H_{\rm II}$, phases. In agreement with experiment, it was found that the transition from $H_{\rm II}$ to L_α occurs upon increasing the solvent content or decreasing the temperature. It was also confirmed that an increase in the length of the hydrocarbon tail or decrease in the head-group volume stabilizes the inverted hexagonal phase.

In a series of papers, Schick and coworkers used a flexible chain model to study bilayer membranes. This model is known to be incapable of producing the main-chain transition to the gel phase, L_β, due to the excessive entropy of a flexible chain. Nevertheless, in the liquid crystalline phase, L_α, it is expected to account reasonably well for the competition between hydrophobic forces and chain stretching. In particular, Netz and Schick [307] used a standard flexible diblock copolymer model in the presence of a solvent, modeled by a flexible hydrophilic homopolymer, to study structure and stability of the fluid bilayer phase. It was found that under external compressive stress the bilayer thickness decreases until the bilayer is in thermodynamic coexistence with either the disordered or catenoid lamellar (hexagonally perforated lamellar) phases. This result was used to describe membrane rupture. It was found that the relative areal expansion

at the onset of rupture is about 2%, which is in agreement with experiments on lipid systems. Pores, which appear in the hexagonally-perforated lamellar phase, formed reversibly with stress and were slightly hydrophobic.

Li and Schick [308] used a more detailed microscopic model of a lipid with a charged headgroup, two flexible hydrophobic tails, and a neutral solvent with counter ions. The hydrophobic interactions are described through the usual contact interactions. First, the model is applied to a neutral, anhydrous, lipid and is shown to describe reasonably well the transitions between lamellar, hexagonal and cubic phases. With the addition of a solvent, the system exhibits a re-entrant $H_{\rm II} \rightarrow L_\alpha \rightarrow H_{\rm II}$ transition, a peculiar feature observed experimentally in the dioleoylphosphatidylethanolamine (DOPE)-water system. Addition of a negative charge on the headgroup leads to an effective increase of the head-group volume and drives the transition from the $H_{\rm II}$ to the L_α phase, also in agreement with experiments. In a second paper, Li and Schick [309] extend their approach to study mixtures of cationic, anionic and neutral lipids. This model provides a detailed description of the pH-tunable $L_\alpha - H_{\rm II}$ phase transition in mixed lipid systems, which could play an important role in liposomal drug delivery systems [310].

We used the SCF approach with the Gaussian chain model to elucidate the evolution and free energy costs of intermediates involved in the fusion of bilayer membranes [311, 312]. This study goes beyond the previous work on laterally homogeneous bilayers and provides a description of complicated structural rearrangements that occur during the fusion reaction. Detailed results of this approach are presented in Sec 3.4. Here we mention important modifications necessary to study such complicated problems within the field-theoretic framework.

In practice, the SCF theory in its common implementation is only capable of identifying thermodynamic, locally stable configurations of a system. Such structures can correspond to stable configurations of a system or metastable *intermediate states* encountered along the transformation of the system towards a stable structure. In studying activated processes (e.g., rupture, fusion or fission of membranes), however, one should also be able to describe properties of *transition states* which correspond to saddle points of the SCF free energy functional. Unfortunately, finding a saddle point of a functional poses a serious numerical problem. To address this issue we propose the use of *reaction coordinate constraints* [293]. In some cases, using either physical intuition, qualitative input from numerical simulations, or SCF fluctuation calculations [287], one can identify the unstable directions of a saddle point and stabilize them by applying a suitable constraint. Such a constraint, for instance, can be a restriction on the symmetry of the segment density distribution, or a direct constraint on the field variables.

As an example, consider nucleation of a hole in a bilayer membrane. First, we confine the possible solutions to be axially symmetric, and to have a mirror symmetry with respect to the bilayer mid-plane. We further constrain the possible segmental density field configurations by requiring that in the bilayer mid-plane, the interface between the hydrophilic and hydrophobic segments be localized along a circle of some prescribed radius, which plays the role of a reaction coordinate. This constraint can be imposed via a Lagrange multiplier field and results in a minimal modification of the usual set of SCF equations. In general, for an arbitrary value of the constraint, the value of the corresponding Lagrange multiplier field is non-zero, which means that the corresponding configuration of the system is not a solution of the original unconstrained problem. Therefore the details as to how the constraint is applied matters. Nevertheless, exactly at the points where the Lagrange multiplier field vanishes, the solutions coincide with those of the unconstrained system, and it is an extremum, a minimum, of the free energy along the reaction coordinate path, i.e., these points are intermediate states. Furthermore, an extremum which is a maximum of the free energy along the reaction coordinate path, corresponds to a saddle point of the unconstrained problem, i.e. to the transition states of the system along the

considered reaction coordinate. This approach provides a wealth of additional information that cannot be accessed by the standard, non-constrained, calculations.

Yet another approach that uses the collective density degrees of freedom as the basic degrees of freedom is the Density Functional Theory (DFT). This formalism has its roots in the quantum many-body theory, where it is widely used for calculating electronic structure of many-atomic systems. Similar ideas have been applied to the description of simple classical fluids, in particular to the studies of vapor-liquid and liquid-solid interfaces, nucleation of new phases (see Ref. [313] for an application to hole nucleation in amphiphilic bilayers), and solvation of extended solutes. One of the major advantages of this approach is the systematic incorporation of liquid state packing effects on the level of segments. Chandler and co-workers [314] have developed an approach to study properties of inhomogeneous molecular systems, which combines molecular simulations and DFT. Despite the fact that the DFT is formally an exact framework it is limited by the accuracy of the approximate density functional. The common approach to construct an approximate density functional relies on mean-molecular field ideas, similar to those utilized in the SCF framework [255]. In particular, the interacting many-particle problem is reduced to that of a reference system consisting of non-interacting particles in an effective external field chosen so that it results in distributions equivalent to those in the original interacting system. Not surprisingly, in complete analogy with the SCF theory, the problem can be divided into two coupled sub-problems. First, one determines the mean-molecular fields produced by a given density distributions. Second, one evaluates the thermal averages of the density operators in the presence of these fields. The major difference between the DFT and SCF theory approaches lies in the microscopic details utilized to obtain the expressions for the mean-molecular fields. In particular, in the DFT framework, the fields are customarily obtained within a linear response theory of a bulk uniform fluid to a weak perturbation. For example [315, 316], the mean-molecular field $w_\alpha(\mathbf{r})$ acting on a segment of type α can be approximated by

$$w_\alpha(\mathbf{r}) = V_\alpha(\mathbf{r}) - \sum_\beta \int d\mathbf{r}' c_{\alpha\beta}^{\mathrm{bulk}}(\mathbf{r}-\mathbf{r}') \left[\rho_\beta(\mathbf{r}') - \rho_\beta^{\mathrm{bulk}}\right], \tag{49}$$

where $\rho_\beta(\mathbf{r}')$ and $\rho_\beta^{\mathrm{bulk}}$ are the local density and the bulk density of site type β, respectively, $V_\alpha(\mathbf{r})$ denotes the "bare" external fields (e.g., interactions with confining surfaces) and $c_{\alpha\beta}^{\mathrm{bulk}}(\mathbf{r}-\mathbf{r}')$ is the bulk direct correlation function between segments of the types α and β. The direct correlation function provides information about microscopic pair correlations in the system. In the mesoscopic SCF approaches discussed above, these microscopic correlations are usually treated on more phenomenological grounds and replaced by a simple contact interaction. The additional microscopic detail of the DFT approaches comes with the additional cost of calculating the direct correlation functions of a molecular fluid. This can be obtained either from simulations (see Eq. 37) or from various integral equation approaches. Despite the much more elaborate microscopic input to the DFT framework, it is *a priori* not clear whether the density functional itself, obtained in the linear response approximation, is accurate in the strongly inhomogeneous systems such as self-assembled bilayer membranes. More sophisticated relations between fields and densities have been utilized, e.g., to capture the equation of state of polymers in bad solvents [317, 318, 319] or the local structure of the segment fluid [320, 321].

Frink et al. applied the DFT approach to study coarse-grained lipid bilayers [322] using a freely jointed chain model for the lipid tails. The direct correlation functions of the bulk disordered system were obtained from the polymer reference interaction site model (P-RISM) [323, 324, 325, 326] in conjunction with the Percus-Yevick closure. Additional single chain Monte Carlo simulations had to be performed to obtain the intramolecular structure factor, which is a necessary input to the P-RISM approach. The bilayer solutions obtained with this

DFT framework have structural properties that are in a reasonable agreement with experimental DPPC data. Interestingly, the model even predicts a highly ordered bilayer phase at a sufficiently low temperature, which has an apparent resemblance to the ordered gel phase, L_β. Nevertheless, the disorder-order transition appears to be continuous, in contradiction with the experimentally observed first-order main chain transition. The reason for this discrepancy presumably lies in the high entropy of the flexible chain model. A more accurate treatment would require the inclusion of chain stiffness to properly describe the main chain transition. Furthermore, in their comparison of this DFT approach to the MD simulations of the same model system, Frischknecht et al. [327] found no ordering transition in the latter at all. Therefore, despite the overall agreement with the MD simulations at relatively high temperatures, it seems that the DFT approach can become qualitatively inaccurate at low temperatures.

2.4. Phenomenological Hamiltonians

While the coarse-grained models discussed above retain the notion of lipid molecules, phenomenological Hamiltonians take the coarse-graining idea one step further and describe the configuration by the collective density of hydrophilic and hydrophobic entities or the spatial position of interfaces. These approaches address the universal properties of amphiphilic systems, and are stripped down to essential ingredients. This permits a study of wide parameter ranges, and a systematic exploration of universal properties and mechanisms. The form of the Hamiltonian is usually dictated by symmetry considerations. The few parameters of the Hamiltonian can be established through comparison of simple properties which result from the calculation, such as interface tension or fluctuation spectra, either with experiments or with simulation results of more detailed models. Two major approaches can be distinguished: (i) Ginzburg-Landau type models which describe the system via collective densities of hydrophilic and hydrophobic entities, (ii) Helfrich Hamiltonians which conceive of the system as an assembly of infinitely thin interfaces characterized by their elastic constants. We briefly discuss both approaches in turn.

2.4.1. Ginzburg-Landau type models

Ginzburg-Landau type models resemble the field-theoretic approach summarized above because they describe the system via collective densities. Their staring point is a free energy functional $\mathcal{H}[\phi]$ that, in the simplest case, describes the free energy of a system with a spatially varying distribution of hydrophilic particles. Within the Random Phase Approximation [4] one can derive such a Hamiltonian from the field-theoretic formulation of a microscopic model. This technique is useful for rationalizing the general form of the Hamiltonian, but the assumption of weak segregation between hydrophilic and hydrophobic entities inherent in the Random Phase Approximation is not valid in biological systems. Hence the approach is often quantitatively unreliable. Typically, the Hamiltonian is constructed via an expansion in terms of an order parameter such as the difference between hydrophilic and hydrophobic densities, $\phi(\mathbf{r})$, and its spatial derivatives, $\nabla\phi$. Only the lowest terms consistent with isotropy of space are retained;

$$\mathcal{H}[\phi] = \int \mathrm{d}^3\mathbf{r} \ \left[f(\phi) + g(\phi)(\nabla\phi)^2 + c(\nabla^2\phi)^2 \right] \tag{50}$$

The function $f(\phi)$ determines the phases of the homogeneous system. Generically, it exhibits two or more minima. The function f can take the form of a polynomial, as in the original Ginzburg-Landau model of phase separation, or the form of a piecewise parabolic function of ϕ [328]. The second term determines the free energy costs of interfaces. In phases characterized by an *extensive* amount of interface, such as a microemulsion, the coefficient in this term must become negative, at least for some composition range, in order to generate these stable interfaces.

The third term with $c > 0$ guarantees that spatial variation in the order parameter will not grow indefinitely, and therefore ensures the stability of the system.

Although simple, this form of Hamiltonian suffices to reproduce many structures observed in lipid-water mixtures including disordered structures like microemulsions and complex periodic phases like the gyroid morphology [329]. Typically, the spatial derivatives are discretized on a regular cubic lattice. Then, the densities at the different lattice nodes are the degrees of freedom and the derivatives give rise to nearest and next-nearest neighbor interactions. The statistical mechanics of the model can be studied with Monte Carlo simulations [330] which includes thermal fluctuations. The fluctuations are important, e.g., for the formation of microemulsions. Alternatively, one seeks spatially modulated structures that minimize the Hamiltonian, and thereby one ignores fluctuations [329].

The attractive features of this type of model is the computational ease with which fluctuations or complex spatial structures can be investigated. Rather large systems can be studied over a wide parameter range, and often one can obtain analytic solutions in various asymptotic regimes. The connection between the model parameters and biological systems often remains qualitative, and we shall not discuss this approach further but rather refer to a comprehensive review [149].

2.4.2. Helfrich's curvature Hamiltonian and its numerical implementation

Another popular description consists of describing a membrane as an infinitely thin sheet that is characterized by a small number of elastic properties: spontaneous curvature and bending moduli. These coarse-grained parameters encode the architecture of the constituent lipids and the way they pack in the bilayer. In its simplest form the Hamiltonian is written as an expansion in the invariants that can be constructed from the local principal curvatures, C_1 and C_2 [331, 332, 333]:

$$\mathcal{H} = \int \mathrm{d}^2 A \, \left(\gamma + \frac{\kappa_b}{2}(C_1 + C_2 - C_0)^2 + \bar{\kappa} C_1 C_2 \right) \tag{51}$$

where C_0 is denoted the spontaneous curvature, and the integration is extended over the entire surface. The coefficient γ is the lateral membrane tension, κ_b and $\bar{\kappa}$ are the bending rigidity and saddle-splay modulus. This expansion is appropriate if the curvature is small compared to the characteristic curvature set by the inverse bilayer thickness or additional non-linear elastic effects. For homogeneous membranes of fixed topology, the integral over the Gaussian curvature, $C_1 C_2$, is an invariant (Gauss-Bonnet theorem), and the term proportional to $\bar{\kappa}$ contributes only a constant. The saddle-splay modulus is, however, important if the membrane topology changes, e.g., pore formation, fusion or fission. Membranes are often characterized as being tensionless, i.e., by $\gamma = 0$. In this case, one can constrain the average membrane area to a fixed value, A_0, and utilize a term that is proportional to the square of the deviation of the membrane area, A, from it,

$$\Delta\mathcal{H}_A = \frac{\kappa_a}{2}(A - A_0)^2 \tag{52}$$

to describe the small area compressibility of the membrane. Such a model is able to describe successfully the large-length scale behavior of interfaces, membranes, and vesicles and their fluctuations. It has been the starting point for analytical calculations, such as the renormalization of elastic constants by fluctuations of the local membrane position [334]. Furthermore, the model can very efficiently be studied by computer simulations. Much effort has been focused on exploring, for instance, the shape of vesicles and their fluctuations [335, 336, 337, 338, 339, 52, 340, 341, 342, 343, 344, 345].

There also have been attempts to successively incorporate more local details into the description by first applying the curvature Hamiltonian to each monolayer of a bilayer membrane and

then to augment it by terms that account for the tilting of hydrocarbon tails [346, 347]. These techniques have been applied to estimate the free energy of localized, highly curved membrane structures as they occur at the edge of a bilayer [348] or in morphological changes of the bilayer structure, e.g., in transitions from the micellar to the inverted hexagonal phase [346] or in the fusion of membranes [349, 350, 351, 352]. The description of topological changes, e.g., pore formation, is difficult, however.

One important simplification of the general curvature Hamiltonian (51) is achieved when overhangs of the membrane can be neglected. In this case the sheet can be described by a single-valued function, $z = h(x, y)$. In this Monge representation the mean and Gaussian curvature, H and K, are given by

$$H = \frac{C_1 + C_2}{2} = \frac{(1 + h_x^2)h_{yy} + (1 + h_y^2)h_{xx} - 2h_x h_y h_{xy}}{2(1 + h_x^2 + h_y^2)^{3/2}} \tag{53}$$

and

$$K = \frac{h_{xx}h_{yy} - h_{xy}^2}{(1 + h_x^2 + h_y^2)^2} \tag{54}$$

where $h_x \equiv \partial h/\partial x$ denote the derivative with respect to one of the two lateral coordinates.

If the amplitude of fluctuations are small, then one can approximate $2H \approx h_{xx} + h_{yy} = \triangle h$ and Eq. (51) takes the simple form (with $C_0 = 0$):

$$\mathcal{H} \approx \int \mathrm{d}x\mathrm{d}y \sqrt{1 + h_x^2 + h_y^2} \left(\gamma + \frac{\kappa}{2}(\triangle h)^2 \right) \tag{55}$$

$$\approx \gamma A + \int \mathrm{d}x\mathrm{d}y \left(\frac{\gamma}{2}|\nabla h|^2 + \frac{\kappa}{2}(\triangle h)^2 \right) \tag{56}$$

Often this approximation is utilized to extract the interface tension and bending rigidity from computer simulations of small membrane patches [353, 137, 111, 354, 174, 17, 182, 355]. To this end, one determines the local position of the membrane, $h(x, y)$, from the simulation. Utilizing the Fourier spectrum of interface fluctuations, $h(\mathbf{k})$,

$$h(\mathbf{x}) = \frac{1}{L^2} \sum_{\mathbf{k}} h(\mathbf{k}) \exp[i\mathbf{k} \cdot \mathbf{x}] = \frac{1}{(2\pi)^2} \int \mathrm{d}^2\mathbf{k}\, h(\mathbf{k}) \exp[i\mathbf{k} \cdot \mathbf{x}] \tag{57}$$

$$h(\mathbf{k}) = \int \mathrm{d}^2\mathbf{x}\, h(\mathbf{x}) \exp[-i\mathbf{k} \cdot \mathbf{x}] \tag{58}$$

one diagonalizes the Hamiltonian (56)

$$\mathcal{H}[h(\mathbf{k})] = \frac{1}{(2\pi)^2} \int \mathrm{d}^2\mathbf{k} \, \left(\frac{\gamma}{2}k^2 + \frac{\kappa}{2}k^4 \right) |h(\mathbf{k})|^2 = \frac{1}{L^2} \sum_{\mathbf{k}} \left(\frac{\gamma}{2}k^2 + \frac{\kappa}{2}k^4 \right) |h(\mathbf{k})|^2 \tag{59}$$

which shows that the different Fourier modes of the local interface position are independent. The statistical mechanics of the interface position can be described by the partition function

$$\mathcal{Z}_{\mathrm{int}} = \int \mathcal{D}h \, \exp\left[-\frac{\mathcal{H}[h]}{k_B T} \right] \tag{60}$$

where the functional integral $\int \mathcal{D}h$ sums over all local positions of the interface. Since the Hamiltonian is the sum of independent, harmonic degrees of freedom, $h(\mathbf{k})$, the Fourier modes are uncorrelated and Gaussian distributed around zero. Their variance is given by the equipartition theorem:

$$\frac{1}{L^2} \left(\gamma k^2 + \kappa k^4 \right) \langle |h(\mathbf{k})|^2 \rangle = k_B T \tag{61}$$

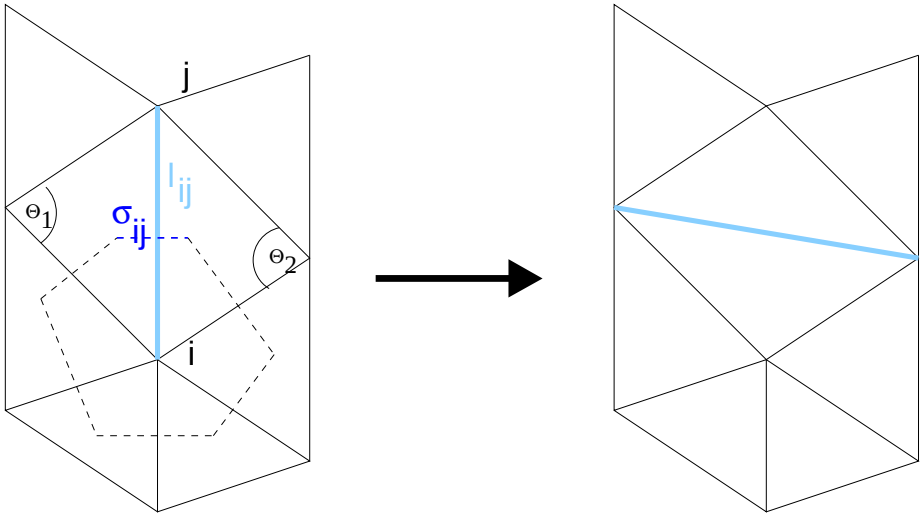

Figure 5. Dynamic triangulation of fluid membranes. The bonds between vertices i and j has length l_{ij}, and the length of the dual tether, σ_{ij} is indicated. The bond that connects vertices i and j is flipped. In order to conserve the triangular nature of the network each vertex must initially be connected to at least four neighbors.

On short length scales, $k > (\gamma/\kappa)^{1/2}$, the bending stiffness dominates and $|h(k)|^2 \sim k^{-4}$. The large scale fluctuations are controlled by the surface tension, γ, and obey $|h(k)|^2 \sim k^{-2}$. This method has successfully been employed to extract the tension and bending rigidity from simulations of interfaces in polymer blends [159, 356, 357], polymer-solvent interfaces [317] liquid crystals [358, 359], and lipid bilayers [353, 137, 111, 354, 174, 17, 182, 355]. To do so, one numerically determines the position, h, of the interface, or bilayer, in sub-columns centered around (x_i, y_j) and with lateral size Δ (block analysis [360, 356]). The distance between the grid points, Δ, is a compromise: if the discretization is too fine, the instantaneous composition profile along a column will strongly fluctuate. Composition fluctuations may affect the estimate of the interface position. If Δ is too large, however, the Fourier modes with large wavevector are averaged out and the spectrum is underestimated. This spectral damping is a function of the product of the spatial resolution Δ and the wavevector q. It only becomes irrelevant in the limit $\Delta q \ll 1$. Cooke and Deserno [175] explicitly calculated the strength of the spectral damping assuming that the smooth interface location is averaged inside each column. In this case, the spectrum of the grid-averaged fluctuations $h(\mathbf{k})_{\text{grid}}$ and the original spectrum, $h(\mathbf{k})$ are related via

$$|h(\mathbf{k})_{\text{grid}}|^2 = |h(\mathbf{k})|^2 \left[\frac{\sin(\Delta k_x/2)}{(\Delta k_x/2)} \frac{\sin(\Delta k_y/2)}{(\Delta k_x/2)}\right]^2 \tag{62}$$

This discretization artifact becomes important when the fluctuation spectrum of very small membrane patches is studied by atomistic simulations or when the crossover between the tension-dominated and bending rigidity-dominated part of the spectrum occurs at rather large wave vectors (i.e., $\gamma > 0$). A possible way to deal with these discretization artifacts is to divide out the *a priori*, k-dependent spectral damping factor.

The full Hamiltonian of Eq. (51) has to be used to describe large amplitude fluctuations of microemulsions and of closed vesicles. To this end one triangulates the surface. A typical snapshot is presented on the right hand side of Fig. 1. The vertices are connected by tethers that define the internal topology of the sheet. If the topology is fixed, the membrane will exhibit only elastic response that is characteristic, *inter alia*, of polymerized membranes. If one allows for changes of the internal topology in the course of the simulation (dynamic triangulation) [361, 336, 362], one can mimic the in-plane fluidity. The vertices diffuse in this fluid membrane. A common strategy consists in cutting and re-attaching tethers between the four beads of two neighboring triangles. Such an elementary move is sketched in Fig. 5.

The self-avoidance of the membrane is modeled by an excluded volume interaction between vertices at positions, $\mathbf{R}_i$. The strength and range of the excluded volume interaction and the interactions along tethers can be chosen so as to avoid crossings. Let $\mathbf{n}_i$ denote the surface normal of a triangle, i. The discretization of the mean curvature, $H = \mathbf{n} \cdot \triangle\mathbf{R}$ at vertex i takes the form

$$H_i = \frac{1}{\sigma_i}\mathbf{n}_i \cdot \sum_{j\in n.n.(i)} \frac{\sigma_{ij}}{l_{ij}}(\mathbf{R}_i - \mathbf{R}_j) \tag{63}$$

where the sum runs over all tethers ij that are connected to the vertex i. The length of such a tether is l_{ij}, $\sigma_{ij} = l_{ij}(\cot\Theta_1 + \cot\Theta_2)/2$ is the length of the corresponding tether in the dual lattice which is created from the intersections of the perpendicular bisectors of the bonds. Θ_1 and Θ_2 are the angles opposite to the link ij in the two triangles that border the link. The quantity $\sigma_i = \frac{1}{4}\sum_{j\in n.n.(i)} \sigma_{ij} l_{ij}$ represents the area of the virtual dual cell. Using this expression and the fact that the local normal $\mathbf{n}$ is collinear to $\triangle\mathbf{R}$ in three dimensional space, one obtains

$$\mathcal{H} = \frac{\kappa}{2}\int \mathrm{d}^2A\, H^2 = \frac{\kappa}{2}\int \mathrm{d}^2A\, (\triangle\mathbf{R})^2 \tag{64}$$

$$= \frac{\kappa}{2}\sum_i \frac{1}{\sigma_i}\left[\sum_{j\in n.n.(i)} \frac{\sigma_{ij}}{l_{ij}}(\mathbf{R}_i - \mathbf{R}_j)\right]^2 \tag{65}$$

for $\gamma = 0$. We have omitted the integral over the Gaussian curvature which does not depend on the membrane configuration if the the topology is preserved.

If one assumes that all triangles are equilateral, $\sigma_{ij} = l_{ij}/\sqrt{3}$, the equation above reduces to

$$\mathcal{H} = \frac{\sqrt{3}\kappa}{2}\sum_{\langle\alpha,\beta\rangle} (\mathbf{n}_\alpha - \mathbf{n}_\beta)^2 = \sqrt{3}\kappa \sum_{\langle\alpha,\beta\rangle} (1 - \mathbf{n}_\alpha \cdot \mathbf{n}_\beta) \tag{66}$$

where $\mathbf{n}_\alpha$ denotes the normal vector of the triangle α. In the general case of randomly triangulated surfaces, however, this latter expression suffers from deficiencies. Most intriguingly, use of the expression (66) for a randomly triangulated sphere recovers the expected result, while a random triangulation of the cylinder in conjunction with Eq. (66) fails to yield the result of the continuum description [363].

Generalizations of this class of models have be utilized to study freezing of vesicles [364, 365] or mixed membranes [366, 367]. These models can also be employed in conjunction with a hydrodynamic description of the surrounding solvent [340, 368, 369, 370].

3. An example of an integrated approach: fusion of membranes

3.1. Motivation and open questions

One example of a collective phenomena in membranes is the fusion of two apposing lipid bilayers. It is a basic ingredient in a multitude of important biological processes ranging from

synaptic release, viral infection, endo- and exocytosis, trafficking within the cell, and fertilization [24, 25, 26, 27, 28, 29, 30]. The fusion process can be roughly divided into two steps [30]: first the two membranes to be fused are brought into close apposition. Fusion peptides embedded in the membranes play an important role during this initial step. They ensure that only specific membranes are brought into close proximity with one another. One way to accomplish this is for a fusion protein, embedded in one of the membranes, to be is inserted into the apposing membrane, followed by a conformational change of the protein. This active mechanism imparts energy into the system. The specific role of proteins in the fusion process, their spatial arrangement and conformational changes, have attracted much interest for they are of great importance in regulating fusion [27, 371]. The second step consists of the fusion event itself in which the topology changes from two apposing bilayer of two vesicles to a fusion pore in a now-single vesicle. There is evidence that this second step is dictated by the amphiphilic nature of the bilayer constituents [372, 26, 373], for fusion occurs in very different systems ranging from tiny, highly curved, synaptic vesicles to whole cells. Moreover, sophisticated fusion peptides are not necessary to initiate fusion between laboratory vesicles. The simple depletion force that arises on the addition of water-soluble polymer (polyethylene glycol, PEG) to a vesicle solution [374, 375, 376], shear [377], or sonication [377] serve equally well in inducing it. Another important piece of evidence comes from synthetic, polymer-based, membranes made of amphiphilic polymers [378, 162, 379, 380, 381, 382]. The behavior of these polymersomes resembles those of the much smaller and more fragile vesicles comprised of biological lipids and, in the absence of proteins, includes processes like fusion and fission [379, 377]. This all suggests that fusion is a universal collective phenomenon. Therefore coarse-grained models are well-suited to investigate its underlying mechanism.

While many specific details are known about the first step of the fusion process, much less is known about the second. Generally, fusion is considered a "messy" process because of the drastic disruption of the bilayers' integrity. The time and length scales exclude a direct experimental observation of an individual fusion event. However even in the absence of direct information about the fusion intermediate, much can be inferred from a systematic variation of parameters (e.g., composition of mixed bilayers, or tension), and careful experimental techniques (e.g., electrophysiological measurements of membrane conductance). Some of the main experimental observations are:

1. Lipids that favor a large negative spontaneous curvature of a monolayer, such as DOPE, increase the fusion rate [24, 383].

2. Increasing the tension of the apposed membranes results in an increased fusion rate [384].

3. During fusion, the lipids in the two apposing *cis* leaves mix [375, 372, 385].

4. In some experiments, fusion is leaky. This implies that, correlated in space and time with the fusion event, there is a passage from the interior of the vesicle to the outside solution [386, 387, 388, 389, 390].

5. Some experiments report on the transient mixing of lipids between the *cis*, or most closely apposed, leaf and the *trans*, or farther leaf, of the other membrane [376, 375]. This process is much faster than the flip-flop tunneling of lipids from one leaf to the other in an intact membrane.

The first three observations can be rationalized by the classical model of membrane fusion proposed by Kozlov and Markin in 1983 [391, 392]. They *conjectured* a fusion pathway and

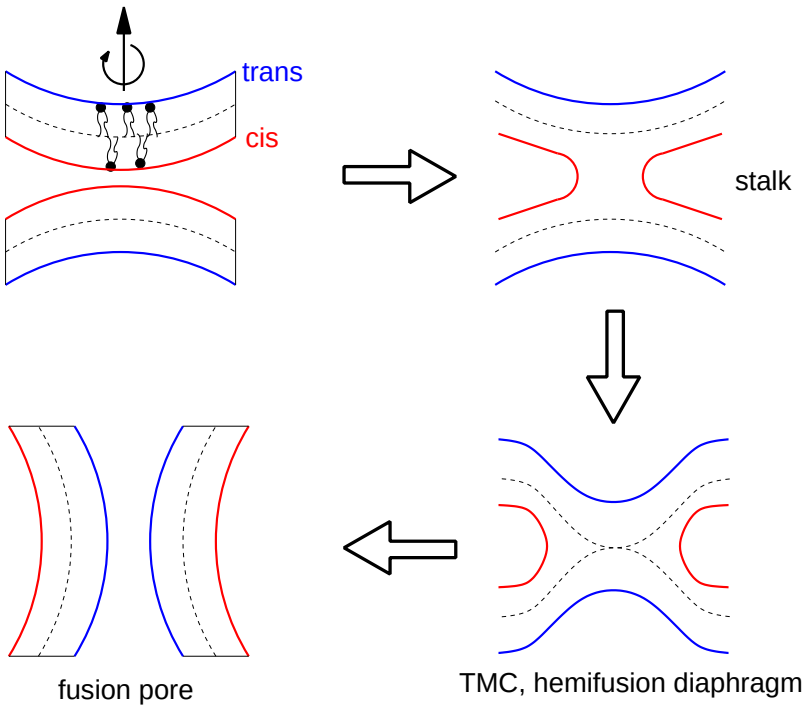

Figure 6. Sketch of the classical fusion path.

calculated the free energy barrier utilizing an effective interface Hamiltonian. The monolayers of the membranes were modeled as thin elastic sheets, and the description was augmented by a free energy penalty for the packing difficulties that arise in the intermediate structures.

In their model the proper fusion process starts with the formation of a stalk (see Fig. 6), a rotationally symmetric connection between the two apposing *cis* monolayers. Once the stalk has formed, the two inner *cis* leaves retract from it leaving a transmembrane contact that consists of a small circular membrane patch built from the two outer *trans* leaves. This transmembrane contact can expand radially to form an extended hemifusion diaphragm. The rupture of this diaphragm creates a fusion pore. The expansion of the fusion pore completes the process. The classical fusion model is able to rationalize the first three observations. (1) Lipids that favor a large negative curvature of a monolayer tend to form an inverted hexagonal phase, and this non-lamellar morphology shares common local geometrical features with the stalk intermediate. (2) An increase of the lateral membrane tension, or free energy per unit area makes more favorable the decrease in membrane area which fusion brings about. (3) The stalk and the outer rim of the hemifusion diaphragm establish a connection between the two inner *cis* leaves along which lipids between the two *cis* monolayers can mix by diffusion. The last two experimental findings, however, cannot be explained. At no time during the classical fusion scenario is there a path between the inside of either vesicle and the outside solution. Also there is never any direct connection between the inner and outer monolayers of a bilayer membrane.

The geometry of the stalk intermediate and the free energy penalty associated with the packing frustration of the hydrocarbon tails is an input into the classical model. Earlier calculations used a toroidal shape of the stalk, and assumed that the thickness of the monolayers remained

constant as a void formed. An *ad-hoc* upper limit of the free energy costs of chain packing was obtained utilizing the macroscopic surface tension of hydrocarbons. The total free energy barrier associated with the formation of a stalk was estimated to be 200 k_BT, a value much too large for fusion to occur in soft matter systems [393]. Subsequent refinements of the model utilizing a catenoid shape and including tilt and splay of the hydrocarbon tails solved this "energy crisis" [349, 352] and yielded a significantly lower barrier of 30 to 40 k_BT. The large variation of the estimated barrier with the assumptions of the model suggests that the effective Hamiltonian representing the monolayers as thin elastic sheets might not be able to accurately describe the highly bent structures of the intermediate. Models that retain the notion of amphiphilic molecules, that incorporate the packing of the molecular conformations in non-lamellar geometries, and that do not assume the structure of the fusion intermediates, are better suited to provide direct insights.

3.2. Model and techniques

By virtue of the experimentally observed universality of the proper fusion event, and due to the concomitant time and length scales that are unattainable with atomistically detailed models, coarse-grained models are well-suited to investigate the basic mechanism of membrane fusion. Ideally, such a coarse-grained model would combine the following characteristics:

1. It describes the architecture of the amphiphilic molecules. The parameters of the model are directly related to experimentally measurable characteristics. The change of the molecular conformations and the associated loss of entropy in a non-planar environment can be calculated.

2. It can be used to observe whether the fusion event does, or does not, occur without prior assumptions about the pathway.

3. It can be solved with a computational technique which permits one to simulate a number of independent fusion events. Note that in experiment, several different outcomes of an encounter between two vesicles can be observed, e.g., adhesion, complete fusion, or rupture.

4. Its various parameters, such as the lipid architecture and thermodynamic conditions, can be explored, and the free energy of the fusion intermediates can be calculated.

The first requirement is best met by a detailed model that mimics as much of the local structure of the bilayer and the surrounding solvent as possible. Such models, however, are computationally very expensive and do not permit the systematic exploration of the fusion process or the calculation of free energy barriers.

In our own investigation, we have chosen the bond fluctuation model (cf. Sec. 2.2). Coarse-grained models strike a balance between specificity of description and efficiency of computation. The bond fluctuation model, in which the amphiphiles are modeled as diblock copolymers on a cubic lattice and the solvent consists of homopolymers of identical length, is certainly one of the coarser, and therefore more computationally efficient, models. Although the model captures only the universal amphiphilic characteristics of the membrane components, it provides a reasonable description of bilayer properties (cf. Tab. 1). This efficient model allowed us to study rather large systems that contain several thousand amphiphiles, and to observe thirty-two fusion events for one set of parameters. Besides computational efficiency, the model has two additional advantages: (1) Much is known about the properties of the model, e.g., interface tension, bilayer compressibility, phase behavior, spectrum of interface fluctuations, etc. (2) The model can be quantitatively compared to the standard Gaussian chain model of the SCF theory without

any adjustable parameter. We use Monte Carlo simulations [51, 161] to provide an unbiased insight into the fusion pathway. Once this is attained, we perform extensive SCF calculations [311, 312] of the same model in order to obtain the free energies of intermediates over a wide range of parameters.

3.3. MC simulation

3.3.1. Separation of time scales

Our Monte Carlo simulations are performed in the canonical ensemble [51, 161]. The molecular conformations are updated by local segment displacements and slithering-snake-like movements. These movements conserve the local densities and thus lead to a diffusive behavior on large length scales. Moreover, the molecules cannot cross each other during their diffusive motion. In this sense we have a slightly more realistic time evolution on local length scales than in dissipative particle dynamics simulations [142], but Monte Carlo simulations cannot include hydrodynamic flow, which might become important on large length scales. We count one attempted local displacement per segment and three slithering-snake-like attempts per molecule as four Monte Carlo steps (MCS). This scheme relaxes the molecular conformation rather efficiently [394]. The time scale of the MC simulations can be compared to experiments by matching the self-diffusion coefficient of the lipids in a single bilayer (see below). At any rate, we do not expect the time sequence to differ qualitatively from that of a simulation with a more realistic dynamics on time scales much larger than a single Monte Carlo step. Most importantly, fusion is thought to be an activated process. Therefore the rate of fusion is dominated by free energy barriers encountered along the fusion pathway, while the details of the dynamics only set the absolute time scale.

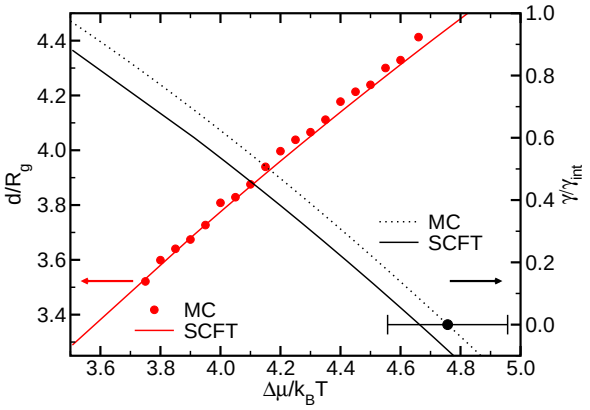

Figure 7. Total thickness of the bilayer membrane, d, measured in units of the radius of gyration, $R_g \approx 7u$, vs. the exchange chemical potential $\Delta\mu$ between amphiphiles and solvent molecules. Membrane tension, γ, as a function of exchange potential, $\Delta\mu$, is shown on the right scale.

We begin our simulation by preassembling flat, tense, bilayers. The tension is dictated by the areal density of amphiphiles, i.e., the thickness of the membrane (cf. Fig. 7). In the lattice MC simulations we cannot simulate at constant pressure or surface tension (which is routinely used in off-lattice models [395, 396]) because the size of the simulation box cannot be changed continuously. The lattice also prevents us from measuring the pressure or tension via the virial

expression (cf. Eq. (33)) or the anisotropy of the virial of the forces. The thickness of a tensionless membrane, however, can be measured by simulating a bilayer patch that spans the periodic boundary conditions of the simulation cell in only one direction but exhibits a free edge in the other direction. The area of the bilayer then will adjust so as to establish zero tension and the thickness can readily be measured in the center of the bilayer patch. Such a tensionless configuration is shown in the middle of Fig. 1.

The dependence of the tension on the exchange potential, $\Delta\mu$, between amphiphiles and solvent can be obtained by simulations in the grand-canonical ensemble where the density is constant but, in addition to the MC moves that renew the molecules' conformations, one "mutates" amphiphiles into solvent molecules and vice versa [397, 398]. These moves change the composition of the system while the thermodynamically conjugate variable, the exchange potential $\Delta\mu$, is controlled.

The excess free energy per unit area, in the thermodynamic limit of infinite area, defines the lateral membrane tension

$$\begin{aligned} \gamma(T,\Delta\mu) &\equiv \lim_{A\to\infty} \frac{\delta\Omega_m(T,\Delta\mu,A)}{A}, \qquad \text{with} \\ \delta\Omega_m(T,\Delta\mu,\mathcal{A}) &\equiv \Omega_m(T,\Delta\mu,V,\mathcal{A}) - \Omega_0(T,\Delta\mu,V) \end{aligned} \tag{67}$$

where A denotes the area of the membrane, and Ω_m and Ω_0 the grand canonical free energy of the system with and without membrane, respectively. In an incompressible system the tension γ can be related to the temperature and chemical potential by means of the Gibbs-Duhem equation

$$\mathrm{d}\gamma(T,\Delta\mu) = -\delta s \ \mathrm{d}T - \delta\sigma_a \mathrm{d}(\Delta\mu), \tag{68}$$

where δs is the excess entropy per unit area, and $\delta\sigma_a$ is the excess number of amphiphilic molecules per unit area. This relation can be exploited to integrate the thickness of the bilayer $d = \sigma_a N/\rho$ with respect to the exchange potential $\Delta\mu$ at constant temperature and calculate the change of the membrane tension [353]. Using the tensionless state as staring point we obtain the relation between the membrane thickness, d and the tension, γ as shown in Fig. 7.

After the bilayer has assembled without defects in a thin film geometry, we stack two bilayers on top of each other with a distance Δ between them. The system of two apposing bilayers is embedded into a three dimensional simulation cell with periodic boundary conditions in all three directions. Configuration bias MC moves [399, 400, 401] are utilized to fill the remaining volume with homopolymer solvent. This starting configuration of flat bilayers mimics the approach of two vesicles whose radii of curvature are much larger than the patch of membrane needed for fusion. Then we let the system evolve and observe the fusion process in the simulation.

Because fusion is a kinetic, irreversible process, the starting condition might have a pronounced influence on the outcome. In Fig. 8 we present the internal energy of the system as a function of MC steps on a logarithmic scale. Immediately after the assembly of the two bilayer system, one observes a rapid decrease of the energy. This corresponds to the relaxation of the bilayer structure after the insertion of the solvent. After $\tau_R \approx 25000$ MCS ($\approx$ 9ns, see below), however, the local internal structure of the bilayer has equilibrated and the energy starts to rise very slowly. This increase is compatible with a logarithmic growth law and stems from thermally excited interface fluctuations that increase the area of the hydrophilic-hydrophobic interface. At the end of this stage, stalks and holes are formed in the simulations. (Here and in the following, we denote a pore across a single bilayer as a "hole" in contrast to the "fusion pore" that spans both bilayers.) Finally, around $\tau_F \approx 8 \cdot 10^6$ MCS, the energy suddenly drops indicating the formation of a fusion pore that reduces the total bilayer area and, therefore, the stored tension. The important point is that there is a difference of two orders of magnitudes between the relaxation

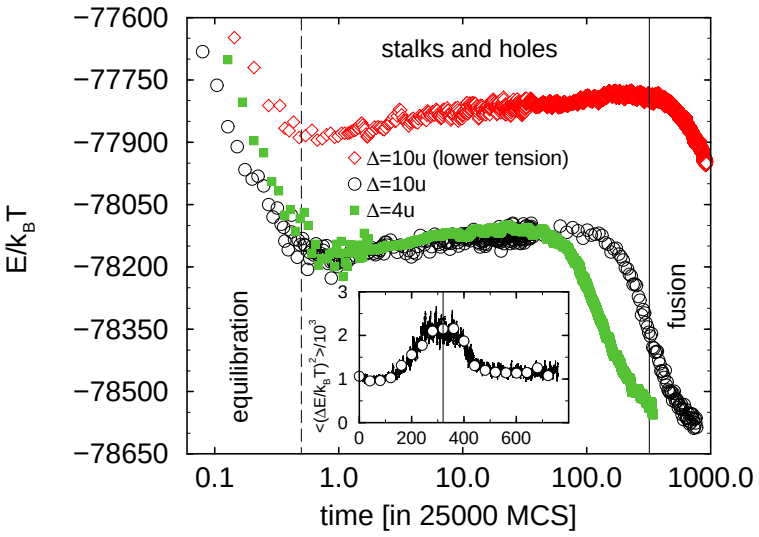

Figure 8. Evolution of internal energy in fusion simulations. The curves correspond to different initial bilayer separations $\Delta = 4u$ (squares) and $\Delta = 10u$ (circles) and bilayer tensions, $\gamma/\gamma_{\rm int} = 0.75$ and 0.375, respectively. To reduce fluctuations, the data are averaged over all 32 configurations at equal time and additionally over small time windows. The large negative value of the energy mirrors the attractive interactions in the solvent. The inset shows the sample-to-sample energy fluctuations as a function of time (for the system with high tension and large membrane separation). Large fluctuations identify the onset of fusion.

time of the local structure of an individual bilayer, and the time scale on which fusion occurs. Due to this separation of time scales between initial relaxation and fusion, we do not expect the preparation of the starting configuration to affect the irreversible fusion process. Similarly we do not expect our results to depend on our particular choice of relaxation moves, as other choices would also lead to relaxation of the bilayers which takes place on a much shorter time scale than does fusion.

The inset of Fig. 8 shows the fluctuations in the energy, i.e., the fluctuations between the thirty-two different runs at equal time. Strong fluctuations indicate energy differences between the independent runs. The peak at around $\tau_F \approx 8{\cdot}10^6$ MCS (for the system with high tension and large separation) indicates that some systems have already formed a fusion pore, and therefore have a lower energy, while other systems have only stalks and holes, and therefore have a higher energy. The width of the peak provides an estimate for the spread of the time during which a fusion pore appears. Specifically, for the system with the lower tension and large initial separation, at time $1.26 \cdot 10^7$ MCS we have observed the formation of stalks in 23 systems while 9 runs have already formed a fusion pore. At time $2.52 \cdot 10^7$ MCS, 20 runs have successfully completed fusion, in 3 configurations only stalks have formed and in 9 runs stalks and holes have appeared but the fusion has not been successfully completed. The figure shows data for two different bilayer tensions and two different distances between the bilayers. Increasing the bilayer tension, and reducing the bilayer distances accelerates the fusion process. Moreover, the slower the fusion process, the clearer is the transition state we observe. Fusion occurs around $8 \cdot 10^6$ MCS and $2 \cdot 10^7$ MCS for the systems at large separation and with high and low tension

respectively.

The lateral diffusion constant of a lipid in a single bilayer is $D \approx 10^{-4}u^2/\mathrm{MCS}$. If we identify the thickness $d_c = 21u$ of hydrophobic core in the tensionless state with 3nm and utilize a typical value for the self-diffusion coefficient of lipids in bilayer membranes, $D \approx 6 \cdot 10^6 \mathrm{nm}^2/\mathrm{s}$, we estimate that one MCS corresponds to 0.36 ps. Thus, the time scale on which we observe fusion is 3μs and 7μs for the tense and less tense bilayers, respectively. This estimate is about an order of magnitude larger than what is observed in the DPD simulations of Shillcock and Lipowsky [402] and about 2 orders of magnitude slower than the fusion process in the Lennard-Jones-type model of Smeijers et al [403]. In the latter study, however, the time scale was not estimated from the comparison of the lipid self-diffusion coefficient in a bilayer but directly from the time of the MD simulations without further rescaling which is likely to underestimate the duration of the fusion process [404].

Unless noted otherwise, we will discuss in the following the data for the larger tension and larger initial bilayer separation. The data for the lower tension are very similar.

An important property of the bilayer which we prepare is its tension, or free energy per unit area. Thermodynamically, a tense bilayer is only metastable, and will eventually rupture. Hole formation reduces the bilayer's area and lead to a stable, tensionless state. Hole formation is an activated process and, indeed, we do observe the rupture of isolated tense bilayers in very long simulation runs. Since vesicles have to be stable for long times in order to fulfill their carrier and enclosing function, it is reasonable to require that the time scale of hole formation and rupture, τ_H, of an isolated membrane be much larger than the times scale of fusion of two apposed bilayers. Yet in order to undergo fusion, just such long-lived holes must occur at some point along the fusion pathway. It would seem that vesicles could either be stable, or they could undergo fusion, but not both. The question that immediately arises is how membranes actually manage to exhibit these two conflicting properties. We return to this question in Sec. 4.

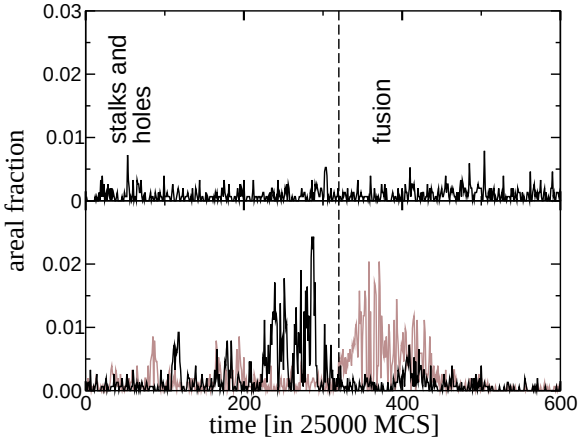

Figure 9. Area of holes vs. time in the system of two apposed bilayers (gray for one bilayer and black for the other on the bottom panel) and in an isolated bilayer (top panel). From Ref. [51]

In Fig. 9 we present time traces of the areal fraction of holes in an isolated tense bilayer and in the two apposed bilayer system. In the isolated bilayer, small holes form and close but the bilayer remains stable on the time scale of the fusion process. In the two apposed bilayer system, however, larger holes form more readily and their occurrence is correlated with the fusion event.

This additional MC data further supports the observation that in our coarse-grained model, there is a clear separation of time scales, $\tau_R \ll \tau_F \ll \tau_H$, between the local relaxation time of

bilayers, τ_R, the time scale, τ_F, to nucleate a fusion pore, and the lifetime of an isolated tense bilayer, τ_H.

3.3.2. Observed fusion pathways

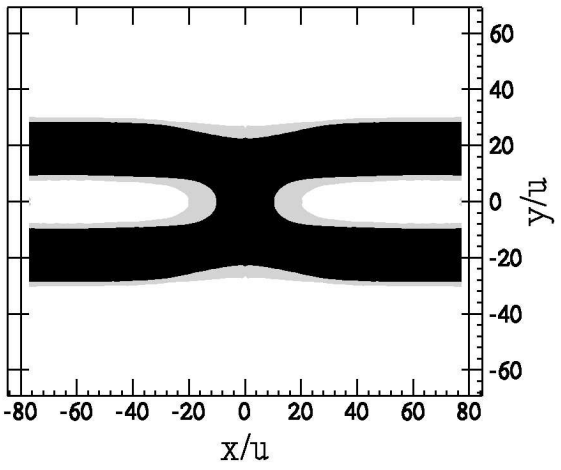

Figure 10. Density distribution of segments in the stalk, averaged over all 32 simulation runs. At each point only the majority component is shown: solvent as white, hydrophobic and hydrophilic segments of amphiphiles as black and gray respectively. From Ref. [51]

During the initial stage of simulations, interface fluctuations of the initially flat bilayers are thermally excited and the bilayers collide with one another. Sometimes these collisions give rise to small local interconnections. For the most part, these contacts are fleeting. Occasionally we observe sufficient rearrangement of the amphiphiles in each bilayer to form a configuration, the stalk, which connects the two bilayers. Once such a stalk has formed, it is rather stable on the time scale τ_F. Density profiles of the hydrophilic and hydrophobic parts of the amphiphiles in the presence of the stalk, obtained by averaging over configurations, are shown in Fig. 10. The dimples in the membranes at each end of the stalk axis are notable. What can barely be seen is a slight thinning of each bilayer a short distance from the axis of the stalk.

Under the specific conditions of our simulations we believe that stalks are only metastable. First, the observed stalks are isolated and their occurrence goes along with a rise of the internal energy. Second, occasionally we observe that stalks disappear without proceeding further to a fusion pore. This behavior indicates that the stalk represents a local (metastable) minimum along the fusion pathway. Once a stalk has formed, we observe that it elongates asymmetrically, and moves around in a worm-like manner. Evidently its elongation does not cost a great deal of free energy.

After stalks are formed, the rate of formation of holes in either of the two bilayers increases. Stalk and hole formation are not only correlated in time but also in space: Holes form close to the stalks. This can be quantified by the hole-stalk correlation function:

$$g(r) \equiv \frac{\sum_{r_s,r_h} \delta(|\mathbf{r}_s - \mathbf{r}_h| - r) P_{sh}(\mathbf{r}_s, \mathbf{r}_h)}{\sum_{r_s,r_h} \delta(|\mathbf{r}_s - \mathbf{r}_h| - r)} \tag{69}$$

where $P_{sh}(\mathbf{r}_s, \mathbf{r}_h)$ is the joint probability that the lateral position $\mathbf{r}_s$ is part of a stalk and $\mathbf{r}_h$ is part of a hole, and $\delta(r)$ is the Dirac delta function. The value of $g(r)$ at large distances r is proportional to the product of the areal fraction of holes and stalks. This correlation function is

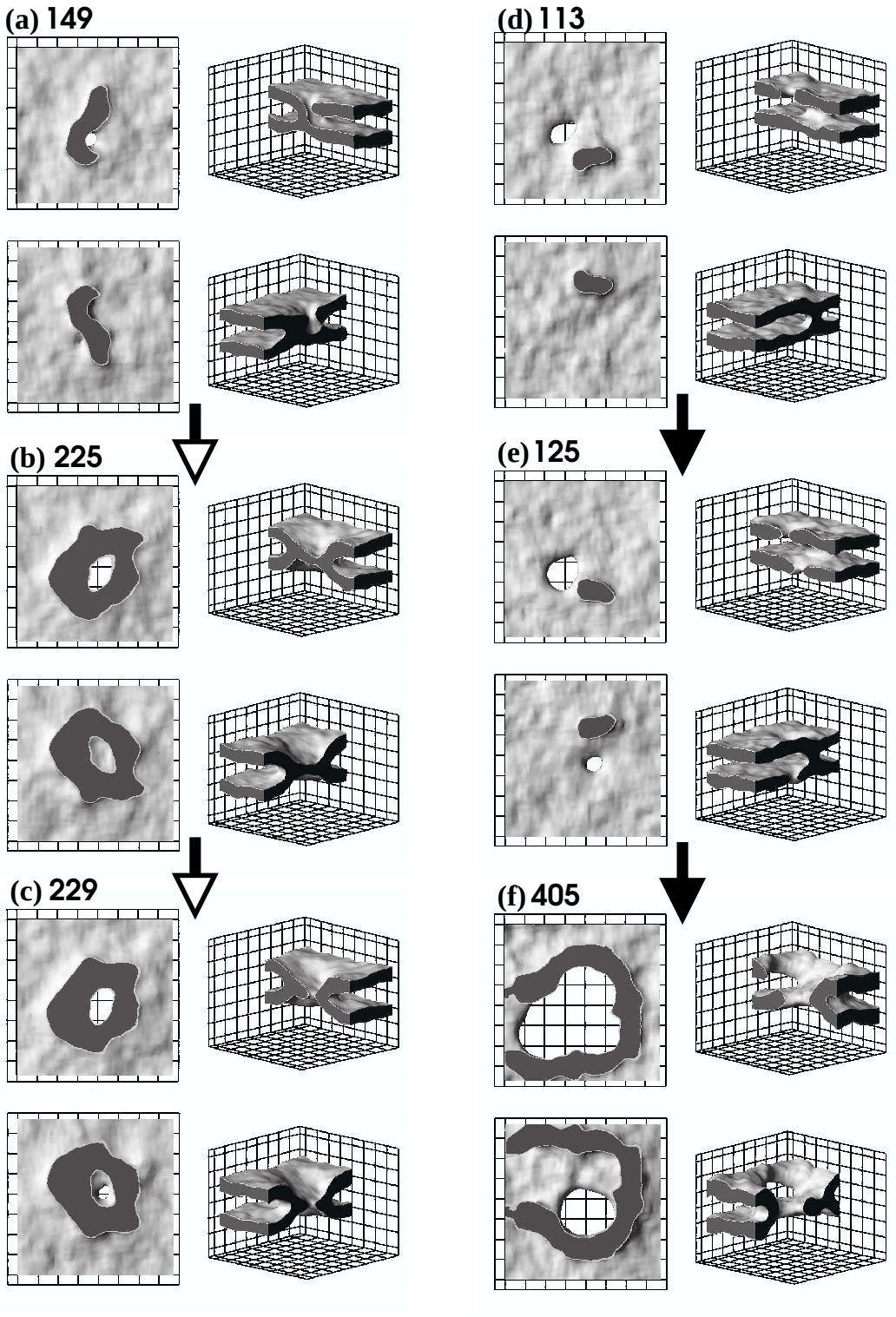

Figure 11. Two observed pathways of fusion process. The snapshots are taken from two representative simulation runs. Each configuration is numbered by the time (in multiples of 25, 000 MCS) at which it was observed. For discussion of the mechanism see text. From Ref. [13]

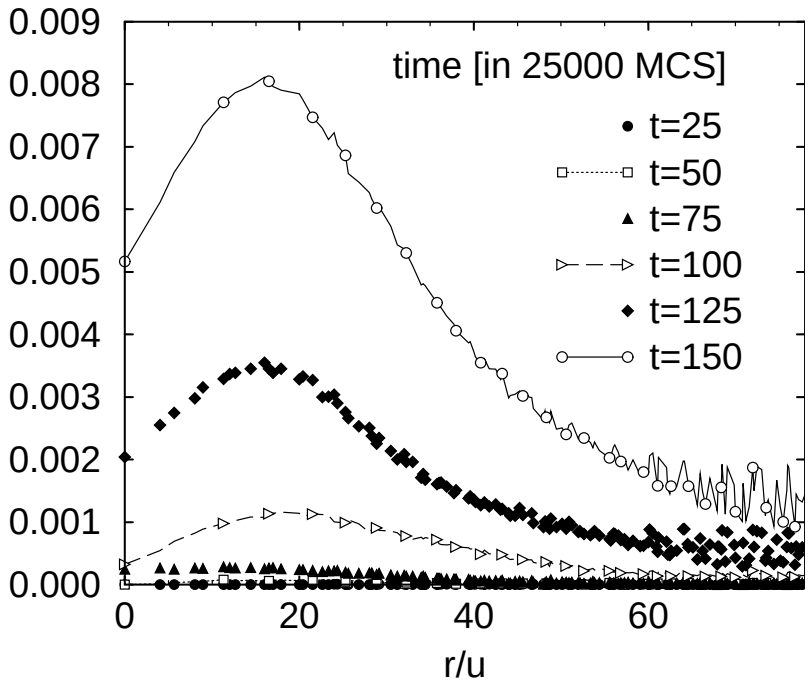

Figure 12. The hole–stalk correlation function, $g(r)$, at early times. From Ref. [51].

shown in Fig. 12. The scale of $g(r)$ increases with time indicating the simultaneous formation of stalks and holes. The figure shows that the correlation peaks at a distance of about 2/3 bilayer thickness, and rapidly decays at larger distances.

Now that a stalk connecting the two bilayers has appeared as well as a hole in one of the bilayers, fusion proceeds along one of two closely related paths. These are depicted in Fig. 11. The snapshots are taken from two representative simulation run. Configurations are numbered by the time (in multiples of 25 000 MCS) at which it was observed. Three-dimensional plots of the local density are shown – the hydrophobic core is depicted as dark gray, the hydrophilic-hydrophobic interface (defined as a surface on which densities of hydrophilic and hydrophobic segments are equal) is light gray. Hydrophilic segments are not shown for clarity. Each configuration is shown from four different viewpoints. Top- and bottom- left sub-panels have been generated by cutting the system along the middle plane parallel to the plane of the bilayer. The top and bottom halves are viewed in the positive (up) and negative (down) direction correspondingly. In these panels one sees the cross-section of connections between bilayers (hydrophobic core of stalks) as dark regions. Holes in the individual bilayers appear as white regions in one of the panels. Top- and bottom- right sub-panels are side views with cuts made by planes perpendicular to the bilayer. The grid spacing is $20u \approx d_c$ (see Tab. 1).

1. A hole appears in one bilayer and the stalk completely surrounds it rather rapidly. The resulting configuration looks very much like a hemifusion diaphragm which has been suggested by many authors as an intermediate stage in fusion [392, 405, 393]. However, this diaphragm is quite different from the hemifusion diaphragm of the classical scenario that consists of two *trans* monolayers of the fusing membranes. In contrast, the diaphragm we

observe in our simulations is made of one of the pre-existing bilayers; i.e., it is comprised of *cis and trans* leaves of the bilayer that did not form a hole. The appearance of a pore in this diaphragm and its expansion completes the formation of the fusion pore.

2. A hole appears in one bilayer and, before the stalk completely surrounds it, a second hole appears in the other bilayer. The stalk continues to surround them both, and align them both during this process. Eventually, the stalk completely encircles both holes and a complete and tight fusion pore is formed. This path is slower than the previous one and the holes tend to expand more during this process.

Once the fusion pore has formed, it expands because it reduces the bilayer area and thereby relieves the tension. Note that in the canonical ensemble, the total tensionless area is fixed from the beginning and the growth of the fusion pore ends when the pore reaches its optimum size determined by the finite size of our simulation cell. Very similar finite-size related effects have been studied for the hole formation in canonical simulations of isolated bilayers [406].

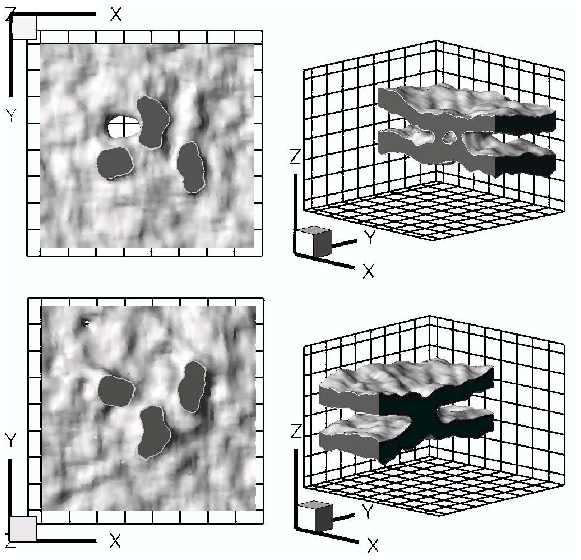

Figure 13. Snapshot from a simulation with small membrane tension and large bilayer distance (cf. Fig. 21) showing multiple stalks and a hole. The configurations are depicted as in Fig. 11.

Occasionally, more than one stalk forms in the simulated bilayer patch. An example of configurations with multiple stalks is shown in Fig. 13. The interactions between stalks have been considered by Lukatsky and Frenkel within an effective interface model [407]. They argue that membrane-mediated interactions lead to an attraction of stalks, and that the collective clustering of stalks, in turn, aids the fusion process. This is compatible with the snapshots presented in Fig. 13 where there is apparently a higher probably of finding two stalks close to each other.

The observed pathway of fusion differs markedly from the classical hypothesis in the following important aspects: First, the fusion intermediates we observe break the axial symmetry which has been assumed in previous calculations. Second, holes in the individual bilayers play an important role in the fusion mechanism. On the one hand, holes give rise to some degree of transient mixing of the amphiphiles in the *trans and cis* leaves of the same membrane that is correlated with the fusion event. Lipids can switch between the two leaves by diffusion along the rim of these holes. On the other hand, the formation of holes in the individual membranes implies a transient content leakage that is correlated in space and time with the fusion event.

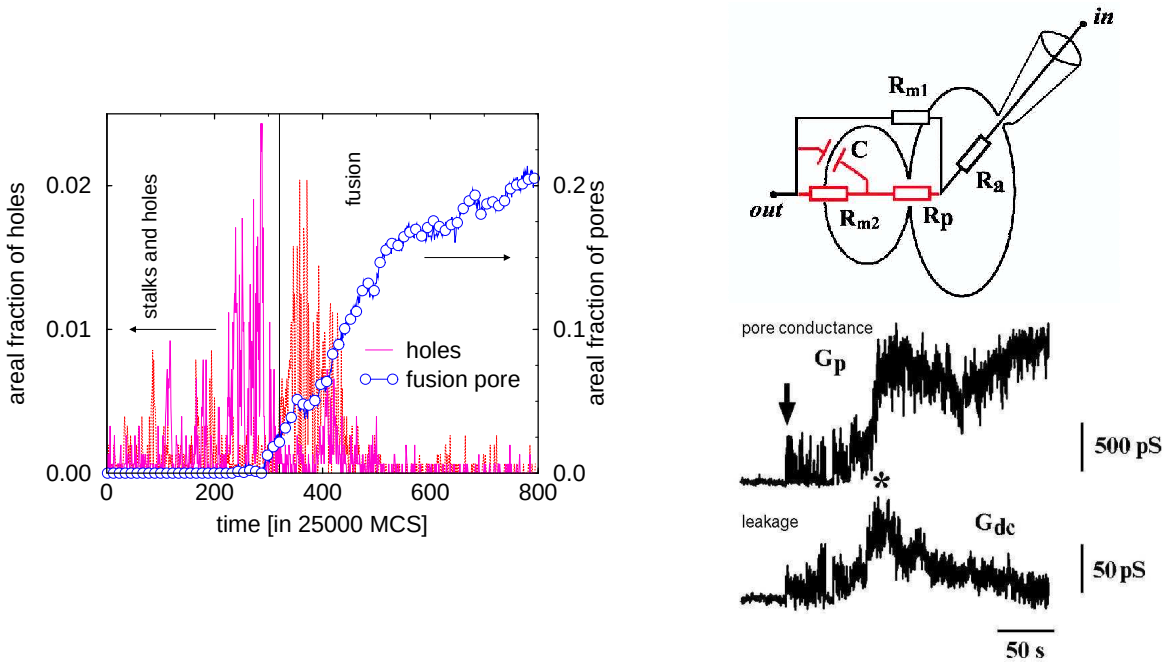

Figure 14. (left) Time dependence of the area of holes (in single bilayers) and the fusion pore in one (out of 32) representative simulation run. Note the different scales for hole and pore areas. From Ref. [51] (right) Electrophysiological experiment on influenza hemagglutinin-mediated fusion of HAb2 and red blood cells. upper panel: equivalent electrical circuit. lower panel: Fusion experiment showing leakage temporarily correlated with fusion. The pore conductance $G_p = 1/R_p$ marks the opening (arrow), flickering and growth of the fusion pore. G_{dc} is the conductance of the HAb2 cell when the fusion pore is closed and is the sum of the conductances of the HAb2 and the red blood cell when the fusion pore is open. It is a measure for the leakiness of the fusion event. Ten out of twelve experiments showed leakage. From Ref. [390]

Such leakage has been observed in recent experiments [388, 390]. In Fig. 14 we present the areal fraction of holes in the individual membranes and the size of the fusion pore from one simulation run. One clearly observes that hole formation precedes the fusion pore. The extent of leakiness that can be observed in experiments depends on the substance that passes through the holes of the vesicles and the fraction of the rim of a pore that is sealed by the stalk. If the stalk is very elongated and covers a substantial fraction of the incipient hole then leakage will be very small. In the same figure, we present electrophysiological experiments by Frolov and co-workers [388, 390] that show the conductance between two fusing vesicles and the conductance between the individual vesicles and the solution. The former quantifies the size of the fusion pore, while the latter indicates the area of holes in the individual membranes. Consistent with the Monte Carlo simulations there is no connectivity between the inside of the vesicle and the outside solution before the fusion event, i.e., the vesicles are tight. Just before a current between the vesicles is observed, however, the experiments reveal a substantial leakage current. Although the simulation and experiments deal with quite different systems, they both observe leakage in contrast to the classical hemifusion hypothesis. This exemplifies the insights into the mechanisms of collective phenomena that one can gain from simulations of coarse-grained membrane models.

3.3.3. Comparison to other coarse-grained models

While this qualitative agreement with experiment is very encouraging, the coarse-grained simulation model differs in many aspects from experiment. In Sec. 2.2 we demonstrated that our model can reproduce many properties of bilayer membranes, and in the previous section we have argued the the time scale of fusion is clearly separated from the relaxation time of local bilayer properties. Therefore we do not expect that including details of the lipid architecture or details of the diffusive dynamics of the MC simulations will qualitatively alter our conclusions.

Nevertheless to gauge the universality of the observation of this specific coarse-grained model, it is very important to relate the findings to results of alternative coarse-grained models. Since the various models include different details, they emphasize different aspects of the fusion process. The simulation studies of fusion differ both in the geometry of the initial state – two apposed planar bilayers, or a planar bilayer in contact with a vesicle or two small vesicles – as well as in the representation of the amphiphiles and the solvent.

Chanturiya et al. [408] investigated the role of tension on fusion within a two-dimensional model of a lipid bilayer. This limitation excluded the possibility of observing complex fusion intermediates.

Noguchi and Takasu [140] studied the fusion of two small bilayer vesicles using a solvent-free model [171] (see Sec. 2.2). The amphiphiles were modeled as a rigid rod comprising one hydrophilic and two hydrophobic beads. Density dependent potentials were tuned to bring about the self-assembly in the absence of solvent. One important difference to the fusion of two planar bilayer membranes consists in the rather small contact zone of the two vesicles and the high curvature of the bilayer membranes. They observed two distinct fusion mechanisms: One mechanism resembled the classical hemifusion mechanism starting from the formation of a stalk and subsequent transmembrane contact. The transmembrane contact, however, did not significantly expand but remained confined to the rather small contact area of the two vesicles. A pore in the transmembrane contact completed the fusion. The other mechanism they saw was the stalk-hole mechanism which we had observed. Their work was completely independent of ours, and was carried out at about the same time. In particular, they observed the elongation of the stalk along the edge of the contact zone between the two vesicles. These observations are visualized in Fig. 15.

The self-assembly of vesicles from a disordered solution and their fusion has been studied using

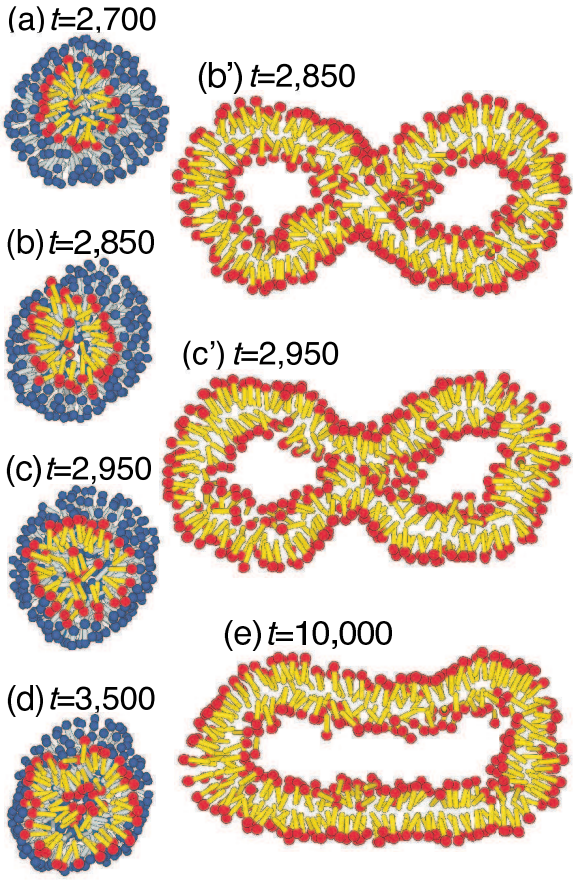

Figure 15. Sequential snapshots of the fusion of two vesicles within the solvent-free model of Noguchi and Takasu [171]. Hydrophilic and hydrophobic segments are represented by spheres and cylinders, respectively. Panel (a) presents a snapshot of the initial stalk between the two apposed vesicles. Panels (b), (c), (d) show cuts perpendicular to the plane of contact while the images (b'), (e), (f), and (c') depict cuts parallel to the plane of contact where the elongation of the stalk is clearly visible. From Ref. [140].

MESODYN simulations [409, 410] of diblock copolymers [411]. The model is similar to the one used in Sec. 3.4 but the use of a very coarse discretization of the molecular architecture permits the study of large system sizes in three dimensions. Interestingly, these calculations also observe the formation of stalks between two apposed vesicles and the formation of holes in the vicinity of stalks in both bilayers (stalk-hole mechanism 2). The subsequent encircling of both holes by the stalk completes the fusion process.

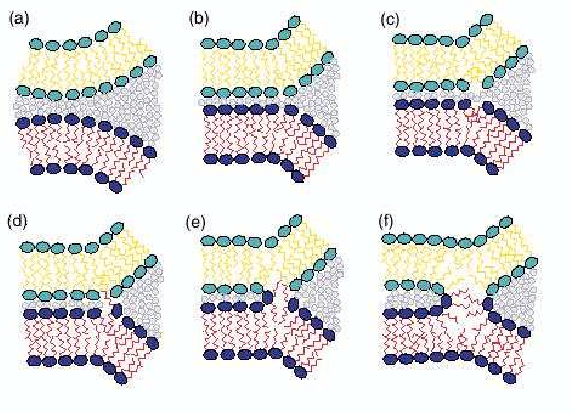

Figure 16. Sketch of stalk formation due to association of splayed lipids suggested by coarse-grained simulations. (a) Two vesicles are brought together and (b) a flat contact forms where, at the edge, the area per lipid in the outer leaflet increases as the membrane is strained. (c) Lipids tilt at the contact and (d) the hydrophobic tails of some amphiphiles begin to splay. (e) Splayed molecules then associate by their tails to form a new hydrophobic core, (f) which expands as the tails extend to form a classical stalk-like structure. From Ref. [412].

Stevens, Hoh and Woolf [412] also studied the fusion of two small vesicles that had been pushed together via an external force. The double-tailed amphiphiles were described by a bead-spring model of eleven particles, and the solvent as consisting of single particles. Their simulation showed a single pathway to fusion, the stalk-hole mechanism. As in Noguchi and Takasu's second mechanism, they found a highly asymmetric expansion of the stalk along the edge of the contact zone. Most notably, the simulations provided a detailed description of stalk formation. Since the hydrocarbon tails were modeled as semi-flexible chains, they were found to tilt at the rim of the contact zone between the vesicles. The model also afforded the possibility of double-tailed lipids bridging between the *cis*-layers of the two apposed vesicles. The authors argue that this effect is important for nucleating the initial stalk. The details of the stalk formation inferred from the simulations are sketched in Fig. 16.

Utilizing a similar coarse-grained bead-spring model [413], Smeijers et al [403] also provide a detailed description of stalk formation and emphasize the role of fluctuations that give rise to microscopic hydrophobic patches of the bilayers. In contrast to the simulations of Stevens et al [412], however, stalks do not necessarily form at the edge of the contact zone. One important difference between Smeijers' simulations and others is the absence of tension in the vesicles that have been prepared by spontaneous self-assembly from a disordered solution. For the small vesicles considered in the simulations, the curvature suffices to induce fusion. For two planar bilayers they observed the formation of stalks but no fusion [404]. In these simulations the stalk-hole mechanism was observed (see Fig. 17) significantly more often than the radial expansion of the stalk.

Even more details of the lipid architecture are incorporated in the systematically coarse-

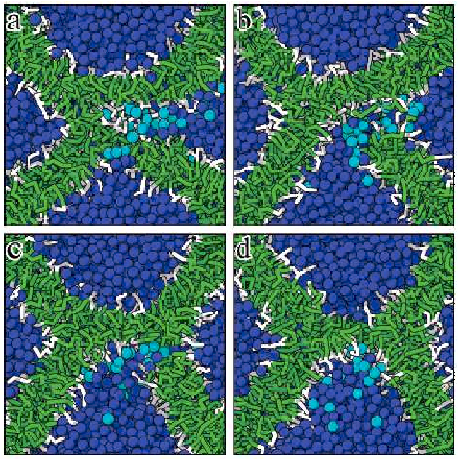

Figure 17. Fusion of two tensionless vesicles observed in a coarse-grained bead-spring model [413]. Shown is a cross-section along the vesicle-vesicle axis. Solvent is shown as dark blue spheres, and the solvent particles that enter the bottom vesicle highlighted light blue. (a) Some solvent enters the vesicle and initializes a hole in the lower vesicle (26.5 ns). (b) The hole is evident (26.8 ns). (c and d) As the stalk encircles the hole and the last solvent particles enter the vesicle, a hemifusion diaphragm is formed by the two monolayers of the upper vesicle (27.0 ns and 27.2 ns). From Ref. [403]

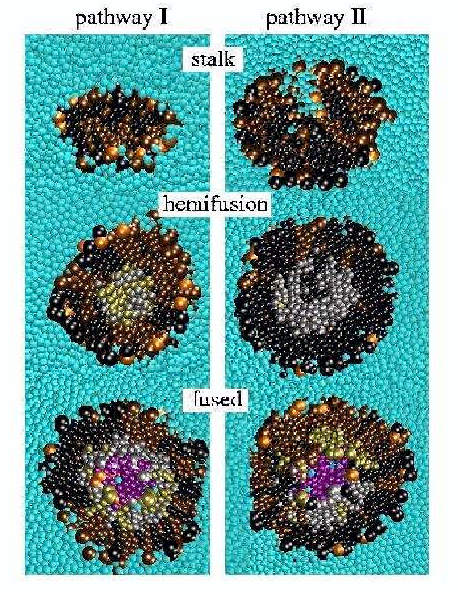

Figure 18. Comparison of the transition from stalk to opening of the fusion pore in both pathways observed for the fusion of mixed DPPC/DPPE vesicles. Slabs perpendicular to the fusion axis are shown, cutting through the stalk or hemifusion diaphragm. Lipid headgroups are represented by large spheres. Different colors distinguish between lipids in the inner (yellow/silver) and outer monolayer (brown/black) and between the two vesicles (brown and yellow vs. black and silver). Orange spheres denote the ethanolamine site of PE, blue spheres denote exterior water, purple spheres interior water. Note the differences in stalk structure (bent in pathway II) and in the composition of the HD (mixed in pathway I, almost entirely from a single vesicle in pathway II). From Ref. [414] (suppl. information).

grained representation of Marrink and Mark [14] who studied fusion of two very small vesicles [414]. This model corroborates the tilting of the amphiphilic tails in the stalk. Marrink and Mark observe two pathways: the classical hemifusion mechanism (pathway I) and the stalk-hole mechanism, with an elongated stalk (pathway II). Importantly, transient pores in one of the bilayers were observed in the vicinity of the stalk in the second mechanism. The two observed pathways are depicted in Fig. 18.

The simulation model of Shillcock and Lipowsky takes a step towards an even more coarse-grained approach utilizing a DPD-model [142]. This allows them to study a large number of fusion events between a tense planar bilayer and a tense vesicle [402]. The larger degree of coarse-graining also allows them to systematically vary the tension of the two membranes. While they do not discuss the detailed mechanism of the fusion, they find that successful fusion is limited to a narrow range of rather high tensions. If the tension is too high, however, the membranes rupture instead of fusing. If the tension is below some threshold, the two apposed membranes do not fuse but rather adhere on the time scale of the simulations. This strong tendency to adhere has not been reported in other simulation models. Thus it does not appear to be a universal characteristic, and it remains unclear which specific property of the model is responsible for this feature.

Utilizing a DPD-model, Li and Liu investigated the structure of the fusion intermediates [415]. They found an asymmetric elongation of stalks similar to our observation. For rather symmetric amphiphiles, however, the elongated stalks expanded into an axially symmetric transmembrane contact, while for more asymmetric lipids, holes formed in the individual membranes in four out of five simulation runs.

Taken together, the different coarse-grained simulation studies provide a consistent picture of the microscopic details of membrane fusion. In particular, the stalk-hole mechanism appears to be a viable alternative to the classical hemifusion mechanism. Although the different lattice, bead-spring, and soft DPD models differ substantially in their microscopic interactions, and in the fusion geometry, planar bilayer or highly curved vesicle, they all observe the non-axially symmetric elongation of the stalk and transient holes in the individual membranes in the vicinity of a stalk. This is also compatible with the experimental observation of transient leakage in some experiments.

It is difficult to determine from the above results the conditions under which the classical fusion mechanism or the stalk-hole mechanism is the favored one. Field-theoretic methods, however, are well suited to explore model parameters and to answer this, and other, questions.

3.4. SCF calculations

One advantage of our coarse-grained model is the fact that it can be mapped onto the standard Gaussian chain model that is routinely utilized in SCF calculations [288, 285]. The length scale, R_e, and the incompatibility χN, can be extracted from the simulations. Further, simulation results of the bond fluctuation model have quantitatively been compared to SCF calculations for many properties [416, 417, 418, 419, 158, 356, 255]. The degree of the quantitative agreement without any adjustable parameter can be gauged from Fig. 7.

The SCF theory approach allows us to calculate the free energy of axially symmetric intermediates utilizing the radius of the structures as a reaction coordinate. First, we examine the dependence of the intermediates along the classical hemifusion path as a function of the bilayer tension and lipid architecture. Then, we proceed to estimate the free energy of the alternative fusion intermediates observed in the simulations by patching together radially symmetric structures. These SCF calculations go beyond the phenomenological approaches that utilize effective interface Hamiltonians in two crucial aspects: (1) They retain the notion of amphiphilic

molecules and calculate the changes of the molecular conformations in the complex, spatially inhomogeneous environment. No assumptions about the chain packing or stretching have to be made. (2) Only the radius (reaction coordinate) and the topology of the intermediate is dictated. The detailed geometry of the intermediate structure is optimized as to minimize the free energy that comprises contributions both from the interface between hydrophobic and hydrophilic components, and from the loss of configurational entropy due to changes of the chain conformations.

3.4.1. Axially symmetric configurations along the classical fusion pathway

The free energy of an axially symmetric stalk that connects the two apposed bilayer membranes as a function of its radius is shown in Fig. 19. The free energy profiles exhibit two maxima – the first one, S_0, corresponds to the formation of an initial connection between the bilayers (stalk) and the second one, S_2, corresponds to the expansion of the stalk to a hemifusion diaphragm. These two maxima are separated by a minimum, S_1, that marks the radius of a metastable stalk. The radius of this metastable configuration is set by the bilayer thickness. Density plots of the majority component of the three extremal states are shown in Fig. 19. While the phenomenological calculations focused much effort on calculating the free energy cost of forming a stalk, S_0, the SCF calculations show that the main barrier along the path towards the expanded hemifusion diaphragm is not the formation of the initial stalk, S_0, but it is determined by the expansion, S_2, of the metastable stalk to the diaphragm.

The free energies of the metastable stalk, S_1, and the saddle point, S_2 along the path towards the hemifusion diaphragm are shown in Fig. 20 as a function of the amphiphilic architecture, f, and the bilayer tension, γ. The free energy barrier, S_2, associated with the stalk expansion strongly decreases with tension. Within the classical model, this explains why the fusion rate increases with tension. The free energy of the metastable stalk hardly depends on tension but it decreases substantially as we lower the fraction f of hydrophilic segments and thereby decrease the spontaneous curvature of a monolayer to more negative values. For very asymmetric amphiphiles, those that form the inverted hexagonal phase in the bulk, the free energy of a stalk actually becomes negative. In this case, many stalks are expected to form and to condense on an hexagonal lattice thereby creating a "stalk phase". Such hexagonally perforated lamellar phases have been observed both in diblock copolymers [420, 421] and in lipid/water mixtures [422]. Making the amphiphiles even more asymmetric, we observe that stalks spontaneously elongate and the inverted hexagonal phase forms. On the other hand, if we make the amphiphiles more symmetric, the metastable stalk configuration eventually disappears. In this case, the fusion rate is not determined by the free energy difference between the saddle point S_2 and the metastable stalk S_1 but by the large barrier S_2 only. Thus, the absence of a metastable stalk will strongly suppress fusion.

Both in the classical mechanism, as well as in the alternate stalk-hole fusion mechanism observed in the simulations, stalks play a pivotal role. The limits of metastability of stalks explored by the SCF calculations are compiled in Fig. 21. Most notably, the free energy calculations demonstrate that fusion is restricted to a rather narrow window of amphiphilic architecture characterized by the ratio of spontaneous monolayer curvature and bilayer thickness. This narrow range of spontaneous curvatures extracted from a coarse-grained model is bound by the spontaneous curvatures of two relevant lipids, DOPE and DOPC.

The rupture of the hemifusion diaphragm completes the fusion process. The free energy of a fusion pore in tensionless bilayers as a function of its radius, R, is shown in Fig. 22. For large radii the free energy linearly increases with R, the slope being proportional to the effective line tension of the pore's rim. For very small radii, however, the free energy also increases

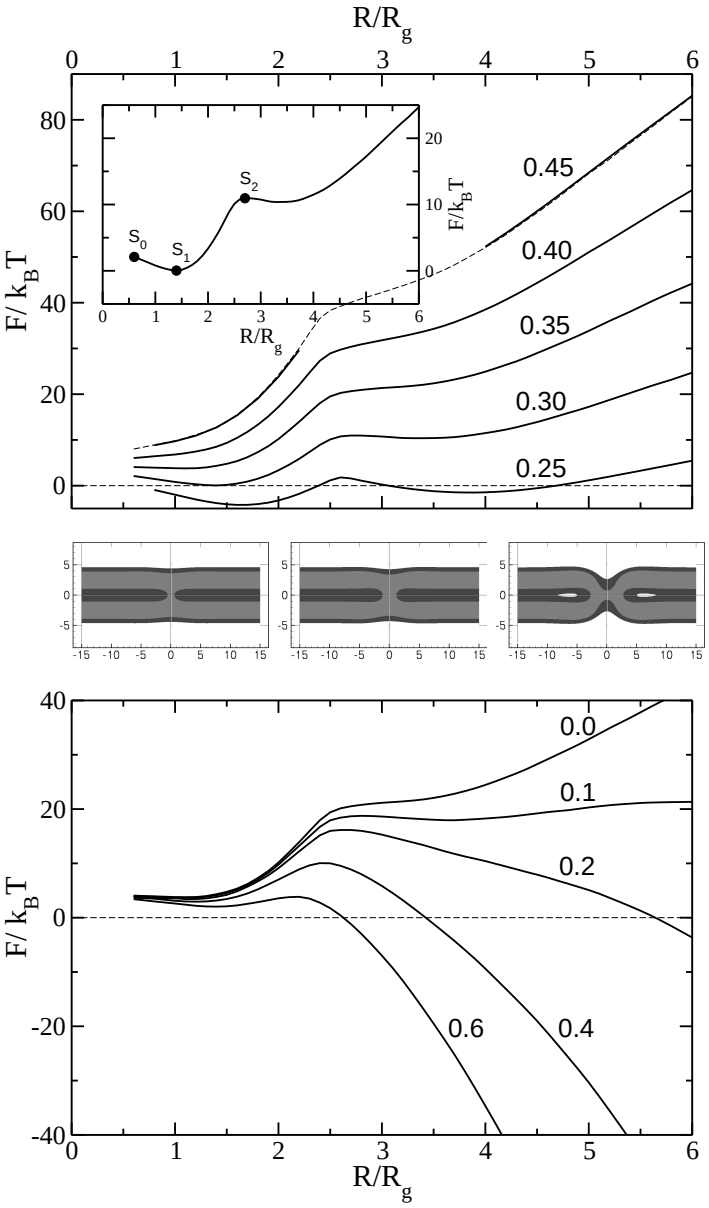

Figure 19. (a) The free energy, F, of the stalk-like structure connecting bilayers of fixed, zero, tension is shown for several different values of the amphiphile's hydrophilic fraction f. In the inset we identify the metastable stalk, S_1, the transition state, S_0, between the system with no stalk at all and with this metastable stalk, and the transition state, S_2, between the metastable stalk and a hemifusion diaphragm. The architectural parameter is $f = 0.30$ for this inset. No stable stalk solutions were found for $f = 0.45$ in the region shown with dashed lines. They were unstable to pore formation. Profiles showing the majority component of the two barriers S_0 and S_2, and the metastable stalk, S_2, are shown below the main panel. (b) The free energy of the expanding stalk-like structure connecting bilayers of amphiphiles with fixed architectural parameter $f = 0.35$ is shown for several different bilayer tensions. These tensions, $\gamma/\gamma_{\rm int}$, are shown next to each curve. From Ref. [311].

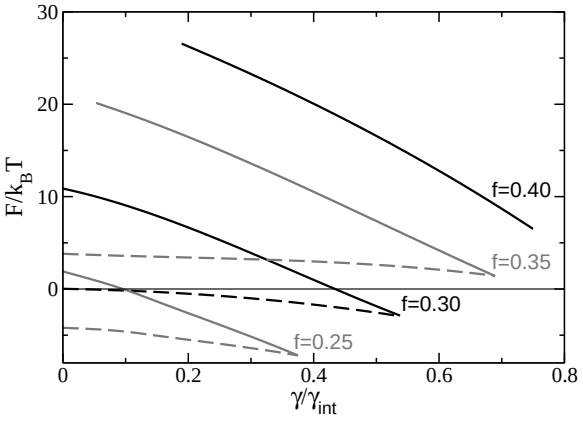

Figure 20. The free energy, F, of the metastable stalks S_1 (dashed lines) and the transition states S_2 (full lines) along the path towards the hemifusion diaphragm are shown as a function of the tension for different architectures $f = 0.25,\ 0.30,\ 0.35,\ 0.40$. Notice that there is no metastable stalk (solution S_1) for $f = 0.4$ at zero tension. From Ref. [311].

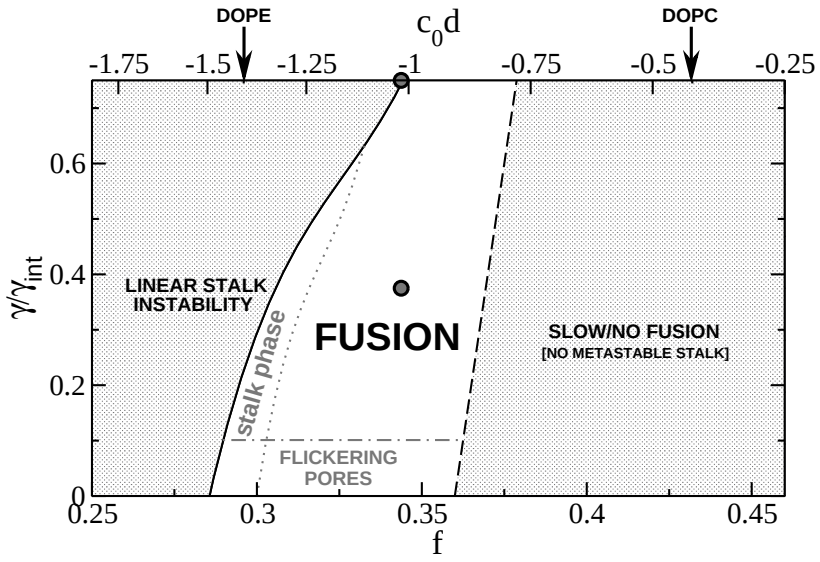

Figure 21. A "phase diagram" of the fusion process in the hydrophilic fraction-tension, (f, γ), plane. Circles show points at which simulations were performed by us. Successful fusion only can occur within the unshaded region. As the tension, γ, decreases to zero, the barrier to expansion of the pore increases without limit as does the time for fusion. As the right-hand boundary is approached, the stalk loses its metastability causing fusion to be extremely slow. As the left-hand boundary is approached, the boundaries to fusion are reduced, as is the time for fusion, but the process is eventually pre-empted due to the stability either of radial stalks, forming the stalk phase, or linear stalks, forming the inverted hexagonal phase. From Ref. [311].

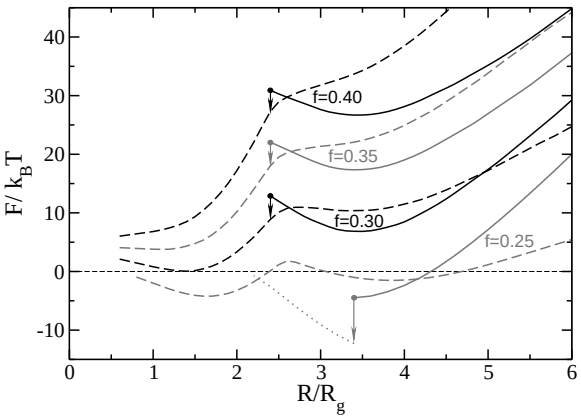

Figure 22. The free energies, F, of a fusion pore (solid lines) and of a stalk (dashed lines) of radius R are shown. The membranes are tensionless and the architecture f of the amphiphiles is indicated in the key. The instability of the fusion pores at small radius is indicated by arrows. For $f = 0.3$, 0.35, and 0.4, the stalk-like structure converts into a pore when it expands to a radius $R \approx 2.4R_g$ at which the free energies of stalk-like structure and pore are equal. For the system composed of amphiphiles of $f = 0.25$, however, the stalk-like structure converts at $R \approx 2R_g$ into an inverted micellar intermediate, IMI, whose free energy is shown by the dotted line. The fusion pore is unstable to this IMI intermediate when its radius decreases to $R \approx 3.4R_g$. Thus the IMI is the most stable structure under these conditions. From Ref. [311].

as we decrease the size of the fusion pore because the head groups begin to repel each other across the pore. Thus, the SCF calculations predict a barrier for the closing of a fusion pore. This prediction qualitatively agrees with the experimental observation of flickering fusion pores at very low tension. In this case, fusion pores once formed do not expand due to the lack of tension, but they do not close either because of the barrier just mentioned. Thus they remain in a metastable state and their radius fluctuates around its preferred value. Experimentally this is detected by a flickering of the current between the two fusion vesicles [423, 424, 425]. The region where flickering pores are expected is also indicated in the fusion diagram (cf. Fig. 21).

3.4.2. Barriers along the stalk-hole path observed in the simulations

The fusion path observed in the simulation differs from the classical hypothesis by the occurrence of non-axially symmetric intermediates and the formation of holes in the individual bilayers.

First, we discuss the free energy of an isolated hole in a single membrane. Hole formation has been investigated by previous simulations [426, 160, 114, 185, 406, 427, 428, 429, 430, 431, 432, 175, 433]. These studies have focused on the fluctuations of the pores, their shape and detailed structure, e.g., the bulging at the rim (see Fig. 23 middle panel). The results indicate that hole formation is well described by classical nucleation theory [434, 435]. Fig. 23 presents the free energy of a hole as a function of its radius R measured in units of the radius of gyration R_g of the amphiphilic molecules. While previous SCF calculations [307] conceived holes as weakly segregated equilibrium structures (the hexagonally perforated phase) of tense bilayers the holes that form at large incompatibility must be stabilized by an external constraint (see Sec. 2.3) and correspond to unstable structures, in agreement with simulation and experiment. For a tensionless membrane, $\gamma = 0$, the free energy linearly increases with its radius, and from

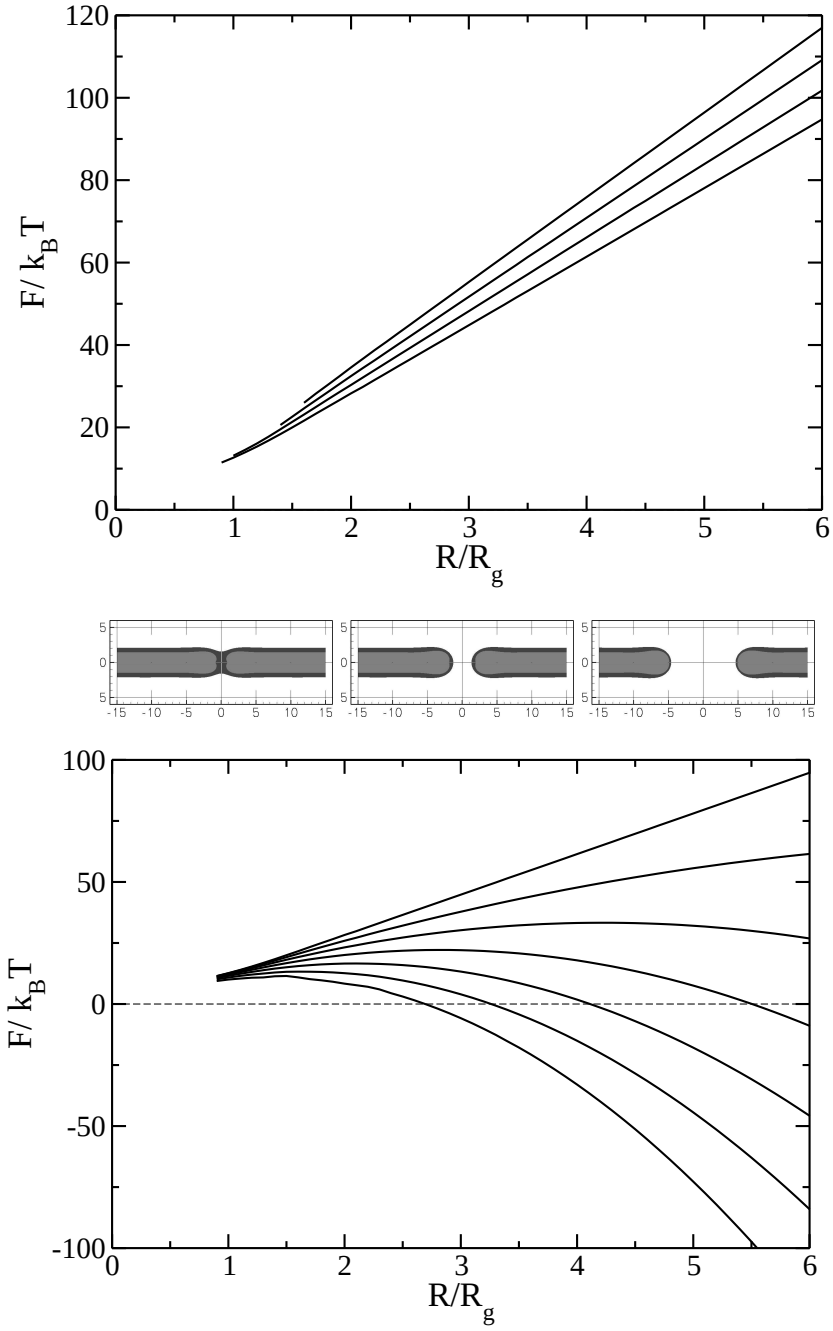

Figure 23. (a) Free energy of a hole in an isolated bilayer as a function of R/R_g at zero tension for various amphiphile architectures, f. From top to bottom the values of f are 0.29, 0.31, 0.33, and 0.35. (b) Same as above, but at fixed $f = 0.35$ and various tensions $\gamma/\gamma_{\rm int}$. From top to bottom, $\gamma/\gamma_{\rm int}$ varies from 0.0 to 0.6 in increments of 0.1. From Ref. [312].

the asymptotic behavior one can identify the line tension, λ of the hole's rim. Upon increasing the membrane tension, the free energy curves adopt a parabolic shape expected from classical nucleation theory, $F_{\rm hole}(R) = 2\pi R\lambda - \pi R^2\gamma$ [434, 435]. Note that the free energy barrier, $\Delta F^* = \pi\lambda^2/\gamma$, is on the order of a few tens of the thermal energy scale, k_BT, for the parameters utilized in the MC simulations of the bond fluctuation model. Although tense membranes are metastable and eventually will rupture, the high barrier makes the homogeneous nucleation of a hole in a bilayer an unlikely event on the time scale on which fusion occurs. Thus, isolated bilayer membranes are stable (cf. also Fig. 9)

In contrast to the above calculation of the free energy of a hole in a bilayer, the direct calculation of the free energy of the stalk-hole intermediate is much more difficult. The reason is that whereas the former structure is axially symmetric, the latter is not. As noted, the axially symmetry is broken explicitly. This means that one has to calculate the free energy of an intrinsically three-dimensional structure. This is computationally very demanding. Moreover, the choice of a suitable reaction coordinate is less obvious for the complex, non-axially-symmetric intermediates of the stalk-hole mechanism. For these practical reasons we estimate the free energy of the intermediates observed in the simulations by patching together axially symmetric configurations calculated within SCF theory. Two structures, the elongated stalk and the stalk-hole complex, are considered.

The geometry of the elongated stalk, which is observed before a hole forms next to it, is characterized by the arc of a circle of radius, R, and length $2\pi R\alpha$, with $0 \leq \alpha \leq 1$. We decompose the free energy of this structure into the contribution of its two end caps, which each resemble half of a metastable, circular stalk, and a fraction, α, of a ring-shaped stalk, or inverted micellar intermediate (IMI) (see Fig.24),

$$F_{\rm es} = F_{\rm stalk} + \alpha F_{\rm IMI}(R). \tag{70}$$

By constructing the free energy via the simple addition of the free energy of axially symmetric structures and not allowing for additional optimization of the shape, we will overestimate the free energy of the intermediate.

After a hole forms next to the stalk, the geometry of the stalk-hole complex can be characterized by the radius of the hole, $R-\delta$, where δ is radius of the metastable stalk, and the fraction α of the hole's rim that is covered by the stalk. The geometry of the latter configuration resembles a hemifusion diaphragm. Thus we can approximate the free energy of the stalk-hole complex by

$$F_{\rm sh} = \alpha F_{\rm HD}(R) + (1-\alpha)F_{\rm hole}(R-\delta) \tag{71}$$

where we neglect the free energy costs of the two end points of the stalk. The free energy of these two saddle-shaped point defects presumably is small.

These free energy estimates allow us to explore the free energy landscape, $F(R,\alpha) = \min[F_{\rm es}, F_{\rm sh}]$ of the fusion process as a function of the two reaction coordinates, the radius of the elongated stalk, R and the fraction α of the hole's rim covered by the stalk. Here, we additionally have assumed that a pore will form with a negligible barrier when the stalk-hole free energy, $F_{\rm sh}$, is lower than the free energy of an elongated stalk, $F_{\rm es}$. The formation of a hole in the vicinity of a stalk produces a ridge in the free energy landscape. This is, of course, a simplification, but we expect the corresponding free energy barrier to be small. The main effect of this simplification is that the locus of transitions between the extended stalk and the stalk-hole complex is a sharp ridge, while in a more complete description it would occur over a range of values over which the free energy of the two competing structures differs by order k_BT. Once the hole has formed, the free energy decreases as the stalk surrounds the hole (increasing α), and the stalk-hole intermediate expands (increasing R).

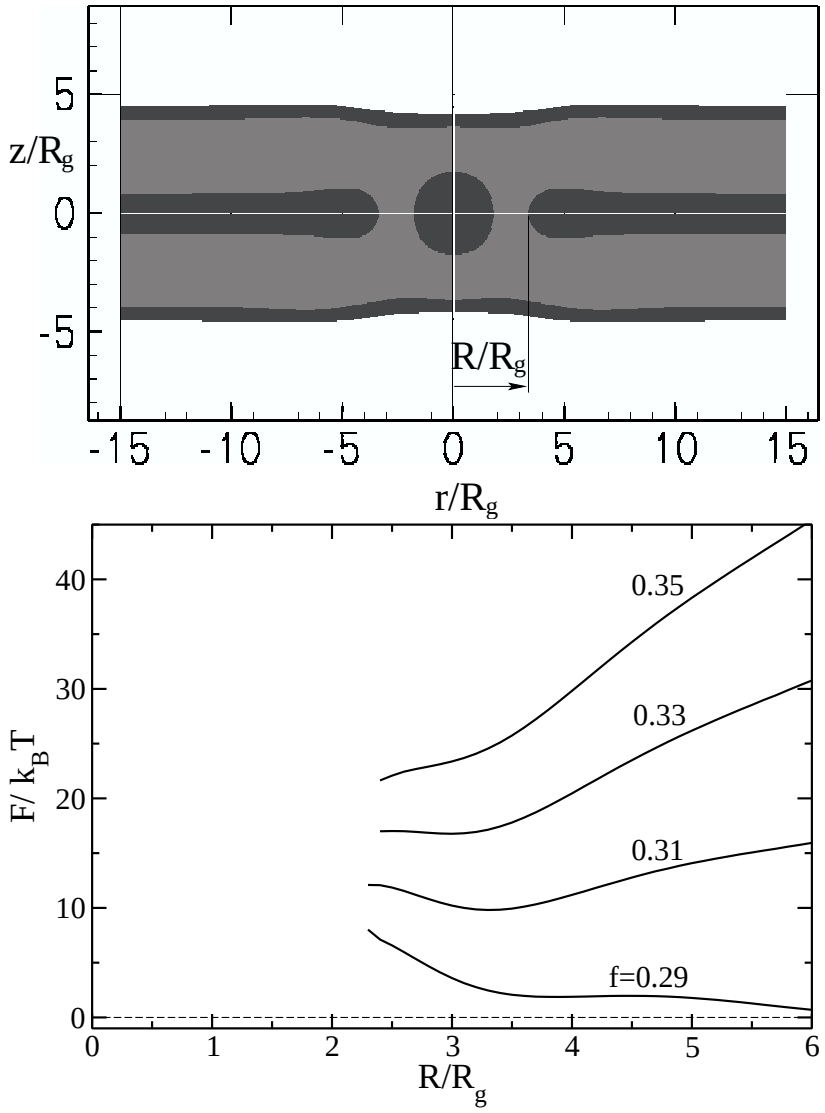

Figure 24. (a) Density profile of an IMI – an elongated stalk that closes in itself forming a circular structure. The amphiphiles are characterized by $f = 0.3$. The radius of the IMI, in units of the radius of gyration, R/R_g is 3.4. (b) Free energy of an IMI as a function of R/R_g at zero tension for various amphiphile architectures, f From Ref. [312].

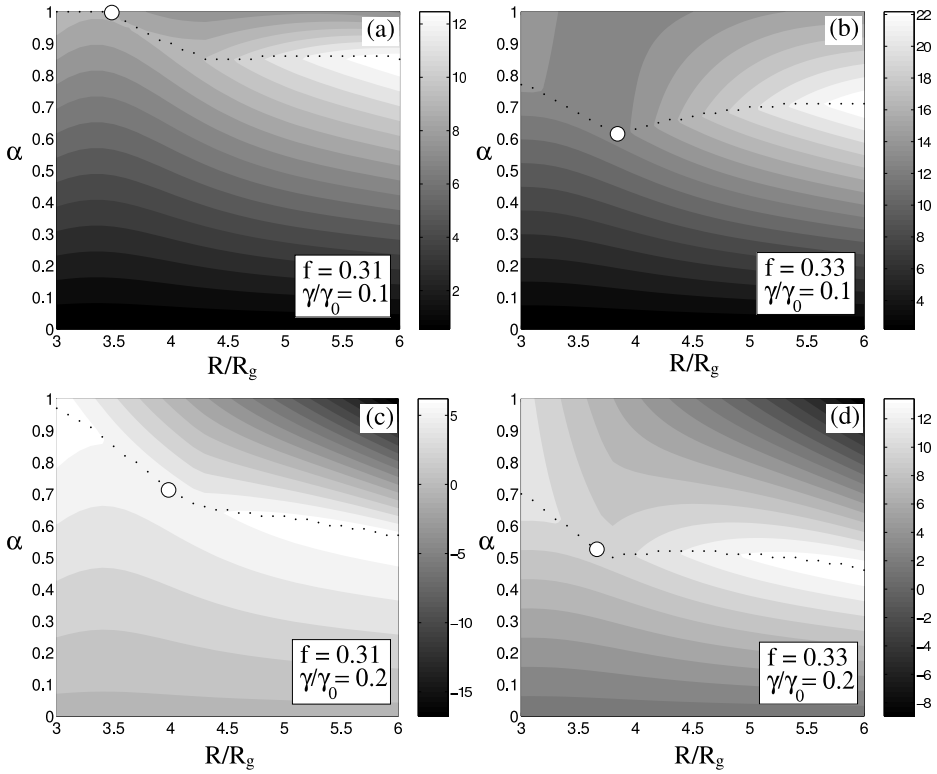

Figure 25. Four free energy landscapes (in units of k_BT) of the fusion process, plotted as a function of the radius, R (in units of R_g) and circumference fraction α. The architecture of the amphiphiles, f, and the value of the tension, $\gamma/\gamma_{\rm int}$, are given. The dotted line shows a ridge of possible transition states, separating two valleys. The region close to the $\alpha = 0$ line corresponds to a barely elongated stalk intermediate (see Eq. (70)). The other valley, close to $\alpha = 1$ states, corresponds to a hole almost completely surrounded by an elongated stalk. The saddle point on the ridge, denoted by a white dot, corresponds to the optimal, lowest free energy, transition state. From Ref. [312].

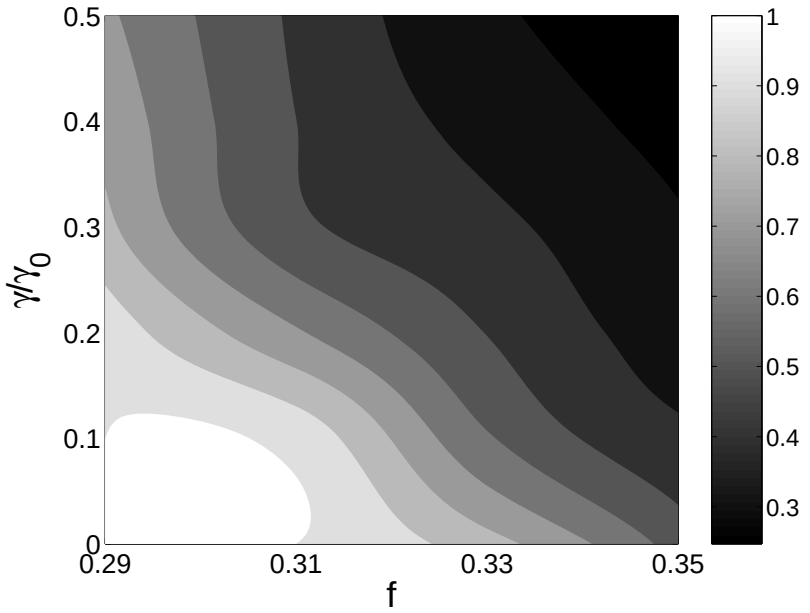

Figure 26. Plot of α^*, which corresponds to the optimal transition state in the stalk-hole mechanism, as a function of architecture of the amphiphiles and the tension of the membrane. Small values of α^* (dark) correspond to leaky fusion events. From Ref. [312].

The minimum of the free energy along the ridge $F_{\rm es}(R,\alpha) = F_{\rm sh}(R,\alpha)$ defines the transition state characterized by R^* and α^*. The value, α^*, is an important characteristic of the fusion intermediate. The larger α^*, the larger is the fraction of the hole's rim that is surrounded by the stalk when the hole is formed. Thus, larger values of α^* correspond to the tighter fusion events while small values of α^* suggest that fusion is leaky and possibly competes with rupture. The value of α^* as a function of tension, γ, and amphiphilic architecture, f, is shown in Fig. 26. Small values of the tension and small values of f, i.e., large negative curvatures, favor tight fusion. Stalks expand more readily because the line tension of the stalk decreases with f (cf. Fig. 23); the line tension, λ_H, of a hole increases for small f; and holes expand less quickly for smaller tension.

In Fig. 27 we compare the free energy of the fusion intermediates along the classical hemifusion path with that of the stalk-hole mechanism as a function of tension and architecture. In agreement with experimental observation, the fusion barrier in both scenarios is the lower the more negative is the spontaneous curvature of the monolayers and the larger the membrane tension is. For the parameters studied, the stalk-hole mechanism has a slightly smaller free energy barrier than that of the classical hemifusion path. The free energy difference, however, amounts only to a few k_BT indicating that the stalk-hole mechanism is a viable alternative to the classical hemifusion path, but that the choice of the pathway will depend on specific details of the system. This is in agreement with the simulation data.

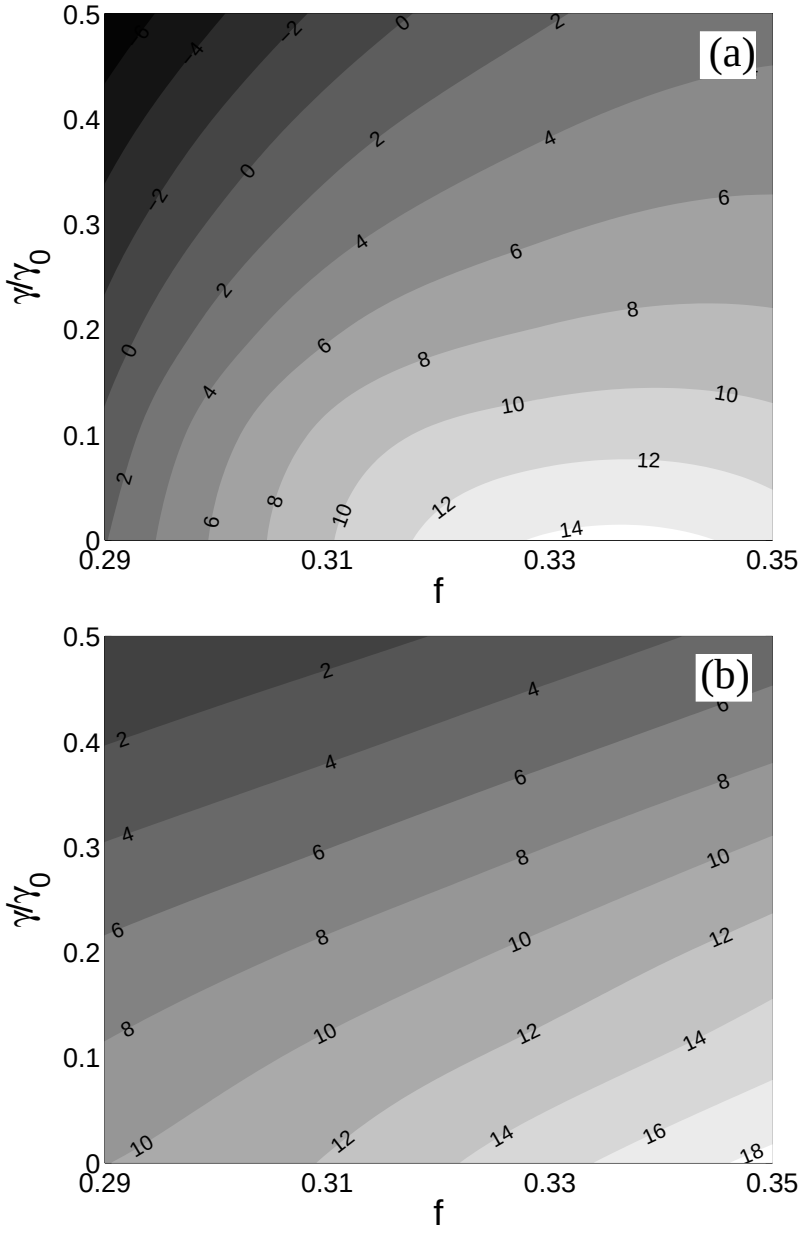

Figure 27. Free energy barriers measured relative to the initial metastable stalk, in units of k_BT, in (a) the new stalk-hole complex mechanism, and (b) the standard hemifusion mechanism. From Ref. [312].

4. Conclusion and outlook

We hope that we have demonstrated that coarse-grained models are a valuable tool for investigating universal collective phenomena in bilayer membranes. These models bridge the gap between atomistic simulations that are limited to rather small time and length scales, and phenomenological models that ignore much of the internal structure of the bilayer. They allow for direct insights into processes that involve many lipids and take place on time scales of milliseconds and length scales of micrometers.

With a specific example, the fusion of membranes, we have illustrated what can be learned from studying coarse-grained models. The apparent universality of membrane fusion that is observed experimentally and the separation of time scales between the local structural relaxation in an individual membrane and the fusion process make it a suitable subject of such models. A rather simple model already yields direct information about the fusion pathway that cannot easily be obtained otherwise, and leads to experimentally verifiable predictions. For high membrane tension and asymmetric lipid architecture, the SCF calculations predict transient leakage that is correlated in time and space with the fusion event. This is observed in simulation of coarse-grained models [140, 161, 51, 414, 415, 403] that substantially differ in their interactions and is corroborated by electrophysiological experiments [388, 390]. Moreover, the coarse-grained models resolve the overt contradiction between the stability of isolated membranes or vesicles that is necessary for their function and the fusion process that involves hole formation in the two apposed membranes. This can be understood as follows. The line tension of holes in the membranes is reduced by the presence of stalks. Therefore, the rate of hole formation is dictated by heterogeneous nucleation at stalks, which is much greater than the rate of homogeneous nucleation in an unperturbed bilayer. The study of fusion also illustrates the fruitful interplay between particle-based simulations and field-theoretic techniques. The latter technique provides quantitative free energy estimates of the fusion barrier and permits the exploration of a wide range of molecular architectures and membrane tensions. It reveals that fusion is strongly suppressed outside a narrow range of monolayer curvatures (see "phase diagram" in Fig. 21). This result suggests ways to control fusion by tuning the stability of stalks and the formation of holes.

The increase of computing resources and algorithmic advances will allow atomistic simulations to explore phenomena at ever larger time and length scales. The role of coarse-grained models, however, will not merely consist in studying problems that are not yet accessible by atomistic simulations. Rather the reduction of the complexity of the system will highlight the relevant ingredients and allow for a systematic quantitative analysis. Thus, coarse-grained models will provide insight into specific mechanisms and principles as well as the degree of universality. Coarse-grained models can explore a variety of conformational properties, thermodynamic quantities (such as phase behavior, bending elastic constants, tension and areal compressibility) and dynamic characteristics (e.g., structural relaxation of the bilayer, dynamics of undulations, lateral diffusion of lipids) simultaneously, and the parameters of the model system can be varied independently and over a wide range. The wealth of information these models provide concerning equilibrium and dynamic properties can be compared both to experiment and to simpler phenomenological approaches in order to assess the validity of the model description. In this way, coarse-grained models identify interesting parameter regimes, test phenomenological concepts, and permit systematic exploration of collective phenomena in biological membranes.

A variety of coarse-grained models has been devised in recent years which differ in the degree of molecular detail, the type of interactions, and the representation of the solvent. In view of the richness and complexity of collective phenomena in membrane physics, no single model will

emerge that captures all aspects. "Systematic" coarse-graining procedures [12, 210, 14, 15, 16, 17] or tightly coupled multi-scale simulation techniques [210, 436, 251, 229, 437] will provide information about the specific interactions that have to be incorporated into coarse-grained models to describe the phenomena of interest.

There are a host of biological problems that can be studied by the kind of coarse-grained models we have discussed, and we expect their use in biological physics to increase greatly in the near future. The formation of bilayers and vesicles [136, 171, 438, 439, 411, 175, 382] has been investigated. The studies of different bilayer phases [187, 180, 206, 191, 175], of the kinetics of phase transition [207, 208], of self-assembly [171, 438, 439, 411], and of phase separation in membrane consisting of different components [440, 114, 441, 192, 442, 443, 444, 445, 446, 447, 233] have already yielded important information about these fascinating systems. Other important questions that can be tackled by coarse-grained models include the interaction between membranes, between membranes and solid substrates, and the interplay between membrane collective phenomena and peptides, proteins and polymers [448, 449, 450, 451, 452, 183, 453], or active components (e.g., ion pumps [454, 455, 456, 457, 183], or fusion proteins [404, 458]).

We close by considering a simple, but important, application to an area which has received much study recently; the possibility of phase separation in the plasma membrane. The basic idea is that the plasma membrane enclosing the cell, rather than being a homogeneous mixture of lipids and cholesterol, may in fact be rather inhomogeneous, with regions of saturated lipids, like sphingomyelin, and cholesterol, aggregated and floating, like "rafts", in a sea of unsaturated lipids, like most phosphatidylcholines. The field grew quickly when it was observed that some signaling proteins preferred the raft environment. As a consequence, these proteins were not distributed randomly throughout the plasma membrane, but were concentrated in the rafts and could therefore function more efficiently.

This seems to be a system which could be studied by coarse-grained models [459]. One object would be to capture the relevant properties of cholesterol which appears to order the saturated lipids in its vicinity [460]. With a suitable model, one can then calculate phase diagrams and compare them to the several experimental ones.

As interesting as this would be, and it would be very interesting indeed, one could then try to understand the observation that rafts act as a nucleation site for the fusion process. One sees how "...way leads onto way" and to the study of ever more complex phenomena, those which are characteristic of biological systems.

Acknowledgment

It is a great pleasure to acknowledge stimulating discussions with V. Frolov. We also acknowledge K. Ch. Daoulas, S. J. Marrink and H. Noguchi for a critical reading of the manuscript. Financial support was provided by the Volkswagen Foundation and the NFS under grant DMR-0140500 and 0503752. The simulations were performed at the von Neumann Institute for Computing at Jülich, Germany.

REFERENCES

1. M. Daoud and C. E. Williams. *Soft Matter Physics, Springer Verlag, Berlin*, 1995.
2. R. G. Larson. *The structure and rheology of complex fluids,Oxford University Press, New York*, 1999.
3. P. M. Chaikin and T. C. Lubensky. *Principles of condensed matter physics, Cambridge University Press, Cambridge*, 1995.
4. P.G. de Gennes. *Scaling Concepts in Polymer Physics, Cornell University Press, Ithaca and London*, 1979.

5. K. F. Freed. *Renormalization Group Theory of Macromolecules, Wiley-Interscience*, 1987.
6. J. des Cloizeaux and G. Jannink. *Polymers in solution: Their modeling and structure, Oxford Science Publications, Oxford*, 1990.
7. L. Schäfer. *Excluded volume effects in polymer solutions, Springer, Berlin*, 1999.
8. J. Baschnagel, K. Binder, P. Doruker, A. A. Gusev, O. Hahn, K. Kremer, W. L. Mattice, F. Müller-Plathe, M. Murat, W. Paul, S. Santos, U. W. Suter, and V. Tries. Bridging the gap between atomistic and coarse-grained models of polymers: Status and perspectives. *Adv. Polym. Sci*, 152:41–156, 2000.
9. M. Müller. *Mesoscopic and continuum models in Encyclopedia of Physical Chemistry and Chemical Physics*, II:2087–2110, 2001.
10. F. Müller-Plathe. Coarse-graining in polymer simulation: From the atomistic to the mesoscopic scale and back. *Chem. Phys. Chem.*, 3:754–769, 2002.
11. K. Kremer and F. Müller-Plathe. Multiscale simulation in polymer science. *Mol. Sim.*, 28:729–750, 2002.
12. J.C. Shelley, M.Y. Shelley, R.C. Reeder, S. Bandyopadhyay, and M.L. Klein. A coarse grain model for phospholipid simulations. *J. Phys. Chem. B*, 105:4464, 2001.
13. M. Müller, K. Katsov, and M. Schick. Coarse-grained models and collective phenomena in membranes: Computer simulation of membrane fusion. *J. Polym. Sci. B: Polymer Physics*, 41:1441–1450, 2003.
14. S.J. Marrink, A.H. de Vries, and A.E. Mark. Coarse grained model for semiquantitative lipid simulations. *J. Phys. Chem. B*, 108:750, 2004.
15. S.O. Nielsen, C.F. Lopez, G. Srinivas, and M. L. Klein. Coarse grain models and the computer simulation of soft materials. *J. Phys.: Condens. Matter*, 16:R481, 2004.
16. S. Izvekov and G.A. Voth. A multiscale coarse-graining method for biomolecular systems. *J. Phys. Chem. B*, 109:2469, 2005.
17. E.S. Boek, J.T. Padding, W.K. den Otter, and W.J. Briels. Mechanical properties of surfactant bilayer membranes from atomistic and coarse-grained molecular dynamics simulations. *J. Phys. Chem. B*, 109:19851, 2005.
18. R. B. Gennis. *Biomembranes, Springer Verlag, New York*, 1989.
19. R. Lipowsky and E. Sackmann. *Structure and dynamics of membranes – from cells to vesicles, Vol 1 of Handbook of biological physics, Elsevier, Amsterdam*, 1995.
20. K. Simons and E. Ikonen. Functional rafts in cell membranes. *Nature*, 387:569–572, 1997.
21. D. A. Brown and E. London. Functions of lipid rafts in biological membranes. *Ann. Rev. Cell Developmental Biology*, 14:111–136, 1998.
22. A. Pralle, P. Keller, E. L. Florin, K. Simons, and J. K. H. Horber. Sphingolipid-cholesterol rafts diffuse as small entities in the plasma membrane of mammalian cells. *J. Cell Bio.*, 148:997–1007, 2000.
23. C. Dietrich, L. A. Bagatolli, Z. N. Volovyk, N. L. Thompson, M. Levi, K. Jacobson, and E. Gratton. Lipid rafts reconstituted in model membranes. *Biophys. J.*, 80:1417–1428, 2001.
24. L. Chernomordik, M.M. Kozlov, and J. Zimmerberg. Lipids in biological membrane fusion. *J. Membr. Biol.*, 146:1–14, 1995.
25. J. R. Monck and J. M. Fernandez. The fusion pore and mechanisms of biological membrane fusion. *Curr. Opin. Cell Biol.*, 8:524–533, 1996.
26. J. Zimmerberg and L. V. Chernomordik. Membrane fusion. *Adv. Drug Deliv. Rev.*, 38:197–205, 1999.
27. R. Jahn and H. Grubmüller. Membrane fusion. *Curr. Opinion in Cell Biol.*, 14:488–495, 2002.
28. A. Mayer. Membrane fusion in eukaryotic cells. *Ann. Rev. Cell and Dev. Biol.*, 18:289–315,

2002.
29. L.K. Tamm, J. Crane, and V. Kiessling. Membrane fusion: a structural perspective on the interplay of lipids and proteins. *Curr. Opin. Struct. Biol.*, 13:453–466, 2003.
30. R. Blumenthal, M. J. Clague, S.R. Durell, and R.M. Epand. Membrane fusion. *Chem. Rev.*, 103:53–69, 2003.
31. H. Potter. Electroporation in biology - methods, applications, and instrumentation. *Analytical Biochemistry*, 174:361–373, 1988.
32. T. Y. Tsong. Electroporation of cell-membranes. *Biophys. J.*, 60:297–306, 1991.
33. A. Barnett and J. C. Weaver. Electroporation - a unified, quantitative theory of reversible electrical breakdown and mechanical rupture in artificial planar bilayer-membranes. *Bioelectrochemistry and Bioenergetics*, 25:163–182, 1991.
34. D. C. Chang. *Guide to Electroporation and Electrofusion, Academic Press, San Diego*, 1992.
35. J. C. Weaver and Y. A. Chizmadzhev. Theory of electroporation: A review. *Bioelectrochemistry and Bioenergetics*, 41:135–160, 1996.
36. O. G. Mouritsen and K. Jorgensen. A new look at lipid-membrane structure in relation to drug research. *Pharmaceutical Research*, 15:1507–1519, 1998.
37. A. Fahr, P. van Hoohevest, S. May, N. Bergstrand, and M. L. S. Leigh. Transfer of lipophilic drugs between liposomal membranes and biological interfaces: Consequences for drug delivery. *Europ. J. Pharmaceutical Sciences*, 26:251–265, 2005.
38. L. P. Kadanoff. *Statistical Physics: Statics, Dynamics and Renormalization, World Scientific Pub Co.*, 2000.
39. K. A. Dill, S. Bromberg, K. Z. Yue, K. M. Fiebig, D. P. Yee, P. D. Thomas, and H. S. Chan. Principles of protein-folding - a perspective from simple exact models. *Protein Science*, 4:561–602, 1995.
40. M. Karplus and A. Sali. Theoretical-studies of protein-folding and unfolding. *Current Opinion in Structural Biology*, 5:58–73, 1995.
41. J. E. Shea and C. L. Brooks. From folding theories to folding proteins: A review and assessment of simulation studies of protein folding and unfolding. *Ann. Rev. Phys. Chem.*, 52:499–535, 2001.
42. O. G. Mouritsen and M. Bloom. Models of lipid-protein interactions in membranes. *Ann. Rev. Biophys. Biomol. Structure*, 22:145–171, 1993.
43. T. Gil, J. H. Ipsen, O. G. Mouritsen, M. C. Sabra, M. M. Sperotto, and M. J. Zuckermann. Theoretical analysis of protein organization in lipid membranes. *Biochimica et Biophysica Acta-Reviews on Biomembranes*, 1376:245–266, 1998.
44. D. P. Tieleman, H. J. C. Berendsen, and M. S. P. Sansom. Voltage-dependent insertion of alamethicin at phospholipid/water and octane/water interfaces. *Biophys. J.*, 80:331–346, 2001.
45. M. W. Maddox and M. L. Longo. A monte carlo study of peptide insertion into lipid bilayers: Equilibrium conformations and insertion mechanisms. *Biophys. J.*, 82:244–263, 2002.
46. C. F. Lopez, S. O. Nielsen, P. B. Moore, and M. L. Klein. Understanding nature's design for a nanosyringe. *Proc. Natl. Acad. Sci. USA*, 101:4431–4434, 2004.
47. B.L. de Groot and H. Grubmüller. Water permeation across biological membranes: Mechanism and dynamics of aquaporin-1 and glpf. *Science*, 294:2353–2357, 2001.
48. E. Tajkhorshid, P. Nollert, M. O. Jensen, L. J. W. Miercke, J. O'Connell, R. M. Stroud, and K. Schulten. Control of the selectivity of the aquaporin water channel family by global orientational tuning. *Science*, 296:525–530, 2002.
49. L. Saiz, S. Bandyopadhyay, and M. L. Klein. Effect of the pore region of a transmembrane ion channel on the physical properties of a simple membrane. *J. Phys. Chem. B*, 108:2608–2613,

2004.
50. L. Saiz and M. L. Klein. Structural properties of a highly polyunsaturated lipid bilayer from molecular dynamics simulations. *Biophys. J.*, 81:204–216, 2001.
51. M. Müller, K. Katsov, and M. Schick. A new mechanism of model membrane fusion determined from monte carlo simulation. *Biophys. J.*, 85:1611–1623, 2003.
52. G. Gompper and D. M. Kroll. Phase-diagram and scaling behavior of fluid vesicles. *Phys. Rev. E*, 51:514–525, 1995.
53. K.V. Damodaran, M. Kenneth, J. Merz, and B.P. Gaber. Structure and dynamics of the dilauroylphosphatidylethanolamine lipid bilayer. *Biochemistry*, 31:7656, 1992.
54. H. Heller, M. Schäfer, and K. Schulten. Molecular dynamics simulation of a bilayer of 200 lipids in the gel and in the liquid-crystal phases. *J. Phys. Chem.*, 97:8343, 1993.
55. M. Tuckerman, B.J. Berne, and G.J. Martyna. Reversible multiple time scale molecular dynamics. *J. Chem. Phys.*, 97:1990, 1992.
56. J.C. Phillips, R. Braun, W. Wang, J. Gumbart, E. Tajkhorshid, E. Villa, C. Chipot, R. Skeel, L. Kale, and K. Schulten. Scalable molecular dynamics with namd. *J. Comp. Chem.*, 26:1781, 2005.
57. E. Lindahl, B. Hess, and D. van der Spoel. Gromacs 3.0: a package for molecular simulation and trajectory analysis. *J. Mol. Model*, 7:306, 2001.
58. D. van der Spoel, E. Lindahl, B. Hess, G. Groenhof, A.E. Mark, and H.J.C. Berendsen. Gromacs: Fast, flexible, and free. *J. Comp. Chem.*, 26:1701–1718, 2005.
59. M. Christen, P.H. Hünenberger, D. Bakowies, R. Baron, R. Bürgi, D.P. Geerke, T.N. Heinz, M.A. Kastenholz, V. Kräutler, C. Oostenbrink, C. Peter, D. Trzesniak, and W.F. van Gunsteren. The gromos software for biomolecular simulation: Gromos05. *J. Comp. Chem.*, 26:1719–1751, 2005.
60. W.R.P. Scott, P.H. Hünenberger, I.G. Tironi, A.E. Mark, S.R. Billeter, J. Fennen, A.E. Torda, T. Huber, P. Krüger, and W.F. van Gunsteren. The gromos biomolecular simulation program package. *J. Phys. Chem. A*, 103:3596–3607, 1999.
61. A.P. Lyubartsev and A.Laaksonen. Mdynamix - a scalable portable parallel md simulation package for arbitrary molecular mixtures. *Comp. Phys. Comm.*, 128:565–589, 2000.
62. D.A. Case, T.E. Cheatham III, T. Darden, H. Gohlke, R. Luo, K.M. Merz Jr., A. Onufriev, C. Simmerling, B. Wang, and R. Woods. The amber biomolecular simulation programs. *J. Comp. Chem.*, 26:1668–1688, 2005.
63. E. Apra, T.L. Windus, and T.P. Straatsma et al. Nwchem, a computational chemistry package for parallel computers, version 4.7. *Pacific Northwest National Laboratory, Richland, Washington 99352-0999, USA*, 2005.
64. R.A. Kendall, E. Apra, D.E. Bernholdt, E.J Bylaska, M. Dupuis, G.I. Fann, R.J. Harrison, J. Ju, J.A. Nichols, J. Nieplocha, T.P. Straatsma, T.L. Windus, and A.T. Wong. High performance computational chemistry: An overview of nwchem a distributed parallel application. *Comp. Phys. Comm.*, 128:260–283, 2000.
65. J.L. Banks, H.S. Beard, Y. Cao, A.E. Cho, W. Damm, R. Farid, A.K. Felts, T.A. Halgren, D.T. Mainz, J.R. Maple, R. Murphy, D.M. Philipp, M.P. Repasky, L.Y. Zhang, B.J. Berne, R.A. Friesner, E. Gallicchio, and R.M. Levy. Integrated modeling program, applied chemical theory (impact). *J. Comp. Chem*, 26:1752–1780, 2005.
66. W.L. Jorgensen and J. Tirado-Rives. Molecular modeling of organic and biomolecular systems using boss and mcpro. *J. Comp. Chem.*, 26:1689–1700, 2005.
67. W. Smith, I.T. Todorov, and M. Leslie. The dlpoly molecular dynamics package. *Z. Kristallogr.*, 220:563–566, 2005.
68. W. Smith and T.R. Forester. Dlpoly2.0: A general-purpose parallel molecular dynamics

simulation package. *J. Mol. Graphics*, 14:136, 1996.
69. S.J. Plimpton. Fast parallel algorithms for short-range molecular dynamics. *J. Comp. Phys.*, 117:1–19, 1995.
70. H.J. Limbach, A. Arnold, B.A. Mann, and C. Holm. Espresso - an extensible simulation package for research on soft matter systems. *Comp. Phys. Comm.*, 174:704–727, 2006.
71. William Humphrey, Andrew Dalke, and Klaus Schulten. VMD – visual molecular dynamics. *J. Mol. Graphics*, 14:33–38, 1996.
72. *http://pymol.sourceforge.net*.
73. B.R. Brooks, R.E. Bruccoleri, B.D. Olafson, D.J. States, S. Swaminathan, and M. Karplus. Charmm: A program for macromolecular energy, minimization, and dynamics calculations. *J. Comp. Chem.*, 4:187–217, 1983.
74. W.F. van Gunsteren, S.R. Billeter, A.A. Eising, P.H. Hünenberger, P. Krüger, A.E. Mark, W.R.P. Scott, and I.G. Tironi. *Hochschulverlag AG der ETH Zürich*, 1996.
75. W.L. Jorgensen, S.D. Maxwell, and J. Tirado-Rives. Development and testing of the opls all-atom force field on conformational energetics and properties of organic liquids. *J. Am. Chem. Soc*, 118:11225, 1996.
76. G.A. Kaminski, R.A. Friesner, J. Tirado-Rives, and W.L. Jorgensen. Evaluation and reparametrization of the opls-aa force field for proteins via comparison with accurate quantum chemical calculations on peptides. *J. Phys. Chem. B*, 2005:6474, 2001.
77. M. Levitt. Energy calculations and dynamics program. *Molecular Applications Group: Standford and Yeda, Rehovot, Israel*, 1990.
78. R.W. Hockney and J.W. Eastwood. *Computer Simulation using Particles*. IOP, London, 1988.
79. M. Deserno and C. Holm. How to mesh up ewald sums. 1. a theoretical and numerical comparison of various particle mesh routines. *J. Chem. Phys.*, 109:7678, 1988.
80. M. Deserno and C. Holm. How to mesh up ewald sums. 2. an accurate error estimate for the p3m algorithm. *J. Chem. Phys.*, 109:7694, 1988.
81. T. Maggs and V. Rosseto. Local simulation algorithms for coulombic interactions. *Phys. Rev. Lett.*, 88:196402, 2002.
82. J. Röttler and T. Maggs. Local molecular dynamics with coulombic interactions. *Phys. Rev. Lett.*, 93:170201, 2004.
83. I. Pasichnyk and B. Dünweg. Coulomb interactions via local dynamics: A molecular-dynamics algorithm. *J. Phys.: Condens. Matter*, 16:3999–4020, 2004.
84. D. Frenkel and B. Smit. *Understanding Molecular Simulation, Academic Press, Boston*, 1996.
85. D.C. Rapaport. *The Art of Molecular Dynamics Simulation, 2nd Edition*. Cambridge University Press, 2004.
86. D. Frenkel and B. Smit. *Understanding Molecular Simulation, 2nd Edition*. Academic Press, San Diego, 2002.
87. G. M. Torrie and J. P. Valleau. *J. Comput. Phys.*, 23:187, 1977.
88. K. Hukushima and K. Nemoto. Exchange monte carlo method and application to spin glass simulations. *J. Phys. Soc. Japan*, 65:1604–1608, 1996.
89. U. H. E. Hansmann. Parallel tempering algorithm for conformational studies of biological molecules. *Chemical Physics Letters*, 281:140–150, 1997.
90. Y. Sugita and Y. Okamoto. Replica-exchange molecular dynamics method for protein folding. *Chemical Physics Letters*, 314:141–151, 1999.
91. A. Mitsutake, Y. Sugita, and Y. Okamoto. Generalized-ensemble algorithms for molecular simulations of biopolymers. *Biopolymers*, 60:96–123, 2001.

92. J.-P. Ryckaert, G. Ciccotti, and H.J.C. Berendsen. Numerical integration of cartesian equations of motion of a system with constraints – molecular dynamics of n-alkanes. *J. Comp. Phys.*, 23:327, 1977.
93. H.C. Andersen. Rattle: A velocity version of the shake algorithm for molecular dynamics calculations. *J. Comput. Phys.*, 52:24, 1983.
94. B. Hess, H. Bekker, H. J. C. Berendsen, and J. G. E. M. Fraaije. Lincs: A linear constraint solver for molecular simulations. *J. Comput. Chem.*, 18:1463–1472, 1997.
95. H.J.C. Berendsen, J.P.M. Postma, W.F. van Gunsteren, A. DiNola, and J. R. Haak. Molecular dynamics with coupling to an external bath. *J. Chem. Phys.*, 81:3684–3690, 1984.
96. H.C. Anderson. Molecular-dynamics at constant pressure and/or temperature. *J. Chem. Phys.*, 72:2384–2393, 1980.
97. S. Nosé. A unified formulation of the constant temperature molecular dynamics methods. *J. Chem. Phys.*, 81:511, 1984.
98. W.G. Hoover. Canonical dynamics: Equilibrium phase-space distributions. *Phys. Rev. A*, 31:1695, 1985.
99. G.J. Martyna, M.L. Klein, and M. Tuckerman. Nosé–hoover chains: The canonical ensemble via continuous dynamics. *J. Chem. Phys.*, 97:2653, 1992.
100. M. Parrinello and A. Rahman. Starin fluctuations and elastic constants. *J. Chem. Phys.*, 76:2662, 1982.
101. C. Jarzynski. Nonequilibrium equality for free energy differences. *Phy. Rev. Lett.*, 78:2690, 2000.
102. C. Jarzynski. Equilibrium free-energy differences from nonequilibrium measurements: A master-equation approach. *Phy. Rev. E*, 56:5018–5038, 2000.
103. S. Park, F. Khalili-Araghi, E. Tajkhorshid, and K. Schulten. Free energy calculation from steered molecular dynamics simulations using jarzynski's equality. *J. Chem. Phys.*, 119:3559–3566, 2003.
104. S. Park and K. Schulten. Calculating potentials of mean force from steered molecular dynamics simulations. *J. Chem. Phys.*, 120:5946–5961, 2004.
105. T. Speck and U. Seifert. Dissipated work in driven harmonic diffusive systems: General solution and application to stretching rouse polymers. *Eur. Phys. J. B*, 43:521–527, 2005.
106. M. Pasenkiewicz-Gierula, Y. Takaoka, H. Miyagawa, K. Kitamura, and A. Kusumi. Charge pairing of headgroups in phosphatidylcholine membranes: A molecular dynamics simulation study. *Biophs. J.*, 76:1228–1240, 1999.
107. K. Aman, E. Lindahl, O. Edholm, P. Hakansson, and P.-O. Westlund. Structure and dynamics of interfacial water in an l_α phase lipid bilayer from molecular dynamics simulations. *Biophys. J.*, 84:102, 2003.
108. C.F. Lopez, S.O. Nielsen, M.L. Klein, and P.B. Moore. Hydrogen bonding structure and dynamics of water at the dimyristoylphosphatidylcholine lipid bilayer surface from a molecular dynamics simulation. *J. Phys. Chem. B*, 108:6603–6610, 2004.
109. F. Suits and M.C. Pitman. Molecular dynamics investigation of the structural properties of phosphatidylethanolamine lipid bilayers. *J. Chem. Phys.*, 122:244714, 2005.
110. A. H. de Vries, S. Yefimov, A. E. Mark, and S. J. Marrink. Molecular structure of the lecithin ripple phase. *Proc. Natl. Acad. Sci. USA*, 102:5392–5396, 2005.
111. E. Lindahl and O. Edholm. Mesoscopic undulations and thickness fluctuations in lipid bilayers from molecular dynamics simulations. *Biophys. J.*, 76:426, 2000.
112. S.J. Marrink and A. E. Mark. Effect of undulations on surface tension in simulated bilayers. *J. Phys. Chem. B*, 105:6122, 2001.
113. S.J. Marrink and D.P Tieleman. Molecular dynamics simulation of spontaneous membrane

fusion during a cubic-hexagonal phase transition. *Biophys. J.*, 83:2386, 2002.
114. V. Knecht, M. Müller, M. Bonn, S.-J. Marrink, and A.E. Mark. Simulation studies of pore and domain formation in a phospholipid monolayer. *J. Chem. Phys.*, 122:024704, 2005.
115. S.J. Marrink, E. Lindahl, O Edholm, and A.E. Mark. Simulation of the spontaneous aggregation of phospholipids into bilayers. *J. Am. Chem. Soc*, 123:8638–8639, 2001.
116. A.H. de Vries, A.E. Mark, and S.J. Marrink. Molecular dynamics simulation of the spontaneous formation of a small dppc vesicle in water in atomistic detail. *J. Am. Chem. Soc*, 126:4488, 2004.
117. S. Bandyopadhyay, J.C. Shelley, and M.L. Klein. Molecular dynamics study of the effect of surfactant on a biomembrane. *J. Chem. Phys.*, 105:5979, 2001.
118. K. Tu, M.L. Klein, and D.J. Tobias. Constant pressure molecular dynamics investigation of cholesterol effects in a dipalmitoylphosphatidylcholine bilayer. *Biophys. J.*, 75:2147, 1998.
119. C. Hofsäß, E. Lindahl, and O. Edholm. Molecular dynamics simulations of phospholipid bilayers with cholesterol. *Biophys. J.*, 84:2192, 2003.
120. E. Falck, M. Patra, M. Karttunen, M.T. Hyvönen, and I. Vattulainen. Impact of cholesterol on voids in phospholipid membranes. *J. Chem. Phys.*, 121:12676, 2004.
121. Y. Song, V. Guallar, and N.A. Baker. Molecular dynamics simulations of salicylate effects on the micro- and mesoscopic properties of a dipalmitoylphosphatidylcholine bilayer? *Biochemistry*, 44:13425, 2005.
122. L. Koubi, M. Tarek M.L. Klein, and D. Scharf. Distribution of halothane in a dppc bilayer from molecular dynamics calculations. *Biophys. J.*, 78:800, 2000.
123. J. H. Crowe, L. M. Crowe, and D. Chapman. Preservation of membranes in anhydrobiotic organisms - the role of trehalose. *Science*, 223:701–703, 1984.
124. S. B. Leslie, E. Israeli, B. Lighthart, J. H. Crowe, and L. M. Crowe. Trehalose and sucrose protect both membranes and proteins in intact bacteria during drying. *Applied and Environmental Microbiology*, 61:3592–3597, 1995.
125. A.K. Sum, R. Faller, and J.J. de Pablo. Molecular simulation study of phospholipid bilayers and insights of the interactions with disaccharides. *Biophys. J.*, 85:2830–2844, 2003.
126. A.K. Sum and J.J. de Pablo. Molecular simulation study on the influence of dimethylsulfoxide on the structure of phospholipid bilayers. *Biophys. J.*, 85:3636, 2003.
127. C. S. Pereira, R. D. Lins, I. Chandrasekhar, L. C. Freitas, and P. H. Hünenberger. Interaction of the disacceride trehalose with a phospholipid bilayer: a molecular dynamics study. *Biophys. J.*, 86:2273–2285, 2004.
128. M.A. Villareal, S.B. Diaz, E.A. Disalvo, and G.G. Montich. Molecular dynamics simulation study of the interaction of trehalose with lipid membranes. *Langmuir*, 20:7844–7851, 2004.
129. M. Doxastakis, A. K. Sum, and J. J. de Pablo. Modulating membrane properties: The effect of trehalose and cholesterol on a phospholipid bilayer. *J. Phys. Chem. B*, 109:24173–24181, 2005.
130. A. Skibinsky, R. M. Venable, and R. W. Pastor. A molecular dynamics study of the response of lipid bilayers and monolayers to trehalose. *Biophys. J.*, 89:4111–4121, 2005.
131. S. Bandyopadhyay, M. Tarek, and M.L. Klein. Molecular dynamics study of a lipid-dna complex. *J. Phys. Chem. B*, 103:10075, 1999.
132. B.L. de Groot, D.P. Tieleman, P.Pohl, and H. Grubmüller. Water permeation through gramicidin a: Desformylation and the double helix: A molecular dynamics study. *Biophys. J.*, 82:2934, 2002.
133. A. Aksimentiev and K. Schulten. Imaging α-hemolysin with molecular dynamics: Ionic conductance, osmotic permeability, and the electrostatic potential map. *Biophys. J.*, 88:3745, 2005.

134.R.G. Larson, L.E. Scriven, and H.T. Davis. Monte carlo simulation of model amphiphile-oil-water systems. *J. Chem. Phys.*, 83:2411, 1983.
135.F. M. Haas, R. Hilfer, and K. Binder. Phase transitions in dense lipid monolayers grafted to a surface: Monte carlo investigation of a coarse-grained off-lattice model. *J. Chem. Phys.*, 100:15290–15300, 1996.
136.R. Goetz and R. Lipowsky. Computer simulations of bilayer membranes: Self-assembly and interfacial tension. *J. Chem. Phys.*, 108:7397, 1998.
137.R. Goetz, G. Gompper, and R. Lipowsky. Mobility and elasticity of self-assembled membranes. *Phys. Rev. Lett.*, 82:221, 1999.
138.I. Carmesin and K. Kremer. The bond fluctuation method: a new effective algorithm for the dynamics of polymers in all spatial dimensions. *Macromolecules*, 21:819–2823, 1988.
139.T. Dotera and A. Hatano. The diagonal bond method: A new lattice polymer model for simulation study of block copolymers. *J. Chem. Phys.*, 105:8431, 1996.
140.H. Noguchi and M. Takasu. Fusion pathways of vesicles: A brownian dynamics simulation. *J. Chem. Phys.*, 115:9547–9551, 2001.
141.T. Soddemann, B. Dünweg, and K. Kremer. A generic computer model for amphiphilic systems. *Eur. Phys. J. E*, 6:409–419, 2001.
142.J. C. Shillcock and R. Lipowsky. Equilibrium structure and lateral stress distribution of amphiphilic bilayers from dissipative particle dynamics simulations. *J. Chem. Phys.*, 117:5048–5061, 2002.
143.H. Guo, K. Kremer, and T. Soddemann. Nonequilibrium molecular dynamics simulation of shear-induced alignment of amphiphilic model systems. *Phys. Rev. E*, 66:061503, 2002.
144.H. Guo and K. Kremer. Amphiphilic lamellar model systems under dilation and compression: Molecular dynamics study. *J. Chem. Phys.*, 118:7714, 2003.
145.P. G. de Gennes. Exponents for excluded volume problem as derived by wilson method. *Physics Letters A*, A:339, 1972.
146.J. Israelachvili. *Intermolecular & Surface Forces*, pages Academic Press, London, 1992.
147.J. N. Israelachvili, S. Marcelja, and R. G. Horn. Physical principles of membrane organization. *Quarterly Reviews of Biophysics*, 13:121–200, 1980.
148.B. Widom. Some topics in the theory of fluids. *J. Chem. Phys.*, 39:2802, 1963.
149.G. Gompper and M.Schick. *Self-assembling amphiphilic systems, in Phase Transitions and critical phenomena*, Vol. 16:C. Domb and J.L. Lebowitz eds., Academic Press, 1994.
150.R.G. Larson. Molecular simulation of ordered amphiphilic phases. *Chem. Engr. Sci*, 49:2833, 1994.
151.R.G. Larson. Monte carlo simulations of the phase behavior of surfactant solutions. *J. Phys. (France) II*, 6:1441, 1996.
152.B. Li, N. Madras, and A. Sokal. *J. Stat. Phys.*, 80:661, 1995.
153.P. J. Flory. Thermodynamics of high polymer solutions. *J. Chem. Phys.*, 9:660, 1941.
154.M. L. Huggins. Solutions of long chain compounds. *J. Chem. Phys.*, 9:440, 1941.
155.K. Kremer and K. Binder. Monte-carlo simulations of lattice models for macromolecules. *Computer Physics Reports*, 7:259–310, 1988.
156.M. Müller. Bond fluctuation model and other lattice models. *Chap 9.5 of the Handbook of Materials Modeling, Sid Yip (ed), Springer, Netherlands*, 2005.
157.H. P. Deutsch and K. Binder. Interdiffusion and self-diffusion in polymer mixtures - a monte-carlo study. *J. Chem. Phys.*, 94:2294–2304, 1991.
158.M. Müller. Miscibility behavior and single chain properties in polymer blends: A bond fluctuation model study. *Macromol. Theory Simul.*, 8:343–374, 1999.
159.M. Müller and M. Schick. Bulk and interfacial thermodynamics of a symmetric, ternary

homopolymer-copolymer mixture: A monte carlo study. *J. Chem. Phys.*, 105:8885–8901, 1996.
160. M. Müller and M. Schick. Structure and nucleation of pores in polymeric bilayers: a monte carlo simulation. *J. Chem. Phys.*, 105:8282–8292, 1996.
161. M. Müller, K. Katsov, and M. Schick. New mechanism of membrane fusion. *J. Chem. Phys.*, 116:2342–2345, 2002.
162. B. D. Discher, Y-Y. Won, D. S. Ege, J. C-M. Lee, F. S. Bates, D. E. Discher, and D. A. Hammer. Polymersomes: tough vesicles made from diblock copolymers. *Science*, 284:1143–1146, 1999.
163. R. P. Rand and V. A. Parsegian. Hydration forces between phospholipid bilayers. *Biochim. Biophys. Acta*, 988:351–376, 1989.
164. R. P. Rand, N. L. Fuller, S. M. Gruner, and V. A. Parsegian. Membrane curvature, lipid segregation, and structural transitions for phospholipids under dual-solvent stress. *Biochemistry*, 29:76–87, 1990.
165. Z. Chen and R. P. Rand. The influence of cholesterol on phospholipid membrane curvature and bending elasticity. *Biophys. J.*, 73:267–276, 1997.
166. S. Leikin, M. M. Kozlov, N. L. Fuller, and R. P. Rand. Measured effects of dyacilglycerol on structural and elastic properties of phospholipid membrane. *Biophys. J.*, 71:2623–2632, 1996.
167. M. Müller and G. Gompper. Elastic properties of polymer interfaces: Aggregation of pure diblock, mixed diblock, and triblock copolymers. *Phys. Rev. E*, 66:041805, 2002.
168. B. Smit, K. Esselink, P.A.J. Hilbers, N.M. van Os, L.A.M. Rupert, and I. Szleifer. Computer simulations of surfactant self-assembly. *Langmuir*, 9:9, 1993.
169. M. Doi and S.F. Edwards. *The Theory of Polymer Dynamics*. Oxford University Press, New York, 1994.
170. J. M. Drouffe, A. C. Maggs, and S. Leibler. Computer-simulations of self-assembled membranes. *Science*, 254:1353–1356, 1991.
171. H. Noguchi and M. Takasu. Self-assembly of amphiphiles into vesicles: A brownian dynamics simulation. *Phys. Rev. E*, 64:041913, 2001.
172. Z.-J. Wang and D. Frenkel. Modeling flexible amphiphilic bilayers: A solvent-free off-lattice monte carlo study. *J. Chem. Phys.*, 122:234711, 2005.
173. O. Farago. Water-free model for fluid bilayer membranes. *J. Chem. Phys.*, 119:596, 2003.
174. I.R. Cooke, K. Kremer, and M. Deserno. Tunable generic model for fluid bilayer membranes. *Phys. Rev. E*, 72:011506, 2005.
175. I. R. Cooke and M. Deserno. Solvent-free model for self-assembling fluid bilayer membranes: Stabilization of the fluid phase based on broad attractive tail potentials. *J. Chem. Phys.*, 123:224710, 2005.
176. M. H. J. Hagen and D. Frenkel. Determination of phase diagrams for the hard-core attractive yukawa system. *J. Chem. Phys.*, 101:4093, 1994.
177. M. Dijkstra, R. van Roij, and R. Evans. Phase behavior and structure of binary hard-sphere mixtures. *Phys. Rev. Lett.*, 81:2268–2271, 1998.
178. C.N. Likos. Effective interactions in soft condensed matter physics. *Physics Reports*, 348:267–439, 2001.
179. G. Brannigan and F. L. H. Brown. Solvent-free simulations of fluid membrane bilayers. *J. Chem. Phys.*, 120:1059–1071, 2004.
180. G. Brannigan, A. C. Tamboli, and F. L. H. Brown. The role of molecular shape in bilayer elasticity and phase behavior. *J. Chem. Phys.*, 121:3259–3271, 2004.
181. G. Brannigan and F. L. H. Brown. Composition dependence of bilayer elasticity. *J. Chem.*

Phys., 122:074905, 2005.
182.G. Brannigan, P. F. Philips, and F. L. H. Brown. Flexible lipid bilayers in implicit solvent. *Phys. Rev. E*, 72:011915, 2005.
183.G. Brannigan, L. C. L. Lin, and F. L. H. Brown. Implicit solvent simulation models for biomembranes. *Eur. Biophys. J.*, 35:104–124, 2006.
184.R. D. Groot. Mesoscopic simulation of polymer-surfactant aggregation. *Langmuir*, 16:7493–7502, 2000.
185.R.D. Groot and K.L. Rabone. Mesoscopic simulation of cell membrane damage, morphology chance and rupture by nonionic surfactants. *Biophys. J.*, 81:725, 2001.
186.M. Kranenburg, M. Venturoli, and B. Smit. Phase behavior and induced interdigitation in bilayers studied with dissipative particle dynamics. *J. Phys. Chem. B*, 107:11491, 2003.
187.M. Kranenburg, C. Laforge, and B. Smit. Mesoscopic simulations of phase transitions in lipid bilayers. *Phys. Chem. Chem. Phys*, 6:4531, 2004.
188.M. Kranenburg, J.-P. Nicolas, and B. Smit. Comparison of mesoscopic phospholipid-water models. *Phys. Chem. Chem. Phys.*, 6:4142, 2004.
189.M. Kranenburg, M. Venturoli, and B. Smit. Molecular simulations of mesoscopic bilayer phases. *Phys. Rev. E*, 67:060901(R), 2003.
190.M. Kranenburg, M. Vlaar, and B. Smit. Simulating induced interdigitation in membranes. *Biophys. J.*, 87:1596, 2004.
191.M. Kranenburg and B. Smit. Phase behavior of model lipid bilayers. *J. Phys. Chem. B*, 109:6553–6563, 2005.
192.A. Imparato, J. C. Shillcock, and R. Lipowsky. Lateral and transverse diffusion in two-component bilayer membranes. *Eur. Phys. J. E*, 11:21, 2003.
193.G. Illya, R. Lipowsky, and J.C. Shillcock. Effect of chain length and asymmetry on material properties of bilayer membranes. *J. Chem. Phys.*, 122:244901, 2005.
194.V. Ortiz, S. O. Nielsen, D. E. Discher, M. L. Klein, R. Lipowsky, and J. Shillcock. Dissipative particle dynamics simulations of polymersomes. *J. Phys. Chem. B*, 109:17708–17714, 2005.
195.A.F. Jakobsen. Constant-pressure and constant-surface tension simulation in dissipative partcile dynamics. *J. Chem. Phys.*, 122:124901, 2005.
196.A. F. Jakobsen, O. G. Mouritsen, and G. Besold. Artifacts in dynamical simulations of coarse-grained model lipid bilayers. *J. Chem. Phys.*, 122:204901, 2005.
197.P. J. Hoogerbrugge and J. M. V. A. Koelman. Simulating microscopic hydrodynamics phenomena with dissipative particle dynamics. *Europhys. Lett*, 19:155, 1992.
198.J. M. V. A. Koelman and P. J. Hoogerbrugge. Dynamic simulation of hard-sphere suspensions under steady shear. *Europhys. Lett*, 21:363, 1993.
199.P. Warren and P. Espanol. Statistical-mechanics of dissipative particle dynamics. *Europhys. Lett*, 30:191196, 1995.
200.T. Soddemann, B, Dünweg, and K. Kremer. Dissipative particle dynamics: A useful thermostat for equilibrium and nonequilibrium molecular dynamics simulations. *Phys. Rev. E*, 68:46702, 2003.
201.P. Espanol . Hydrodynamics from dissipative particle dynamics. *Phys. Rev. E*, 52:1734, 1995.
202.G. Besold, I. Vattulainen, M. Karttunen, and J.M. Polson. Towards better integrators for dissipative particle dynamics simulations. *Phys. Rev. E*, 62:7611, 2000.
203.I. Vattulainen, M. Karttunen, G. Besold, and J.M. Polson. Integration schemes for dissipative particle dynamics simulations: From softly interacting systems towards hybrid models. *J. Chem. Phys.*, 116:3967, 2002.
204.M. P. Allen. Configurational temperature in membrane simulations using dissipative particle

dynamics. *J. Phys. Chem. B*, 110:3823–3830, 2006.
205. F. A. M. Leermakers and J. M. H. M. Scheutjens. Statistical thermodynamics of association colloids .1. lipid bilayer-membranes. *J. Chem. Phys.*, 89:3264–3274, 1988.
206. O. Lenz and F. Schmid. A simple computer model for liquid lipid bilayers. *Journal Of Molecular Liquids*, 117:147–152, 2005.
207. S. J. Marrink and A. E. Mark. Molecular view of hexagonal phase formation in phospholipid membranes. *Biophys. J.*, 87:3894–3900, 2004.
208. S. J. Marrink, J. Risselada, and A. E. Mark. Simulation of gel phase formation and melting in lipid bilayers using a coarse grained model. *Chem. Phys. Lip.*, 135:223–244, 2005.
209. I. R. Cooke and M. Deserno. Coupling between lipid shape and membrane curvature. *Biophys. J.*, 91:487–495, 2006.
210. G. Ayton and G.A. Voth. Bridging mocroscopic and mesoscopic simulations of lipid bilayers. *Biophys. J.*, 83:3357, 2002.
211. W. Paul, K. Binder, K. Kremer, and D. W. Heermann. Structure property correlation of polymers, a monte-carlo approach. *Macromolecules*, 24:6332–6334, 1991.
212. M. Murat and K. Kremer. From many monomers to many polymers: Soft ellipsoid model for polymer melts and mixtures. *J. Chem. Phys.*, 108:4340–4348, 1998.
213. W. Tschop, K. Kremer, J. Batoulis, T. Burger, and O. Hahn. Simulation of polymer melts. i. coarse-graining procedure for polycarbonates. *Acta Polymerica*, 49:61–74, 1998.
214. P. G. Bolhuis, A. A. Louis, J. P. Hansen, and E. J. Meijer. Accurate effective pair potentials for polymer solutions. *J. Chem. Phys.*, 114:4296–4311, 2001.
215. M. Doi. Octa (open computational tool for advanced material technology). *Macromolecular Symposia*, 195:101–107, 2003.
216. S. K. Ma. *Statistical Mechanics, World Scientific Pub Co Inc*, 1985.
217. L. Yelash, M. Müller, W. Paul, and K. Binder. How well can coarse-grained models of real polymers describe their structure? the case of polybutadiene. *J. Chem. Theo. Comp.*, 2:588–597, 2006.
218. J. Baschnagel, K. Binder, W. Paul, M. Laso, U. W. Suter, I. Batoulis, W. Jilge, and T. Burger. On the construction of coarse-grained models for linear flexible polymer-chains - distribution-functions for groups of consecutive monomers. *J. Chem. Phys.*, 95:6014–6025, 1991.
219. P. Doruker and W. L. Mattice. Reverse mapping of coarse-grained polyethylene chains from the second nearest neighbor diamond lattice to an atomistic model in continuous space. *Macromolecules*, 30:5520–5526, 1997.
220. R. Faller, H. Schmitz, O. Biermann, and F. Müller-Plathe. Automatic parameterization of force fields for liquids by simplex optimization. *J. Comput. Chem*, 20:1009–1017, 1999.
221. H. Meyer, O. Biermann, R. Faller, D. Reith, and F. Müller-Plathe. Coarse graining of nonbonded inter-particle potentials using automatic simplex optimization to fit structural properties. *J. Chem. Phys.*, 113:6264–6275, 2000.
222. C. F. Abrams, L. delle Site, and K. Kremer. Dual-resolution coarse-grained simulation of the bisphenol-a-polycarbonate/nickel interface. *Phys. Rev. E*, 67:021807, 2003.
223. C. F. Abrams and K. Kremer. Combined coarse-grained and atomistic simulation of liquid bisphenol a-polycarbonate: Liquid packing and intramolecular structure. *Macromolecules*, 36:260–267, 2003.
224. R. Faller. Automatic coarse graining of polymers. *Polymer*, 45:3869–3876, 2004.
225. T. Murtola, E. Flack, M. Patra, M. Karttunen, and I. Vattulainena. Coarse-grained model for phospholipid/cholesterol bilayer. *J. Chem. Phys.*, 121:9156, 2004.
226. S. Izvekov and G.A. Voth. Multiscale coarse graining of liquid-state systems. *J. Chem.*

Phys., 123:134105, 2005.
227. Q. Sun and R. Faller. Systematic coarse-graining of atomistic models for simulation of polymeric systems. *Computers & Chemical Engineering*, 29:2380–2385, 2005.
228. G. Milano and F. Müller-Plathe. Mapping atomistic simulations to mesoscopic models: A systematic coarse-graining procedure for vinyl polymer chains. *J. Phys. Chem. B*, 109:18609–18619, 2005.
229. M. Praprotnik, L. delle Site, and K. Kremer. Adaptive resolution molecular-dynamics simulation: Changing the degrees of freedom on the fly. *J. Chem. Phys.*, 123:224106, 2005.
230. Q. Sun and R. Faller. Systematic coarse-graining of a polymer blend: Polyisoprene and polystyrene. *J. Chem. Theo. Comp.*, 2:607–615, 2006.
231. Q. Sun and R. Faller. Crossover from unentangled to entangled dynamics in a systematically coarse-grained polystyrene melt. *Macromolecules*, 39:812–820, 2006.
232. J. R. Silbermann, S. H. L. Klapp, M. Schoen, N. Chennamsetty, H. Bock, and K. E. Gubbins. Mesoscale modeling of complex binary fluid mixtures: Towards an atomistic foundation of effective potentials. *J. Chem. Phys.*, 124:074105, 2006.
233. S. Izvekov and G. A. Voth. Multiscale coarse-graining of mixed phospholipid/cholesterol bilayers. *J. Chem. Theo. Comp.*, 2:637–648, 2006.
234. D. Bedrov, C. Ayyagari, and G. D. Smith. Multiscale modeling of poly(ethylene oxide)-poly(propylene oxide)-poly(ethylene oxide) triblock copolymer micelles in aqueous solution. *J. Chem. Theo. Comp.*, 2:598–606, 2006.
235. G. Prampolini. Parametrization and validation of coarse grained force-fields derived from ab initio calculations. *J. Chem. Theo. Comp.*, 2:556–567, 2006.
236. G. D. Smith and W. Paul. United atom force field for molecular dynamics simulations of 1,4-polybutadine based on quantum chemistry calculations on model molecules. *J. Phys. Chem. A*, 102:1200–1208, 1998.
237. G. D. Smith, W. Paul, M. Monkenbusch, L. Willner, D. Richter, X. H. Qiu, and M. D. Ediger. Molecular dynamics of a 1,4-polybutadiene melt. comparison of experiment and simulation. *Macromolecules*, 32:8857–8865, 1999.
238. G. D. Smith, O. Borodin, D. Bedrov, W. Paul, X. H. Qiu, and M. D. Ediger. C-13 nmr spin-lattice relaxation and conformational dynamics in a 1,4-polybutadiene melt. *Macromolecules*, 34:5192–5199, 2001.
239. S. Krushev, W. Paul, and G. D. Smith. The role of internal rotational barriers in polymer melt chain dynamics. *Macromolecules*, 35:4198–4203, 2002.
240. A. A. Louis. Beware of density dependent pair potentials. *J. Phys.: Condens. Matter*, 14:9187–9206, 2002.
241. P. Ascarelli and R. J. Harrison. Density-dependent potentials and hard-sphere model for liquid metals. *Phys. Rev. Lett.*, 22:385–388, 1969.
242. S. K. Ma. Renormalization group by monte-carlo methods. *Phys. Rev. Lett.*, 37:461–464, 1976.
243. R. H. Swendsen. Monte-carlo renormalization group. *Phys. Rev. Lett.*, 42:859–861, 1979.
244. P. J. Reynolds, H. E. Stanley, and W. Klein. Large-cell monte-carlo renormalization-group for percolation. *Phys. Rev. B*, 21:1223–1245, 1980.
245. G. S. Pawley, R. H. Swendsen, D. J. Wallace, and K. G. Wilson. Monte-carlo renormalization-group calculations of critical-behavior in the simple-cubic ising-model. *Phys. Rev. B*, 29:4030–4040, 1984.
246. D. Reith, M. Pütz, and F. Müller-Plathe. *J. Comput. Chem.*, 24:1624–1636, 2003.
247. R. Faller and D. Reith. Properties of poly(isoprene): Model building in the melt and in solution. *Macromolecules*, 36:5406–5414, 2003.

248.F. Wang and D. P. Landau. Determining the density of states for classical statistical models: A random walk algorithm to produce a flat histogram. *Phys. Rev. E*, 64:056101, 2001.
249.C.F. Lopez, S.O. Nielson, P.B. Moore, J.C. Shelley, and M.L. Klein. Self-assembly of a phospholipid langmuir monolayer using coarse-grained molecular dynamics simulations. *J. Phys.: Condens. Matter*, 14:9431, 2002.
250.R. W. Chang and A. Yethiraj. Solvent effects on the collapse dynamics of polymers. *J. Chem. Phys.*, 114:7688–7699, 2001.
251.R. Chang, G.S. Ayton, and G.A. Voth. Multiscale coupling of mesoscopic- and atomistic-level lipid bilayer simulations. *J. Chem. Phys.*, 122:244716, 2005.
252.M. Doi and S. F. Edwards. *The theory of polymer dynamics*. Oxford, 2001.
253.G. H. Fredrickson. *The equilibrium theory of inhomogeneous polymers*. Oxford, 2006.
254.M. Müller and F. Schmid. Incorporating fluctuations and dynamics in self-consistent field theories for polymer blends. *Adv. Polym. Sci*, 185:1–58, 2005.
255.M. Müller. Comparison of self-consistent field theory and monte carlo simulations. *Soft Matter, G. Gompper and M. Schick (edts)*, 1:179–281, 2005.
256.S. Marcelja. Molecular model for phase transition in biological membranes. *Nature*, 241:451, 1973.
257.S. Marcelja. *Biochem. Biophys. Acta*, 367:165, 1974.
258.P. J. Flory. *Principles of Polymer Chemistry*. Cornell University Press, Ithaca, 1954.
259.W. L. Mattice and U. W. Suter. *Conformational Theory of Large Molecules: the Rotational Isomeric State Model in Macromolecular Systems, Wiley Interscience, New York*, 1994.
260.D. W. R. Gruen. A model for the chains in amphiphilic aggregates. 1. comparison with a molecular dynamics simulation of a bilayer. *J. Phys. Chem.*, 89:146, 1985.
261.D. W. R. Gruen. Statistical mechanical model of the lipid bilayer above its phase-transition. *Biochim. Biophys. Acta*, 595:161, 1980.
262.D. W. R. Gruen. A mean-field model of the alkane-saturated lipid bilayer above its phase-transition. 1. development of the model. *Biophys. J.*, 33:149, 1981.
263.D. W. R. Gruen and D. A. Haydon. A mean-field model of the alkane-saturated lipid bilayer above its phase-transition. 2. results and comparison with experiment. *Biophys. J.*, 33:167, 1981.
264.D. W. R. Gruen. The packing of amphiphile chains in a small spherical micelle. *J. Coll. Int. Sci.*, 84:281, 1981.
265.D. W. R. Gruen. A model for the chains in amphiphilic aggregates. 1. comparison with a molecular-dynamics simulation of a bilayer. *J. Phys. Chem.*, 89:146, 1985.
266.D. W. R. Gruen. A model for the chains in amphiphilic aggregates. 2. thermodynamic and experimental comparison for aggregates of different shape and size. *J. Phys. Chem.*, 89:153, 1985.
267.K. A. Dill and R. S. Cantor. Statistical thermodynamics of short-chain molecule interphases. 1. theory. *Macromolecules*, 17:380, 1984.
268.K. A. Dill, J. Naghizadeh, and J. A. Marqusee. Chain molecules at high densities at interfaces. *Ann. Rev. Phys. Chem.*, 39:425, 1988.
269.J. M. H. M. Scheutjens and G. J. Fleer. Statistical-theory of the adsorption of interacting chain molecules .1. partition-function, segment density distribution, and adsorption-isotherms. *J. Phys. Chem.*, 83:1619–1635, 1979.
270.A. Ben-Shaul and W. M. Gelbart. Theory of chain packing in amphiphilic aggregates. *Ann. Rev. Phys. Chem.*, 36:179, 1985.
271.A. Ben-Shaul. Molecular theory of chain packing, elasticity and lipid-protein interaction in lipid bilayers. *Handbook of biological physics*, 1:359, 1995.

272.A. Ben-Shaul and I. Szleifer. Chain organization and thermodynamics in micelles and bilayers. 1. theory. *J. Chem. Phys.*, 83:3597, 1985.
273.A. Ben-Shaul and I. Szleifer. Chain organization and thermodynamics in micelles and bilayers. 2. model calculations. *J. Chem. Phys.*, 83:3612, 1985.
274.R. Elliott, K. Katsov, M. Schick, and I. Szleifer. Phase separation of saturated and monounsaturated lipids as determined from a microscopic model. *J. Chem. Phys.*, 122:044904, 2005.
275.R. Elliott, I. Szleifer, and M. Schick. Phase diagram of a ternary mixture of cholesterol and saturated and unsaturated lipids calculated from a microscopic model. *Phys. Rev. Lett.*, 96:098101, 2006.
276.S. Marcelja. Chain ordering in liquid crystals. i. even-odd effect. *J. Chem. Phys.*, 60:3599, 1974.
277.S.F. Edwards. *Proc. Phys. Soc.*, 85:613, 1965.
278.E. Helfand and Y. Tagami. Theory of interface between immiscible polymers. *J. Polym. Sci. B: Polymer Letters*, 9:741, 1971.
279.E. Helfand and Y. Tagami. Theory of interface between immiscible polymers. *J. Chem. Phys.*, 57:1812, 1972.
280.E. Helfand and Y. Tagami. Theory of interface between immiscible polymers .2. *J. Chem. Phys.*, 56:3592, 1972.
281.J. M. H. M. Scheutjens and G. J. Fleer. Statistical-theory of the adsorption of interacting chain molecules .2. train, loop, and tail size distribution. *J. Phys.Chem.*, 84:178–190, 1980.
282.K. M. Hong and J. Noolandi. Theory of interfacial-tension in ternary homopolymer-solvent systems. *Macromolecules*, 14:736–742, 1981.
283.K. M. Hong and J. Noolandi. Theory of inhomogeneous multicomponent polymer systems. *Macromolecules*, 14:727–736, 1981.
284.M. W. Matsen and M. Schick. Stable and unstable phases of a diblock copolymer melt. *Phys. Rev. Lett.*, 72:2660–2663, 1994.
285.M. W. Matsen. Self-consistent field theory and its application. *Soft Matter, G. Gompper and M. Schick (edts)*, 1:87–178, 2006.
286.M. W. Matsen and F. S. Bates. Unifying weak- and strong-segregation block copolymer theories. *Macromolecules*, 29:1091–1098, 1996.
287.A. C. Shi, J. Noolandi, and R. C. Desai. Theory of anisotropic fluctuations in ordered block copolymer phases. *Macromolecules*, 29:6487–6504, 1996.
288.M. W. Matsen. The standard gausian model for block copolymer melts. *J. Phys.: Condens. Matter*, 14:R21–R47, 2002.
289.M. W. Matsen. Stabilizing new morphologies by blending homopolymer with block-copolymer. *Phys. Rev. Lett.*, 74:4225–4228, 1995.
290.P. K. Janert and M. Schick. Phase behavior of ternary homopolymer/diblock blends: Microphase unbinding in the symmetric system. *Macromolecules*, 30:3916–3920, 1997.
291.P. K. Janert and M. Schick. Phase behavior of ternary homopolymer/diblock blends: Influence of relative chain lengths. *Macromolecules*, 30:137–144, 1997.
292.P. K. Janert and M. Schick. Phase behavior of binary homopolymer/diblock blends: Temperature and chain length dependence. *Macromolecules*, 31:1109–1113, 1998.
293.M. W. Matsen. Elastic properties of a diblock copolymer monolayer and their relevance to bicontinuous microemulsion. *J. Chem. Phys.*, 110:4658–4667, 1999.
294.F. A. M. Leermakers and J. M. H. M. Scheutjens. Statistical thermodynamics of association colloids. 1. lipid vesicles. *J. Phys. Chem.*, 93:7417, 1989.
295.F. A. M. Leermakers and J. M. H. M. Scheutjens. Statistical thermodynamics of association

colloids. iii. the gel to liquid phase transition of lipid bilayer membranes. *J. Chem. Phys.*, 89:6912, 1988.

296. I. Szleifer, D. Kramer, A. Ben-Shaul, D. Roux, and W. M. Gelbart. Curvature elasticity of pure and mixed surfactant films. *Phys. Rev. Lett.*, 60:1966, 1988.
297. S. M. Oversteegen and F. A. M. Leermakers. Thermodynamics and mechanics of bilayer membranes. *Phys. Rev. E*, 62:8453, 2000.
298. R. A. Kik, J. M. Kleijn, and F. A. M. Leermakers. Bending moduli and spontaneous curvature of the monolayer in a surfactant bilayer. *J. Phys. Chem. B*, 109:14251, 2005.
299. I. Szleifer, D. Kramer, A. Ben-Shaul, W. M. Gelbart, and S. A. Safran. Molecular theory of curvature elasticity in surfactant films. *J. Chem. Phys.*, 92:6800, 1990.
300. L. A. Meijer, F. A. M. Leermakers, and J. Lyklema. Self-consistent modeling of complex molecules with united atom detail in inhomogeneous systems. cyclic and branched foreign molecules in dimyristoylphosphatidylcholine membranes. *J. Chem. Phys.*, 110:6560, 1999.
301. F. A. M. Leermakers, A. L. Rabinovich, and N. K. Balabaev. Self-consistent modeling of hydrated unsaturated lipid bilayers in liquid-crystal phase and comparison to molecular dynamics simulations. *Phys. Rev. E*, 67:011910, 2003.
302. S. J. Suresh and V. M. Naik. Predictive models for interfacial properties of associating systems. a statistical thermodynamic approach. *Langmuir*, 12:6151, 1996.
303. A. L. Rabinovich, P. O. Ripatti, N. K. Balabaev, and F. A. M. Leermakers. Molecular dynamics simulations of hydrated unsaturated lipid bilayers in the liquid-crystal phase and comparison to self-consistent-field modeling. *Phys. Rev. E*, 67:011909, 2003.
304. M. D. Whitmore, J. P. Whitehead, and A.Roberge. Self-consistent field theory of compressible phospholipid membranes at ambient pressure. *Can. J. Phys.*, 76:831, 1998.
305. M. Müller and M. Schick. Calculation of the phase behavior of lipids. *Phys. Rev. E*, 57:6973–6978, 1998.
306. I. Szleifer and M. A. Carignano. Tethered polymer layers. *Advances In Chemical Physics*, 94:165–260, 1996.
307. R.R. Netz and M. Schick. Pore formation and rupture in fluid bilayers. *Phys. Rev. E*, 53:3875, 1996.
308. X.-J. Li and M. Schick. Theory of lipid polymorphism application to phosphatidylethanolamine and phosphatidylserine. *Biophys. J.*, 78:34, 2000.
309. X.-J. Li and M. Schick. Theory of ph-sensitive vesicles of anionic and cationic lipids or anionic and neutral lipids. *Biophys. J.*, 80:1703, 2001.
310. I. M. Hafez, S. Ansell, and P.R. Cullis. Tunable ph sensitive liposomes composed of mixtures of cationic and anionic lipids. *Biophys. J.*, 79:14238–14246, 2000.
311. K. Katsov, M. Müller, and M. Schick. Field theoretic study of bilayer membrane fusion. i. hemifusion mechanism. *Biophys. J.*, 87:3277–3290, 2004.
312. K. Katsov, M. Müller, and M. Schick. Field theoretic study of bilayer membrane fusion: Ii. mechanism of a stalk-hole complex. *Biophys. J.*, 90:915–926, 2006.
313. V. Talanquer and D. W. Oxtoby. Nucleation of pores in amphiphile bilayers. *J. Chem. Phys.*, 118:872–877, 2003.
314. D. Chandler, J. D. McCoy, and S. J. Singer. Density functional theory of nonuniform polyatomic systems. i. general formulation. *J. Chem. Phys.*, 85:597, 1986.
315. A. L. Frischknecht, J. G. Curro, and L. J. Douglas Frink. Density functional theory for inhomogeneous polymer systems. ii application to block copolymer films. *J. Chem. Phys.*, 117:10398, 2002.
316. A. L. Frischknecht, J. D. Weinhold, A. G. Salinger, J. G. Curro, and J. D. McCoy. Density functional theory for inhomogeneous polymer systems. i numerical methods. *J. Chem. Phys.*,

117:10385, 2002.

317.M. Müller and L. G. MacDowell. Interface and surface properties of short polymers in solution: Monte carlo simulations and self-consistent field theory. *Macromolecules*, 33:3902–3923, 2000.

318.M. Müller, L. G. MacDowell, and A. Yethiraj. Short chains at surfaces and interfaces: A quantitative comparison between density-functional theories and monte carlo simulations. *J. Chem. Phys.*, 118:2929–2940, 2003.

319.C. N. Patra and A. Yethiraj. Density functional theory for nonuniform polymers: Accurate treatment of the effect of attractive interactions. *J. Chem. Phys.*, 118:4702–4706, 2003.

320.Y. X. Yu and J. Z. Wu. Density functional theory for inhomogeneous mixtures of polymeric fluids. *J. Chem. Phys.*, 117:2368–2376, 2002.

321.J. Z. Wu. Density functional theory for chemical engineering: From capillarity to soft materials. *AICHE Journal*, 52:1169–1193, 2006.

322.L.J.D. Frink and A.L. Frischknecht. Density functional theory approach for coarse-grained lipid bilayers. *Phys. Rev. E*, 72:041923, 2005.

323.J. G. Curro and K. S. Schweizer. Theory of polymer melts - an integral-equation approach. *Macromolecules*, 20:1928–1934, 1987.

324.K. S. Schweizer and J. G. Curro. Integral-equation theory of polymer melts - intramolecular structure, local order, and the correlation hole. *Macromolecules*, 21:3070–3081, 1988.

325.A. Yethiraj and K. S. Schweizer. Self-consistent polymer integral equation theory: Comparison with Monte Carlo simulations and alternative closure approximations. *J. Chem. Phys.*, 97:1455–1465, 1992.

326.K. S. Schweizer and J. G. Curro. Integral equation theories of the structure, thermodynamics, and phase transitions of polymer fluids. *Adv. Chem. Phys.*, 98:1–142, 1997.

327.A.L. Frischknecht and L.J.D. Frink. Comparison of density functional theory and simulation of fluid bilayers. *Phys. Rev. E*, 72:041924, 2005.

328.G. Gompper and M. Schick. Correlation between structural and interfacial properties of amphiphilic systems. *Phys. Rev. Lett.*, 65:1116–1119, 1990.

329.W. T. Gozdz and R. Holyst. Triply periodic surfaces and multiply continuous structures from the landau model of microemulsions. *Phys. Rev. E*, 54:5012–5027, 1996.

330.G. Gompper and M. Kraus. Ginzburg-landau theory of ternary amphiphilic systems .2. monte-carlo simulations. *Phys. Rev. E*, 47:4301–4312, 1993.

331.P. B. Canham. Minimum energy of bending as a possible explanation of biconcave shape of human red blood cell. *J. Theor. Bio.*, 26:61, 1970.

332.W. Helfrich. Elastic properties of lipid bilayers - theory and possible experiments. *Zeitschrift Naturforschung C*, 28:693–703, 1973.

333.E. A. Evans. Bending resistance and chemically-induced moments in membrane bilayers. *Biophys. J.*, 14:923–931, 1974.

334.L. Peliti and S. Leibler. Effects of thermal fluctuations on systems with small surface tensions. *Phys. Rev. Lett.*, 54:1690–1693, 1985.

335.D. M. Kroll and G. Gompper. Scaling behavior of randomly triangulated self-avoiding surfaces. *Phys. Rev. A*, 46:3119–3122, 1992.

336.D. M. Kroll and G. Gompper. The conformation of fluid membranes - monte-carlo simulations. *Science*, 255:968–971, 1992.

337.G. Gompper and D. M. Kroll. Shape of inflated vesicles. *Phys. Rev. A*, 46:7466–7473, 1992.

338.D. C. Morse and S. T. Milner. Fluctuations and phase-behavior of fluid membrane-vesicles. *Europhys. Lett*, 26:565–570, 1994.

339.D. C. Morse and S. T. Milner. Statistical mechanics of closed fluid membranes. *Phys. Rev.*

E, 52:5918–5945, 1995.
340. M. Kraus, W. Wintz, U. Seifert, and R. Lipowsky. Fluid vesicles in shear flow. *Phys. Rev. Lett.*, 77:3685–3688, 1996.
341. G. Gompper and D. M. Kroll. Fluctuations of polymerized, fluid and hexatic membranes: Continuum models and simulations. *Current Opinion in Colloid & Interface Science*, 2:373–381, 1997.
342. H. G. Dobereiner, E. Evans, M. Kraus, U. Seifert, and M. Wortis. Mapping vesicle shapes into the phase diagram: A comparison of experiment and theory. *Phys. Rev. E*, 55:4458–4474, 1997.
343. U. Seifert. Configurations of fluid membranes and vesicles. *Adv. Phys.*, 46:13–137, 1997.
344. G. Gompper and D. M. Kroll. Membranes with fluctuating topology: Monte carlo simulations. *Phys. Rev. Lett.*, 81:2284–2287, 1998.
345. G. Gompper and D. M. Kroll. Statistical mechanics of membranes: Freezing, undulations, and topology fluctuations. *J. Phys.: Condens. Matter*, 12:A29–A37, 2000.
346. M. Hamm and M. M. Kozlov. Tilt model of inverted amphiphilic mesophases. *Eur. Phys. J. B*, 6:519–528, 1998.
347. J. B. Fournier. Coupling between membrane tilt-difference and dilation: A new "ripple" instability and multiple crystalline inclusions phases. *Europhys. Lett*, 43:725–730, 1998.
348. S. May. A molecular model for the line tension of lipid membranes. *Eur. Phys. J. E*, 3:37–44, 2000.
349. Y. Kozlovsky and M. M. Kozlov. Stalk model of membrane fusion: solution of energy crisis. *Biophys. J.*, 82:882–895, 2002.
350. Y. Kozlowsky, L.V. Chernomordik, and M.M. Kozlov. Lipid intermediates in membrane fusion: Formation, structure and decay of hemifusion diaphragm. *Biophys. J.*, 83:2634, 2002.
351. D.P. Siegel. The modified stalk mechanism of lamellar/inverted phase transitions and its implications for membrane fusion. *Biophys. J.*, 76:291, 1999.
352. S. May. Structure and energy of fusion stalks: The role of membrane edges. *Biophys. J.*, 83:2969–2980, 2002.
353. M. Müller and M. Schick. Structure and nucleation of pores in polymeric bilayers: A monte carlo simulation. *J. Chem. Phys.*, 105:8282–8292, 1996.
354. W. K. den Otter, S. A. Shkulipa, and W. J. Briels. Buckling and persistence length of an amphiphilic worm from molecular dynamics simulations. *J. Chem. Phys.*, 119:2363–2368, 2003.
355. W. K. den Otter. Area compressibility and buckling of amphiphilic bilayers in molecular dynamics simulations. *J. Chem. Phys.*, 123:214906, 2005.
356. A. Werner, F. Schmid, M. Müller, and K. Binder. Intrinsic profiles and capillary waves at homopolymer interfaces: A monte carlo study. *Phys. Rev. E*, 59:728–738, 1999.
357. A. Werner, F. Schmid, and M. Müller. Monte carlo simulations of copolymers at homopolymer interfaces: Interfacial structure as a function of the copolymer density. *J. Chem. Phys.*, 110:5370–5379, 1999.
358. N. Akino, F. Schmid, and M. P. Allen. Molecular-dynamics study of the nematic-isotropic interface. *Phys. Rev. E*, 63:041706, 2001.
359. S. Wolfsheimer, C. Tanase, K. Shundyak, R. van Roij, and T. Schilling. Isotropic-nematic interface in suspensions of hard rods: Mean-field properties and capillary waves. *Phys. Rev. E*, 73:061703, 2006.
360. A. Werner, F. Schmid, M. Müller, and K. Binder. Anomalous size-dependence of interfacial profiles between coexisting phases of polymer mixtures in thin-film geometry: A monte carlo

simulation. *J. Chem. Phys.*, 107:8175–8188, 1997.
361. J. S. Ho and A. Baumgartner. Simulations of fluid self-avoiding membranes. *Europhys. Lett*, 12:295–300, 1990.
362. D. H. Boal and M. Rao. Scaling behavior of fluid membranes in 3 dimensions. *Phys. Rev. A*, 45:R6947–R6950, 1992.
363. G. Gompper and D. M. Kroll. Random surface discretizations and the renormalization of the bending rigidity. *J. Phys. (France) I*, 6:1305–1320, 1996.
364. G. Gompper and D. M. Kroll. Freezing flexible vesicles. *Phys. Rev. Lett.*, 78:2859–2862, 1997.
365. G. Gompper and D. M. Kroll. The freezing of flexible vesicles of spherical topology. *J. Phys. (France) I*, 7:1369–1390, 1997.
366. P. B. S. Kumar and M. Rao. Shape instabilities in the dynamics of a two-component fluid membrane. *Phys. Rev. Lett.*, 80:2489–2492, 1998.
367. P. B. S. Kumar, G. Gompper, and R. Lipowsky. Budding dynamics of multicomponent membranes. *Phys. Rev. Lett.*, 86:3911–3914, 2001.
368. H. Noguchi and G. Gompper. Fluid vesicles with viscous membranes in shear flow. *Phys. Rev. Lett.*, 93:258102, 2004.
369. H. Noguchi and G. Gompper. Dynamics of fluid vesicles in shear flow: Effect of membrane viscosity and thermal fluctuations. *Phys. Rev. E*, 72:011901, 2005.
370. H. Noguchi and G. Gompper. Shape transitions of fluid vesicles and red blood cells in capillary flows. *Proc. Natl. Acad. Sci. USA*, 102:14159–14164, 2005.
371. B. Chen, J. J. Potoff, and I. J. Siepmann. *J. Phys. Chem. B*, 105:3093–3104, 2001.
372. J. Lee and B. R. Lentz. Evolution of lipidic structures during model membrane fusion and the relation of this process to cell membrane fusion. *Biochemistry*, 36:6251–6259, 1997.
373. B. R. Lentz, V. Malinin, Md. E. Haque, and K. Evans. Protein machines and lipid assemblies: current views of cellmembrane fusion. *Curr. Opinion in Struct. Biol.*, 10:607–615, 2000.
374. G. Cevc and H. Richardsen. Lipid vesicles and membrane fusion. *Adv. Drug. Deliv.*, 38:207–232, 1999.
375. K. O. Evans and B. R. Lentz. Kinetics of lipid rearrangements during poly(ethylene glycol)-mediated fusion of highly curved unilamellar vesicles. *Biochemistry*, 41:1241–1249, 2002.
376. B. R. Lentz, W. Talbot, J. Lee, and L.-X. Zheng. Transbilayer lipid redistribution accompanies poly(ethylene glycol) treatment of model membranes but is not induced by fusion. *Biochemistry*, 36:2076–2083, 1997.
377. Y. Zhou and D. Yan. Real-time membrane fusion of giant polymer vesicles. *J. Am. Chem. Soc*, 127:10468–10469, 2005.
378. S. Förster and M. Antonietti. Amphiphilic block copolymers in structure-controlled nanomaterial hybrids. *Adv. Mater.*, 10:195, 1998.
379. L. B. Luo and A. Eisenberg. Thermodynamic size control of block copolymer vesicles in solution. *Langmuir*, 17:6804–6811, 2001.
380. D. E. Discher and A. Eisenberg. Polymer vesicles. *Science*, 297:967–973, 2002.
381. M. Antonietti and S. Förster. Vesicles and liposomes: A self-assembly principle beyond lipids. *Adv. Mater.*, 15:1323–1333, 2003.
382. V. Ortiz, S. O. Nielsen, M. L. Klein, and D. E. Discher. Computer simulation of aqueous block copolymer assemblies: length scales and methods. *J. Polym. Sci. B: Polymer Physics*, 44:1907–1918, 2006.
383. L. Chernomordik. Non-bilayer lipids and biological fusion intermediates. *Chem. Phys. Lip.*, 81:203–213, 1996.
384. J. R. Monck, G.A. de Toledo, and J. M. Fernandez. Tension in granule secretory membranes

causes extensive membrane transfer through the exocytotic fusion pore. *Proc. Natl. Acad. Sci. USA*, 87:7804–7808, 1990.

385. G. B. Melikyan, J. M. White, and F. S. Cohen. Gpi-anchored influenza hemagglutinin induces hemifusion to both red blood cells and planar bilayer membranes. *J. Cell Biol.*, 131:679–691, 1995.

386. T. Shangguan, D. Alford, and J. Bentz. Influenza virus-liposome lipid mixing is leaky and largely insensitive to the material properties of the target membrans. *Biochemistry*, 25:4956–4965, 1996.

387. P. Bonnafous and T. Stegmann. Membrane perturbation and fusion pore formation in influenza hemagglutinin-mediated membrane fusion. *J. Biol. Chem.*, 275:6160–6166, 2000.

388. A. Ya. Dunina-Barkovskaya, A. V. Samsonov, V. S. Pivovarov, and V. A. Frolov. Hemagglutinin-induced fusion of hab2 and plc cells: dynamics of fusion pore conductance. *Membr. Cell Biol.*, 13:567–580, 2000.

389. Md. E. Haque and B. R. Lentz. Influence of gp41 fusion peptide on the kinetics of poly(ethylene glycol)-mediated model membrane fusion. *Biochemistry*, 41:10866–10876, 2002.

390. V. A. Frolov, A. Ya. Dunina-Barkovskaya, A. V. Samsonov, and J. Zimmerberg. Membrane permeability changes at early stages of influenza hemagglutinin-mediated fusion. *Biophys. J.*, 85:1725–1733, 2003.

391. M. M. Kozlov and V. S. Markin. Possible mechanism of membrane fusion. *Biofizika*, 28:255–261, 1983.

392. V. S. Markin and M. M. Kozlov. Primary act in the process of membrane fusion. *Biofizika*, 28:73–78, 1983.

393. D. P. Siegel. Energetics of intermediates in membrane fusion:comparison of stalk and inverted micellar intermediate mechanisms. *Biophys. J.*, 65:2124–2140, 1993.

394. M. Müller and K. Binder. Computer-simulation of asymmetric polymer mixtures. *Macromolecules*, 28:1825–1834, 1995.

395. S. E. Feller and R. W. Pastor. On simulating lipid bilayers with an applied surface tension: Periodic boundary conditions and undulations. *Biophys. J.*, 71:1350–1355, 1996.

396. S.E. Feller and R.W. Pastor. Constant surface tension simulations of lipid bilayers: The sensitivity of surface areas and compressibilities. *J. Chem. Phys.*, 111:1281, 1999.

397. A. Sariban and K. Binder. Critical properties of the flory-huggins lattice model of polymer mixtures. *J. Chem. Phys.*, 86:5859–5873, 1987.

398. A. Sariban and K. Binder. Phase-separation of polymer mixtures in the presence of solvent. *Macromolecules*, 21:711–726, 1988.

399. J. I. Siepmann. A method for the direct calculation of chemical-potentials for dense chain systems. *Molecular Physics*, 70:1145–1158, 1990.

400. M. Laso, J. J. Depablo, and U. W. Suter. Simulation of phase-equilibria for chain molecules. *J. Chem. Phys.*, 97:2817–2819, 1992.

401. J. I. Siepmann and D. Frenkel. Configurational-Bias Monte Carlo: A new sampling scheme for flexible chains. *Mol. Phys.*, 75:59–70, 1992.

402. J. C. Shillcock and R. Lipowsky. Tension-induced fusion of bilayer membranes and vesicles. *Nature Mater*, 4:225, 2005.

403. A. F. Smeijers, A. J. Marvoort, K. Pieterse, and P. A. J. Hilbers. A detailed look at vesicle fusion. *J. Phys. Chem. B*, 110:13212–13219, 2006.

404. A. F. Smeijers, K. Pieterse, A.F. Markvoort, and P. A. J. Hilbers. Coarse-grained transmembrane proteins: Hydrophobic matching, aggregation, and their effect on fusion. *J. Phys. Chem. B*, 110:13614–13623, 2006.

405.L. V. Chernomordik, M. M. Kozlov, G. B. Melikyan, I. G. Abidor, V. S. Markin, and Yu. A. Chizmadzhev. The shape of lipid molecules and monolayer membrane fusion. *Biochim. Biophys. Acta*, 812:643–655, 1985.

406.T. V. Tolpekina, W. K. den Otter, and W. J. Briels. Simulations of stable pores in membranes: System size dependence and line tension. *J. Chem. Phys.*, 121:8014–8020, 2004.

407.D. B. Lukatsky and D. Frenkel. Multiple stalk formation as a pathway of defect-induced membrane fusion. *Eur. Phys. J. E*, 14:3–6, 2004.

408.A. Chanturiya, P. Scaria, O. Kuksenok, and M. C. Woodle. Probing the mechanism of fusion in a two-dimensional computer simulation. *Biophys. J.*, 82:3072–3080, 2002.

409.P. Altevogt, O. A. Evers, J. G. E. M. Fraaije, N. M. Maurits, and B. A. C. van Vlimmeren. The mesodyn project: Software for mesoscale chemical engineering. *J. Mol. Struct. Theochem*, 463:139–143, 1999.

410.B. A. C. van Vlimmeren, N. M. Maurits, A. V. Zvelindovsky, G. J. A. Sevink, and J. G. E. M. Fraaije. Simulation of 3d mesoscale structure formation in concentrated aqueous solution of the triblock polymer surfactants (ethylene oxide)(13)(propylene oxide)(30)(ethylene oxide)(13) and (propylene oxide)(19)(ethylene oxide)(33)(propylene oxide)(19). application of dynamic mean-field density functional theory. *Macromolecules*, 32:646–656, 1999.

411.G. J. A. Sevink and A. V. Zvelindovsky. Self-assembly of complex vesicles. *Macromolecules*, 38:7502, 2005.

412.Mark J. Stevens, Jan Hoh, and Thomas Woolf. Insights into the molecular mechanism of membrane fusion from simulation: evidence for the association of splayed tails. *Phys. Rev. Lett.*, 91:188102–1–188102–4, 2003.

413.A. J. Markvoort, K. Pieterse, M. N. Steijaert, P. Spijker, and P. A. J. Hilbers. The bilayer-vesicle transition is entropy driven. *J. Phys. Chem. B*, 109:22649–22654, 2005.

414.Siewart J. Marrink and Alan E. Mark. The mechanism of vesicle fusion as revealed by molecular dynamics simulations. *J. Am. Chem. Soc.*, 125:11144–11145, 2003.

415.D.-W. Li and X.Y. Liu. Examination of membrane fusion by dissipative particle dynamics and comparison with continuum elastic models. *J. Chem. Phys.*, 122:174909, 2005.

416.M. Müller, K. Binder, and W. Oed. Structural and thermodynamic properties of interfaces between coexisting phases in polymer blends - a monte-carlo simulation. *J. Chem. Soc. Faraday Transactions*, 91:2369–2379, 1995.

417.F. Schmid and M. Müller. Quantitative comparison of self-consistent-field theories for polymers near interfaces with monte-carlo simulations. *Macromolecules*, 28:8639–8645, 1995.

418.M. Müller and A. Werner. Interfaces between highly incompatible polymers of different stiffness: Monte carlo simulations and self-consistent field calculations. *J. Chem. Phys.*, 107:10764–10776, 1997.

419.M. Müller and K. Binder. Wetting and capillary condensation in symmetric polymer blends: A comparison between monte carlo simulations and self-consistent field calculations. *Macromolecules*, 31:8323–8346, 1998.

420.D. A. Hajduk, H. Takenouchi, M. A. Hillmyer, F. S. Bates, M. E. Vigild, and K. Almdal. Stability of the perforated layer (pl) phase in diblock copolymer melts. *Macromolecules*, 30:3788–3795, 1997.

421.Y. L. Loo, R. A. Register, D. H. Adamson, and A. J. Ryan. A highly regular hexagonally perforated lamellar structure in a quiescent diblock copolymer. *Macromolecules*, 38:4947–4949, 2005.

422.L. Yang and H. W. Huang. Observation of a membrane fusion intermediate structure. *Science*, 297:1877–1879, 2002.

423.J.M. Fernandez, E. Neher, and B.D. Gomperts. Capacitance measurements reveal stepwise

fusion events in degranulating mast cells. *Nature*, 312:453–455, 1984.
424.A.E. Spruce, L.J. Breckenridge, A. K. Lee, and W. Almers. Properties of the fusion pore that forms during exocytosis of a mast cell secretory vesicle. *Neuron*, 4:643–654, 1990.
425.A. Chanturiya, L.V. Chernomordik, and J. Zimmerberg. Flickering fusion pores comparable with initial exocytotic pores occur in protein-free phospholipid bilayers. *Proc. Natl. Acad. Sci. USA*, 94:14423–14428, 1997.
426.J. C. Shillcock and D. H. Boal. Entropy-driven instability and rupture of fluid membranes. *Biophys. J.*, 71:317–326, 1996.
427.T.V. Tolpekina, W.K. den Otter, and W.J. Briels. Nucleation free energy of pore formation in an amphiphilic bilayer studied by molecular dynamics simulations. *J. Chem. Phys.*, 121:12060, 2004.
428.H. Leontiadou, A.E. Mark, and S.-J. Marrink. Molecular dynamics simulation of hydrophilic pores in lipid bilayers. *Biophys. J.*, 86:2156, 2004.
429.O. Farago and C.D. Santangelo. Pore formation in fluctuating membranes. *J. Chem. Phys.*, 122:044901, 2005.
430.Z.-J. Wang and D. Frenkel. Pore nucleation in mechanically stretched bilayer membranes. *J. Chem. Phys.*, 123:154701, 2005.
431.C. Loison, M. Mareschal, and F. Schmid. Pores in bilayer membranes of amphiphilic molecules: Coarse-grained molecular dynamics simulations compared with simple mesoscopic models. *J. Chem. Phys.*, 121:1890, 2004.
432.Q. Hu, S. Vswanadham, R.P. Joshi, K.H. Schoenbach, S.J. Beebe, and P.F. Blackmore. Simulations of transient membrane behavior in celles subjected to a high-intensity ultrashort electric pulse. *Phys. Rev. E*, 71:031914, 2005.
433.J. Wohlert, W. K. den Otter, O. Edholm, and W. J. Briels. Free energy of a trans-membrane pore calculated from atomistic molecular dynamics simulations. *J. Chem. Phys.*, 124:154905, 2006.
434.C. Taupin, M. Dvolaitzky, and C. Sauterey. Osmotic-pressure induced pores in phospholipid vesicles. *Biochemistry*, 14:4771–4775, 1975.
435.J. D. Litster. Stability of lipid bilayers and red blood-cell membranes. *Physics Letters A*, A:193–194, 1975.
436.G. Hummer and I. G. Kevrekidis. Coarse molecular dynamics of a peptide fragment: Free energy, kinetics, and long-time dynamics computations. *J. Chem. Phys.*, 118:10762–10773, 2003.
437.M. Praprotnik, L. delle Site, and K. Kremer. Adaptive resolution scheme for efficient hydrid atomistic-mesoscale molecular dynamics simulations of dense liquids. *Phys. Rev. E*, 73:066701, 2006.
438.S. Yamamoto, Y. Maruyama, and S. Hyodo. Dissipative particle dynamics study of spontaneous vesicle formation of amphiphilic molecules. *J. Chem. Phys.*, 116:5842–5849, 2002.
439.S. J. Marrink and A. E. Mark. Molecular dynamics simulation of the formation, structure, and dynamics of small phospholipid vesicles. *J. Am. Chem. Soc*, 125:15233–15242, 2003.
440.G.S. Ayton, J.L. McWhriter, P. McMurty, and G.A. Voth. Coupling field theory with continuum mechanics: A simulation of domain formation in giant unilamellar vesicles. *Biophys. J.*, 88:3855, 2005.
441.R. Faller and S. J. Marrink. Simulation of domain formation in dlpc-dspc mixed bilayers. *Langmuir*, 20:7686–7693, 2004.
442.L. Foret. A simple mechanism of raft formation in two-components fluid membranes. *Europhys. Lett*, 71:508, 2005.
443.S.L. Veatch and S.L. Keller. Miscibility phase diagram of giant vesicles containing sphin-

gomylin. *Phys. Rev. Lett.*, 94:148101, 2005.

444.R. Elliot, K. Katsov, M. Schick, and I. Szleifer. Phase separation of saturated and mono-unsaturated lipids as determined from a microscopic model. *J. Chem. Phys.*, 122:044904, 2005.

445.G.A. Khelashvili, S.A. Pandit, and H.L. Scott. Self-consistent mean-field model based on molecular dynamics: Application to lipid-cholesterol bilayers. *J. Chem. Phys.*, 123:034910, 2005.

446.J. Liu, S. Qi, J.T. Groves, and A.K. Chakraborty. Phase segregation on different length scales in a model cell membrane system. *J. Phys. Chem. B*, 109:199960–199969, 2005.

447.Q. Shi and G. A. Voth. Multi-scale modeling of phase separation in mixed lipid bilayers. *Biophys. J.*, 89:2385–2394, 2005.

448.G. Srinivas, C. F. Lopez, and M. L. Klein. Membrane bound hydraphiles facilitate cation trauslocation. *J. Phys. Chem. B*, 108:4231–4235, 2004.

449.M. Venturoli, B. Smit, and M. M. Sperotto. Simulation studies of protein-induced bilayer deformations, and lipid-induced protein tilting, on a mesoscopic model for lipid bilayers with embedded proteins. *Biophys. J.*, 88:1778–1798, 2005.

450.G. Srinivas, D. E. Discher, and M. L. Klein. Key roles for chain flexibility in block copolymer membranes that contain pores or make tubes. *Nano Letters*, 5:2343–2349, 2005.

451.C. F. Lopez, S. O. Nielsen, G. Srinivas, W. F. Degrado, and M. L. Klein. Probing membrane insertion activity of antimicrobial polymers via coarse-grain molecular dynamics. *J. Chem. Theo. Comp.*, 2:649–655, 2006.

452.M. M. Sperotto, S. May, and A. Baumgaertner. Modelling of proteins in membranes. *Chem. Phys. Lip.*, 141:2–29, 2006.

453.O. Farago, N. Gronbech-Jensen, and P. Pincus. Mesoscale computer modeling of lipid-dna complexes for gene therapy. *Phys. Rev. Lett.*, 96:018102, 2006.

454.J. B. Manneville, P. Bassereau, D. Levy, and J. Prost. Activity of transmembrane proteins induces magnification of shape fluctuations of lipid membranes. *Phys. Rev. Lett.*, 82:4356–4359, 1999.

455.N. Gov. Membrane undulations driven by force fluctuations of active proteins. *Phys. Rev. Lett.*, 93:268104, 2004.

456.P. Girard, J. Prost, and P. Bassereau. Passive or active fluctuations in membranes containing proteins. *Phys. Rev. Lett.*, 94:088102, 2005.

457.L. C. L. Lin, N. Gov, and F. L. H. Brown. Nonequilibrium membrane fluctuations driven by active proteins. *J. Chem. Phys.*, 124:074903, 2006.

458.J. C. Shillcock and R. Lipowsky. The computational route from bilayer membranes to vesicle fusion. *J. Phys.: Condens. Matter*, 18:S1191–S1219, 2006.

459.S. W. Chiu, E. Jakobsson, and H. Larry Scott. Combined monte carlo and molecular dynamics simulation of hydrated lipid-cholesterol lipid bilayers at low cholesterol concentration. *Biophys. J.*, 80:1104–1114, 2001.

460.M. R. Vist and J. H. Davis. Phase equilibria of cholesterol/dipalmitoylphosphatidylcholine mixtures:nuclear magnetic resonance and differential scanning calorimetry. *Biochemistry*, 29:451–464, 1990.